



IMPACTS OF TEMPERATURE-DEPENDENT EMISSIVITY ON THE THERMOMECHANICAL RESPONSE OF STEEL MEMBERS SUBJECTED TO UNIFORM AND LOCALIZED HEATING

Master's Thesis Submitted in Partial Fulfilment of the Requirements for the
Erasmus+ Joint Master's Degree
International Master of Science in Fire Safety Engineering

Gerard Jericho Blanca Ronquillo

Student

Dr David Rush

Supervisor

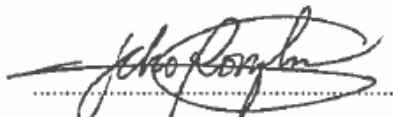
Institute for Infrastructure and Environment
School of Engineering
The University of Edinburgh

Host University

DECLARATION

This thesis is submitted in partial fulfilment of the requirements for the degree International Master of Science in Fire Safety Engineering (IMFSE). This thesis—with an overall word count of 27,201 and a main body word count of 18,606—has never been submitted for any degree or examination to any other university/programme. The author declares that this thesis is original work except where stated. This declaration constitutes an assertion that full and accurate references and citations have been included for all material, directly included and indirectly contributing to the thesis. The author gives permission to make this master's thesis available for consultation and to copy parts of this master's thesis for personal use. In the case of any other use, the limitations of the copyright have to be respected, in particular with regard to the obligation to state expressly the source when quoting results from this master's thesis. The thesis supervisor must be informed when data or results are used.

Signed:



APRIL 29, 2019

Date:

ABSTRACT

Six temperature-dependent emissivity models were used to determine its impact on the thermomechanical behaviour of steel members as compared to using a constant value suggested by the Eurocode. The members—a 3 m beam and a 3 m column—were part of an arbitrarily chosen concrete compartment of office occupancy with dimensions of 5 m × 5 m × 3 m, and which consists of a 1 m × 2 m door and a 1 m × 1 m window openings. Using Abaqus CAE/2018, these members were modelled and subjected to two cases of heating: uniform and localized. The compartment's parametric temperature-time curve and the equivalent ISO 834 standard curve were applied to the members as the uniform heating case, while the localized fire curve was applied as the localized heating case. The results revealed that, on average, the Eurocode overestimated the temperature by as much as 43.09% and underestimated it by 9.33% for the case with an intervening medium between the fire and the surface. The Eurocode prediction for maximum normal stress varied from an overestimation of 56.31% to an underestimation of 9.06%. It generally overestimated the maximum deflection by as high as 48.65%. Lastly, the results for the final deflection varied from an overestimation of 46.67% and underestimation of 10.43%. The variability of the results highlighted the importance of using an appropriate emissivity model to accurately predict the performance of fire-exposed steel members.

ACKNOWLEDGEMENTS

If there is one thing that I learned while doing this thesis that is applicable in real life, it is to be like steel that expands and contracts according to the heat flux that it is being exposed to. Throughout the four months that I used to complete this study, I was faced with a lot of challenges from technical difficulties to repeating simulations all over again because of wrong assumptions to redoing data extraction to the last-minute realization that my data is not fit for a certain type of analysis. But I remained tough despite all of the stress and this study is a proof of that resilient spirit. I could not have finished this if not for the following persons who gave their valuable inputs:

- To my supervisor, Dr David Rush, thank you for this topic. The moment I read this in the IMFSE thesis topics list, I immediately knew that this is what I want to do. Structural modelling is close to my heart because of my huge fascination of the built environment. Despite embarking on a more specific field of study, I believe that this is always going to be my core. Thank you for enlightening me about what is expected of me with this topic. Your suggestions challenged me to do more and it added a palette of colours to this study.
- To Dr Stephen Welch, I really appreciate how you kept on thinking about improving my work even if I am not under your supervision. The papers you gave me about heat transfer were probably my most favourite papers. Because of those, I found out that I had been doing all of my simulations wrong. Thank you for the suggestions and if only I had more time, I would have definitely done those.
- To Jed Aguirre and Jared Mendoza who made me realize that a certain statistical analysis that I wanted to do is not fit for the kind of data that I have, I am grateful to you for answering my questions. If not for you, I would have done something wrong which would have destroyed the credibility of all of my findings.

Apart from the people with direct contributions, I dedicate this thesis to the following people who made this IMFSE journey a dream come true:

- To Dr Bart Merci, Dr Patrick van Hees, and most especially Dr Grunde Jomaas, for their efforts in managing IMFSE. Thank you for believing in my potentials. Your trust is the reason why I strived really hard. Special mention also to Lies Decroos for always attending to our student needs.
- To the 2017 cohort of IMFSE, I am really happy to have met all of you. Thank you for all the wonderful memories and bonding moments. You made the two years of

being away from home less lonely. Special mention to Balsa Jovanovic and Jamie Crum because we have been together since day one, and to Farah Faudzi for all the life advices.

- To Bem and Claire Sajulga, and Jen Hara who served as my second family in Ghent, thank you for always welcoming me to your home. Your positivity in life inspired me a lot.
- To Myla Marquez, Fernando Lit, and Juan Britanico, thank you for being good friends in Edinburgh especially during the times when I needed rest in speaking English and I wanted to speak to fellow Filipinos. Thank you that I always have someone to share the frustrations and joys of thesis writing.
- To Edinburgh University Lawn Tennis Club, thank you for all the fun tennis moments. I am really happy that I was able to let out stress from all the rigors of academic life by playing tennis with you. I also enjoyed playing for the university in some events. Special mention to coach Calum Meston and president-elect Charlie Wingfield-Digby, good luck in the next academic year. Hit more winners, EULTC!
- To my family to whom all of this is for. More than two years ago when I received the big news that I got a scholarship, even I did not know if that was just a dream. You kept asking me, "Are you really leaving?" I took a major decision for our dreams and now I am about to finish it. All the loneliness of being away was worth it. This is the start of something bigger. Thank you for being my inspiration. Thank you for the support. I love you bigtime!
- To God for giving me this opportunity and for the gift of intelligence. Despite all of my shortcomings, You continued to guide me and bless me throughout this journey. My family and I have been through thick and thin throughout the past two years but You gave us hope and endurance. All of this is because of You and for You!

TABLE OF CONTENTS

DECLARATION	i
ABSTRACT	iii
ACKNOWLEDGEMENTS	iv
TABLE OF CONTENTS	vi
LIST OF FIGURES	viii
LIST OF TABLES	xi
LIST OF NOTATIONS	xii
1 INTRODUCTION	1
1.1 Background of the Study	1
1.2 Significance of the Study	2
1.3 Research Objectives	3
1.4 Scope and Limitations	4
2 REVIEW OF RELATED LITERATURE	7
2.1 Radiative Heat Transfer	7
2.1.1 The Nature of Thermal Radiation	7
2.1.2 The Blackbody Idealization	8
2.1.3 Real Surface Radiation and its Related Assumptions	9
2.1.4 Energy Balance for Radiation in a Surface	10
2.1.5 Effect of Intervening Medium	11
2.2 Temperature-dependent Emissivity	13
2.2.1 Factors Affecting the Radiative Properties of Metals	13
2.2.2 Emissivity Models for Steel	15
2.3 Survey of Building Codes About Fire-Exposed Steel Structures	18
2.3.1 Europe: Eurocode	19
2.3.2 USA: International Building Code 2018	20
2.3.3 New Zealand: New Zealand Building Code	21
2.3.4 Australia: National Construction Code 2019	22
2.3.5 Japan: Building Standard Law	23
2.3.6 Hong Kong: Code of Practice for Fire Resisting Construction 1996	23
2.3.7 India: National Building Code of India 2016	24
2.3.8 Singapore: Code of Practice for Fire Precautions in Buildings 2018	24
2.3.9 Philippines: National Structural Code of the Philippines 2015	25
2.3.10 Summary	25
3 METHODOLOGY	27

3.1	General Description	27
3.2	Design Scenario	28
3.3	Fire Curves.....	29
3.3.1	Case 1: Uniform Heating.....	29
3.3.2	Case 2—Scenario 1: Column Fully Engulfed in the Localized Fire.....	30
3.3.3	Case 2—Scenario 2: Column at a Distance from the Localized Fire	31
3.3.4	Case 2—Scenario 3: Beam Directly Above the Localized Fire	31
3.4	Software and Model Preparation	33
3.5	Heat Transfer Modelling	34
3.6	Material Properties of Steel.....	36
3.7	Verification of the User Subroutines	38
4	RESULTS AND DISCUSSION	39
4.1	Temperature.....	39
4.1.1	Case 1: Uniform Heating.....	39
4.1.2	Case 2: Localized Heating	45
4.2	Stress.....	51
4.2.1	Case 1: Uniform Heating.....	51
4.2.2	Case 2: Localized Heating	56
4.3	Deflection.....	58
4.3.1	Case 1: Uniform Heating.....	58
4.3.2	Case 2: Localized Heating	61
4.4	Quantitative Comparison of the Impact of Temperature-dependent Emissivity	64
4.4.1	Temperature.....	64
4.4.2	Stress.....	65
4.4.3	Deflection.....	66
5	CONCLUSIONS.....	69
6	RECOMMENDATIONS.....	71
	REFERENCES	73
	APPENDICES.....	77
A	Design Load	77
B	Temperature-time Curves: Parametric and Equivalent ISO 834.....	79
C	Localized Fire Curve	81
D	Benchmarking Procedure for the Software	82
E	Static Model Verification.....	84
F	Benchmarking Procedure for the User Subroutines	86

LIST OF FIGURES

Figure 2-1. Spectral and directional distributions of radiation. Adapted from (Incropera et al., 2007).....	8
Figure 2-2. Spectral (a) and directional (b) emission of a blackbody and a real surface. Adapted from Incropera et al. (2007).	9
Figure 2-3. View factor between surfaces i and j. Adapted from Incropera et al. (2007)	11
Figure 2-4. Schematic diagram for fire emissivity calculation. Adapted from Hostikka (2003a).	12
Figure 2-5. Topography differences in surfaces with equal σ_h : (a) gradual slopes, (b) steep slopes. Adapted from Modest (2013).	14
Figure 2-6. Temperature-dependent emissivity models.....	18
Figure 3-1. Methodological framework.	27
Figure 3-2. Sketch of the compartment: (a) perspective view and (b) framing plan. Highlighted in red are the structural elements being investigated.....	28
Figure 3-3. Temperature-time curves of a fully-developed fire in the compartment.....	29
Figure 3-4. Heat release rate curve and flame height as a function of time for the localized fire.	30
Figure 3-5. Temperature-time curve along the height of the column fully engulfed in the localized fire. The legend corresponds to the height from the floor in m.	30
Figure 3-6. Incident radiant heat flux to the target surfaces of the column at a distance of 1 m from the fire. The legend corresponds to the height from the floor in m.....	31
Figure 3-7. Incident radiant heat flux to the target surfaces of the beam 2 m above the fire. The legend corresponds to the distance from the beam midspan in m.	32
Figure 3-8. Ceiling jet temperature along the length of the beam. The legend corresponds to the distance from the beam midspan in m.....	33
Figure 3-9. Abaqus model of the structural members: (a) column and (b) beam.....	34
Figure 3-10. Yield strength of steel.	36
Figure 3-11. Elastic modulus of steel.....	36
Figure 3-12. Specific heat of steel.	37
Figure 3-13. Thermal conductivity of steel.	37
Figure 3-14. Stress-strain relationship of steel at elevated temperatures. The legend is in °C.	37
Figure 4-1. Temperature distribution along the beam: (a) parametric curve at $t = 2200$ s and (b) ISO 834 standard curve at $t = 870$ s. The legend is in °C.	39
Figure 4-2. Temperature profile across the beam midspan cross section: (a) parametric curve and (b) ISO 834 standard curve. The legend is in °C.....	40
Figure 4-3. Temperature evolution of the specified point in the beam under parametric curve heating: (a) whole duration and (b) heating period.....	41
Figure 4-4. Temperature evolution of the specified point in the beam under ISO 834 standard curve heating.....	42

Figure 4-5. Temperature distribution along the column: (a) parametric curve at $t = 2300$ s and (b) ISO 834 standard curve at $t = 870$ s. The legend is in $^{\circ}\text{C}$.	42
Figure 4-6. Temperature profile across the column cross section at a height of 2.425 m above the floor: (a) parametric curve and (b) ISO 834 standard curve. The legend is in $^{\circ}\text{C}$.	43
Figure 4-7. Temperature evolution of the specified point in the column under parametric curve heating: (a) whole duration and (b) heating period.	44
Figure 4-8. Temperature evolution of the specified point in the column under ISO 834 standard curve heating.	44
Figure 4-9. Temperature distribution along the column (Case 2—Scenario 1). The legend is in $^{\circ}\text{C}$.	46
Figure 4-10. Temperature profile across the column (Case 2—Scenario 1) cross section at a height of 0.175 m above the floor. The legend is in $^{\circ}\text{C}$.	46
Figure 4-11. Temperature evolution of the specified point in the column (Case 2—Scenario 1).	47
Figure 4-12. Temperature distribution along the column (Case 2—Scenario 2). The legend is in $^{\circ}\text{C}$.	47
Figure 4-13. Temperature profile across the column (Case 2—Scenario 2) cross section at a height of 0.45 m above the floor. The legend is in $^{\circ}\text{C}$.	48
Figure 4-14. Temperature evolution of the specified point in the column (Case 2—Scenario 2).	48
Figure 4-15. Temperature distribution along the beam (Case 2—Scenario 3). The legend is in $^{\circ}\text{C}$.	49
Figure 4-16. Temperature profile across the beam midspan cross section (Case 2—Scenario 3). The legend is in $^{\circ}\text{C}$.	50
Figure 4-17. Temperature evolution of the specified point in the beam (Case 2—Scenario 3).	50
Figure 4-18. Normal stress at different points across the beam midspan cross section under parametric curve heating.	52
Figure 4-19. Temperature variation along the height of the beam cross section under parametric curve heating at chosen timesteps.	52
Figure 4-20. Evolution of the normal stress in the specified point of the beam under parametric curve heating.	53
Figure 4-21. Evolution of the normal stress in the specified point of the beam under parametric curve heating.	53
Figure 4-22. Normal stress at different points across the column cross section under parametric curve heating.	54
Figure 4-23. Evolution of the normal stress in the specified point of the column under parametric curve heating.	55
Figure 4-24. Evolution of the normal stress in the specified point of the column under ISO 834 standard curve heating.	55
Figure 4-25. Evolution of the normal stress in the specified point of the column (Case 2—Scenario 1).	56
Figure 4-26. Normal stress at different points across the cross section of the column (Case 2—Scenario 2).	57

Figure 4-27. Evolution of the normal stress in the specified point of the column (Case 2–Scenario 2).....	57
Figure 4-28. Evolution of the normal stress in the specified point of the beam (Case 2–Scenario 3).....	58
Figure 4-29. Deformed shape of the beam (scaled 10×): (a) parametric curve at t = 2212 s and (b) ISO 834 standard curve at t = 870 s. The legend is in m.....	59
Figure 4-30. Evolution of the vertical deflection of the beam midspan: (a) parametric curve and (b) ISO 834 standard curve.....	60
Figure 4-31. Deformed shape of the column (scaled 10×): (a) parametric curve at t = 2292 s and (b) ISO 834 standard curve at t = 870 s. The legend is in m.....	60
Figure 4-32. Evolution of the vertical deflection of the column top section: (a) parametric curve and (b) ISO 834 standard curve.....	61
Figure 4-33. Deformed shape of the column (scaled 10×): (a) engulfed by the fire at t = 1396 s and (b) distant from the fire at t = 1590 s. The legend is in m.	62
Figure 4-34. Evolution of the vertical deflection of the column top section (Case 2–Scenario 1).....	62
Figure 4-35. Evolution of the horizontal deflection of the column top section (Case 2–Scenario 2).....	63
Figure 4-36. Deformed shape of the beam above the localized fire (scaled 10×) at t = 1401 s.	63
Figure 4-37. Evolution of the vertical deflection of the beam midspan (Case 2–Scenario 3)..	64

LIST OF TABLES

Table 4-1. Comparison of the effect of temperature-dependent emissivity on the surface temperature.....	65
Table 4-2. Comparison of the effect of temperature-dependent emissivity on the maximum stress.....	65
Table 4-3. Comparison of the effect of temperature-dependent emissivity on the maximum deflection.....	66
Table 4-4. Comparison of the effect of temperature-dependent emissivity on the final deflection.....	67

LIST OF NOTATIONS

Subscripts

a	Ambient surroundings
bo	Boundary surface
$cond$	Conduction
$conv$	Convection
eff	Effective
f	Fire source
g	Gas or smoke
i	Radiation source
j	Target surface
net	Net energy
rad	Radiation
s	Surface

Latin Letters

A	Surface area
c_{sh}	Specific heat
D	Fuel diameter
E	Total emissive power
E_a	Modulus of elasticity
E_b	Total emissive power of a blackbody
F	View factor
f_y	Yield strength
f_p	Proportionality limit
G	Total irradiation
H	Distance from the centre of the fuel to the ceiling
h	Heat transfer coefficient
J	Radiosity
k	Thermal conductivity

$k\rho c$	Thermal inertia
L	Path length
Q	Heat release rate
Q''	Heat flux
R	Distance between the centres of two surfaces
r	Horizontal distance from the plume centreline to any point in the compartment
T	Absolute temperature (unless otherwise stated)
T_r	Absolute effective radiant temperature
t	Time

Greek Letters

α	Absorptivity
ε	Emissivity
θ	Angle between the normal of the target surface and the line of sight from the source to the target surface
K_m	Effective absorption coefficient
λ	Wavelength
η	Stoichiometric ratio
ρ	Reflectivity
σ	Stefan-Boltzmann constant
σ_h	Root-mean-square height of the surface roughness
τ	Transmissivity
γ_s	Soot yield

1 INTRODUCTION

1.1 Background of the Study

The ultimate goal of fire safety is to protect lives, properties, and the environment. In the perspective of structural design, fire safety strategies focus on the prevention of collapse of the structure so as to evacuate occupants and provide access to firefighters. In an economic viewpoint, stakeholders require as minimal damage to the structure as possible so that repair costs can be lessened and service of the building can be continued in the earliest possible time. These goals demonstrate the importance of understanding the response of structural members exposed to high temperatures.

The performance of structural members subjected to fires is influenced by the rate by which heat is being transferred into them from the fire, smoke, and boundary surfaces. Fire resistance is of small importance in the early stages of the fire but as the fire grows into full room involvement, its significance increases (Buchanan & Abu, 2017). For large-scale fires, radiation is the dominant heat transfer mechanism (de Ris, 1979). Its intensity depends on the material's emissivity ε , among other factors, which is assumed in several literatures as a constant value. However, the definition of emissivity suggests that it is closely related to the temperature of the radiating body (Incropera, Dewitt, Bergman, & Lavine, 2007).

It is a common design practice in structural fire engineering to adopt constant radiative coefficients, such as emissivity and absorptivity, for thermal radiation between fire gas and solid construction materials (Wang & Tan, 2008). Steel is among the most widely used construction materials in the world and is favoured because of its ability to be formed into complex forms and shapes aside from its high strength. In fact, the global stock of iron currently in use, steel's primary component, amounts to 18 billion metric tons with another 79 billion metric tons worth of ground reserves that can be economically extracted (Müller, Wang, & Duval, 2011). Its material properties such as effective yield strength f_y , and modulus of elasticity E_s are characterized by a number of codes as a function of the temperature. Similarly, Eurocode 3 Part 1-2 uses temperature-dependent values for proportional limit f_p , specific heat c_{sh} , and thermal conductivity k (CEN, 2005b). Same as with these properties, emissivity is also temperature-dependent as revealed by a couple of researches and this is contrary to code provisions.

Rush (2013) provided a brief discussion of these researches that were done to capture the variation of emissivity with respect to temperature. This includes experiments by Paloposki

& Liedquist (2005), and Bentz, Hanssen, & Wilthan (2009), as well as literature values from Drysdale (2011) and Kay, Kirby, & Preston (1996). Similarly, Jiang, Main, Weigand, & Sadek (2018), Sadiq, Wong, Tashan, Al-Mahaidi, & Zhao (2013), Hamerlinck, Twilt, & Stark (1990), and Touloukian & DeWitt (1970) also reported the temperature dependence of the emissivity of steel. Except for the summarized researches by Kay et al. (1996), these references revealed that, generally, emissivity increases with increasing temperature. A thorough discussion of these studies is presented in Subsection 2.2.2.

Radiation is an important physical phenomenon for structural members exposed to fire. However, building codes and performance-based design guidelines for structural steel around the world do not seem to properly account for it because of the simplification in their approach/assumptions, i.e., using a constant emissivity value (CEN, 2005b; Pettersson, Magnusson, & Thor, 1976; Wickström, 2016) and giving it little attention by not being explicitly considered in simplified equations and analysis (Paloposki & Liedquist, 2005). This simplification has to be improved especially because fire engineers now have better understanding of the fire phenomenon and have access to new and state-of-the-art researches on the properties of different materials related to radiation, and advanced analytical and modelling techniques. After all, a better structural fire strategy starts with a more realistic application of the concept of heat transfer.

1.2 Significance of the Study

The quality of a design calculation is only as good as the assumptions used. Researches about finding the temperature dependence of the emissivity of steel were done primarily because using a constant value overestimates the temperature of the steel member. Ghojel & Wong (2005) and Wang & Tan (2008) claimed that using the conventional formulations, particularly for emissivity, of Eurocode 3 Part 1-2 yields higher temperatures for steel members exposed to fire. Additionally, Jiang et al., (2018) demonstrated that there are huge temperature differences on the exposed side of composite slabs with different constant values of emissivity. It was shown that the evolution of temperature was faster for higher values.

Overestimation of the temperature of the structural elements has implications on the determination of the sizes of the members and the level of fire protection that should be applied. Although the cost of fire protection differs according to the project, it accounts for about 20-30% of the total cost of the steel frame for multi-storey projects (Gardner & Ng, 2006). Reducing

the level of structural fire protection or even its total elimination translates to savings in costs and time of construction, and effective utilization of interior space during the construction phase and actual usage of the building (Gardner & Ng, 2006). These are all directly related to the economic benefits of accurate prediction of the temperature of structural members.

Apart from the economic implications, reductions in the level of fire protection in steel buildings also affects the environment. The production of metals such as steel results in the release of pollutants: directly during mining and processing, and indirectly due to the consumption of raw materials and utilities such as in power generation and manufacturing of reagents and explosives (Norgate, Jahanshahi, & Rankin, 2007). The steel production industry is responsible for 7% of the global anthropogenic carbon dioxide (CO₂) emissions (Kim & Worrell, 2002). Meanwhile, it accounts for 4.7% of the European Union's (EU) emission equivalent to 182 million tons of CO₂ (Morfeldt, Nijs, & Silveira, 2015). Similarly, the manufacturing of other passive fire protection materials such as thermal insulations and intumescent paints also contribute to the depletion and destruction of natural resources, directly or indirectly.

Overall, the impact of accurate determination of the thermal response of steel members which starts with the use of more realistic values for the thermal properties spans more than just the structure being designed or assessed. If the raw materials needed for the construction of a building can be reduced, the client and other stakeholders, and the environment will benefit in an economic and sustainable manner, respectively. In this way, fire engineers fulfil the goals of protecting people, properties, and the environment.

1.3 Research Objectives

The main objective of this study is to determine the impact of using a more realistic emissivity model, i.e., emissivity value that varies with temperature, in the thermal and structural response of steel elements at two types of heating scenario: uniform and localized. Specifically, this study aims to accomplish the following:

- a) Perform a survey of the provisions of different building codes and guidelines related to radiative heat transfer.
- b) Review and summarize related literatures about radiation and researches done about the temperature-dependent behaviour of the emissivity of steel.
- c) For uniform heating, select an arbitrary enclosure size, determine the parametric temperature-time curve inside the enclosure using Annex A of Eurocode 1 Part 1-2 and

the equivalent BS EN 1363-1 standard fire curve which, according to BSI (1999), is technically related to ISO 834.

- d) For localized heating, model the fire using Annex C of Eurocode 1 Part 1-2.
- e) Apply the temperature-dependent emissivity models to simulate the thermal and structural response of beams in flexure and columns in compression with arbitrarily chosen loads exposed to the different heating scenarios.
- f) Compare and analyse the results obtained (temperature, stress, and deflection) from using a constant emissivity value to that from a temperature-dependent emissivity value.

1.4 Scope and Limitations

Majority of the work done in this research involved the use of computer simulation. The finite element analysis software Abaqus CAE/2018 was used to model and simulate the response of the steel members with certain loading while being exposed to several heating scenarios. Therefore, this study was bound by the capabilities of this software. Verification of the modelling procedure and setup was done by comparison of results using the Gillie (2009) benchmark and by manual calculations using fundamental concept of mechanics.

The temperatures used in the computer simulation were determined using analytical techniques in the form of various spreadsheets coded by the author. These heating scenarios were represented by temperature-time curves and heat release rate curves which were created using the provisions of Eurocode 1 Part 1-2. These curves served as the quantitative representation of the fire scenarios in the enclosure of arbitrary boundary dimensions and opening sizes. This could be seen as the performance-based approach to the problem because it was based on actual enclosure configuration. On the other hand, the use of the BS EN 1363-1 standard curve served as the prescriptive approach to the problem. The gap between these two approaches was bridged through the use of the concept of time equivalence.

Although several emissivity models were used, the determination of which is the best model is out of the scope of this study. Moreover, because the focus of this research is about the emissivity of steel, other thermal and mechanical properties were all taken from Eurocode 3 Part 1-2 for simplicity. Likewise, other heat transfer properties (mainly convective) other than radiative heat transfer were also taken from the same code. The author recognizes the fact that convective heat transfer varies according to the temperature. However, the simplification of using a single value of convective heat transfer were justified by de Ris (1979) and a study by

Sadiq et al. (2013) which showed that the effect of a varying convective heat transfer coefficient is only evident at temperatures lower than 300 °C.

2 REVIEW OF RELATED LITERATURE

2.1 Radiative Heat Transfer

2.1.1 The Nature of Thermal Radiation

Radiation is a mode of energy transfer through the emission of electromagnetic energy in the form of waves or particles and this transport requires no medium, i.e., it can travel through a vacuum (Halliday, Resnick, & Walker, 2011). There are several forms of radiation but for the purpose of fire safety engineering, thermal radiation is of particular interest. Thermal radiation is the energy emitted by matter due to its finite temperature (Incropera et al., 2007). Any matter radiates continuously due to the agitation of its atoms and molecules as a result of its internal energy which is proportional to its temperature at equilibrium state (Siegel & Howell, 1992).

Although all kinds of matter emit radiation, the behaviour differs according to the type of the material. Radiation from gases and semi-transparent solids such as glass is a volumetric phenomenon wherein the local emission of the particles is integrated throughout the whole volume (Incropera et al., 2007). On the other hand, radiation from most solids and liquids is a surface phenomenon wherein the radiation from the interior molecules are absorbed by the adjacent ones and the emission originates from the molecules within 1 μm from the exposed surface (Incropera et al., 2007). The radiative properties of gases is a function of the pressure, temperature, composition, and the presence of other particles such as soot and ash (Siegel & Howell, 1992). Conversely, the radiative properties of solids depend on the surface roughness and degree of polish, purity, thickness of coating, temperature, and wavelength and angle of radiation (Siegel & Howell, 1992).

The radiation emitted by a surface can be characterized by its spectral (pertaining to variation with respect to the wavelength) and directional (pertaining to variation with respect to the direction of propagation) distributions (Incropera et al., 2007). This is illustrated in Fig. 2-1. Due to the spectral and directional distribution of radiation, it is more convenient to refer to the related quantities as already integrated in all directions at all wavelengths. The definitions in this paragraph and the subsequent paragraph were all taken from Incropera et al. (2007). The rate by which radiant energy leaves a surface is called total emissive power E . A surface which emits the same intensity of radiation in all directions is called a diffuse emitter.

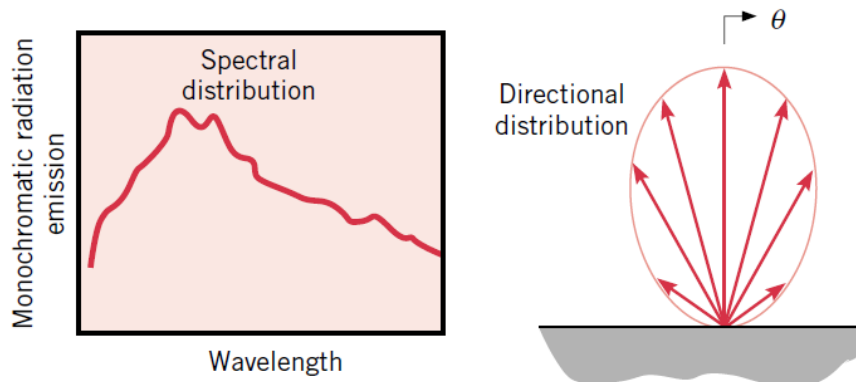


Figure 2-1. Spectral and directional distributions of radiation. Adapted from (Incropera et al., 2007).

The same concept applies to radiation coming to a surface which is termed as incident radiation. If total emissive power is the rate per unit area by which radiation leaves an emitting surface, the rate per unit area by which radiation is incident to a surface is called total irradiation G . Irradiation causes an increase in the temperature of the receiving surface which makes it emit radiation. However, a portion of the irradiation can also be reflected by the surface. The sum of the emission and reflection as a result of irradiation is called radiosity J .

2.1.2 The Blackbody Idealization

When a body receives radiation, some of it will be reflected, transmitted, and absorbed. An idealization of this body that perfectly absorbs all incident radiation is called a blackbody (Incropera et al., 2007; Siegel & Howell, 1992). Additionally, no surface can emit more energy than a blackbody at any given temperature and wavelength, and that this emitted radiation is directionally independent, i.e., it is a diffuse emitter (Incropera et al., 2007). Another property of a blackbody is that its total emitted radiation in a vacuum is a function only of the temperature, and this was verified by Planck's quantum arguments and other experiments (Siegel & Howell, 1992).

Planck's study led to the derivation of the Stefan-Boltzmann Law which allowed for the calculation of the total emissive power of a blackbody, E_b , just by knowing its absolute temperature (Incropera et al., 2007). In equation form,

$$E_b = \sigma T^4 \quad (2.1)$$

where σ is the Stefan-Boltzmann constant equal to $5.67 \times 10^{-8} \text{ W/m}^2\cdot\text{K}^4$ and T is the absolute temperature in K (Incropera et al., 2007).

2.1.3 Real Surface Radiation and its Related Assumptions

Because of the ideal properties of a blackbody, it serves as the reference for the behaviour of real surfaces. Therefore, a ratio of the radiation emitted by a surface to that of a blackbody at the same temperature can be defined. This surface radiative property is called emissivity ε (Incropera et al., 2007). However, the same as with other radiation quantities, it may also vary depending on the wavelength and direction of radiation. This can be seen in Fig. 2-2. Additionally, as the definition suggests, it is directly related to the temperature and this dependency is the backbone of this study.

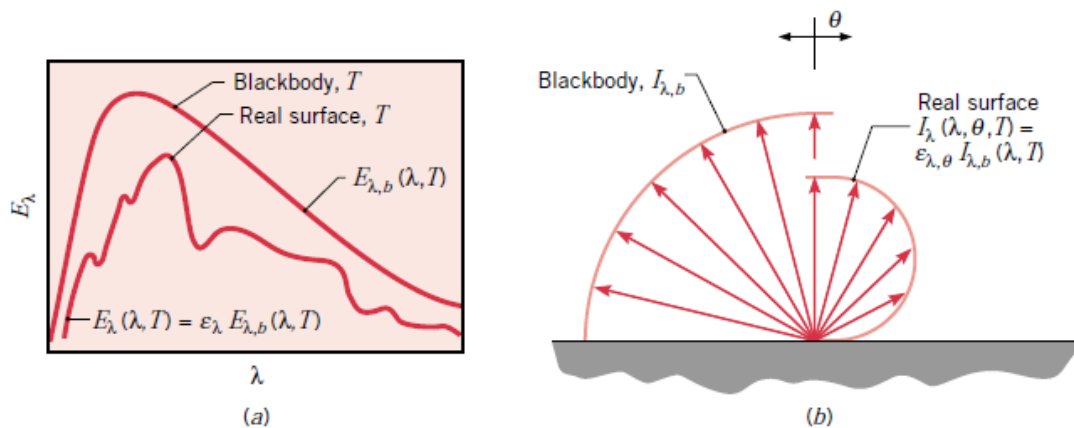


Figure 2-2. Spectral (a) and directional (b) emission of a blackbody and a real surface. Adapted from Incropera et al. (2007).

Portions of the irradiation being absorbed, reflected, and transmitted by the surface are influenced by properties called absorptivity α , reflectivity ρ , and transmissivity τ , respectively (Incropera et al., 2007). These properties are related by

$$\alpha + \rho + \tau = 1 \quad (2.2)$$

Most materials of construction are opaque such that they do not allow radiation to pass through them, in which case, $\tau = 0$. An exemption to this is glass, for example.

In an ideal isothermal enclosure, a material can only emit what it can absorb. This is known as the Kirchhoff's Law (Incropera et al., 2007) and can be simplified as

$$\varepsilon = \alpha \quad (2.3)$$

This has been proven true only when there is no net heat transfer in the surface which, nonetheless, is still a good approximation for actual surfaces. The validity of this approximation is based on experiments which shows that the surrounding radiation field has no significant

effect on the emissivity and absorptivity because the material can maintain local thermodynamic equilibrium in most instances (Siegel & Howell, 1992). Therefore, it is based not on a simplification of the problem but on actual material behaviour.

Another common assumption is that real surfaces acts as diffuse-grey bodies. Diffuse signifies that the absorptivity and emissivity are independent of the direction while grey signifies that both are independent of the wavelength (Siegel & Howell, 1992). This means that diffuse-grey bodies absorb a fixed fraction of the incident radiation and emit a fixed fraction of blackbody radiation for all directions and wavelengths (Siegel & Howell, 1992). Although a common assumption, it is essentially a simplification of a complex material behaviour especially the grey body part. A surface emits differently depending on the spectral region which means that this assumption only holds for certain regions in the spectrum (Incropera et al., 2007). Despite being a reasonable assumption for many practical applications, there should be caution on its use especially when there is a wide separation between the spectral regions of the irradiation and emission (Incropera et al., 2007).

2.1.4 Energy Balance for Radiation in a Surface

Unless otherwise specified, the following discussion is based on Mooney (1992). Given a source i and a surface j , the incident radiation or irradiation from the source to the surface, G_{i-j} , is defined below. The total irradiation from all possible sources to the surface j , G_j , is shown after.

$$G_{i-j} = F_{i-j}J_i \quad (2.4)$$

$$G_j = \sum_i F_{i-j}J_i \quad (2.5)$$

where F_{i-j} is the view factor and J_i is the radiosity coming from source i . The view factor is given below in equation form (Incropera et al., 2007) with the parameters illustrated in Fig. 2-3. Because of the complexity of the equation, several formulas can be found in literatures such as the SPFE Handbook and Karlsson & Quintiere (2000) to calculate the view factor which depends on the configuration of the source and the receiving surface.

$$F_{i-j} = \frac{1}{A_i} \int_{A_i} \int_{A_j} \frac{\cos \theta_i \cos \theta_j}{\pi R^2} dA_i dA_j \quad (2.6)$$

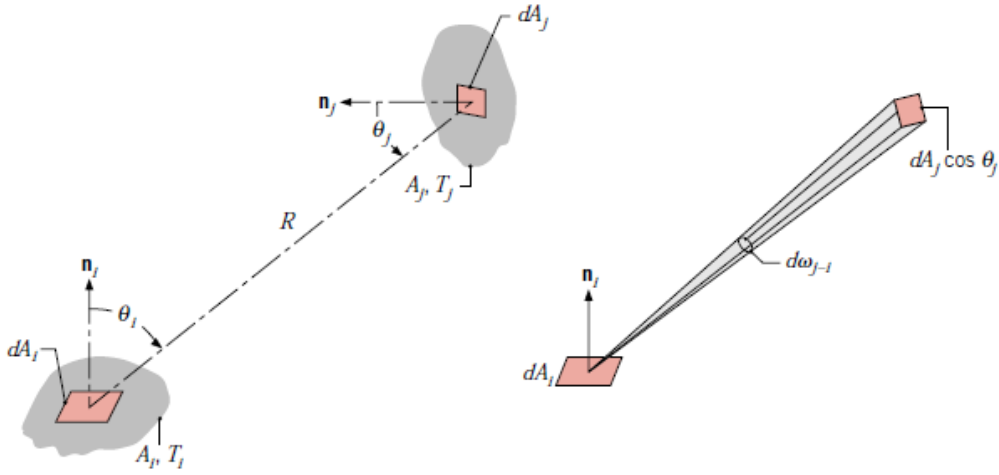


Figure 2-3. View factor between surfaces i and j . Adapted from Incropera et al. (2007)

The surface j absorbs a portion of the total irradiation which is equal to the absorptivity multiplied by the total irradiation. As a convention, any energy going to the surface is taken as positive and vice-versa. Applying the Kirchhoff's Law leads to the surface energy balance

$$E_{net,j} = \left(a_j \sum_i F_{i-j} J_i \right) - \varepsilon_j \sigma T_j^4 \quad (2.7)$$

$$E_{net,j} = \varepsilon_j (G_j - \sigma T_j^4) \quad (2.8)$$

where $E_{net,j}$ is the net energy in surface j and T_j is the absolute temperature of surface j . The first term of both equations represents the absorbed portion into the surface while the second term represents the emitted portion from the surface. Additionally, the radiosity J_i for which irradiation G_j depends is the sum of the emission and reflection coming from source i . This can be written as

$$J_i = \varepsilon_i \sigma T_i^4 + (1 - \varepsilon_i) G_i \quad (2.9)$$

where G_i is the irradiation to source i and T_i is the absolute temperature of source i .

2.1.5 Effect of Intervening Medium

The energy balance discussed in Subsection 2.1.4 can be considered as either radiation in a vacuum or the medium between the two surfaces is non-participating. However, in real life applications, the medium can absorb, scatter, and emit radiation. Combustion gases like H_2O and CO_2 can radiate only over certain bands of wavelength while soot radiates continuously

throughout the whole spectrum (Karlsson & Quintiere, 2000). Same as with real surfaces, the gases can be assumed to be grey such that their properties are independent of the wavelength, and that the Kirchhoff's Law also applies (Karlsson & Quintiere, 2000).

The absorptivity a_g and emissivity ε_g of a grey gas can be calculated using the equation

$$a_g = \varepsilon_g = 1 - e^{-\kappa_m L} \quad (2.10)$$

where κ_m is the effective absorption coefficient which depends on the type of fuel and L is the path length (Karlsson & Quintiere, 2000). A study by Hostikka (2003a) correlated the stoichiometric ratio η which determines the amount of air in the fire gases with the path length L and soot yield Y_s to determine the gas emissivity at different temperatures. Figure 2-4 illustrates the parameters needed for calculating the fire gas emissivity.

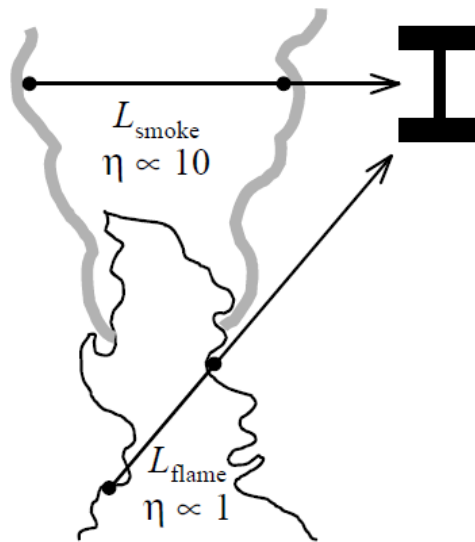


Figure 2-4. Schematic diagram for fire emissivity calculation. Adapted from Hostikka (2003a).

Another study by Guo-wei, Guo-qing, & Li-li (2014) stressed the important contribution of the smoke radiation to the thermal response of steel members in localized fires. A formula to calculate the smoke emissivity using the smoke temperature was introduced as adapted from Edwards & Matavosian (2009) which is expressed as

$$\varepsilon_g = 0.458 - 1.29 \times 10^{-4} (T_g - 273) \quad (2.11)$$

where T_g is the smoke temperature in °C.

In the case of a blackbody surface receiving radiation from a fire source, considering the effect of an intervening medium, i.e., smoke, the energy balance in the form of a radiant heat flux $Q''_{\text{net,rad}}$ can be represented as

$$\dot{Q}''_{net,rad} = \epsilon_g \sigma T_g^4 + (1 - \epsilon_g)[F_f \sigma T_f^4 + (1 - F_f) \sigma T_a^4] - \sigma T_s^4 \quad (2.12)$$

where F_f is the view factor from the fire source to the surface, T_f is the effective radiation temperature of the fire source in K, T_a is the ambient temperature in K, and T_s is the surface temperature in K (Karlsson & Quintiere, 2000). The first term is the smoke contribution, the second term is composed of the contributions from the fire source and the ambient surroundings, while the last term is the emission from the surface. The above equation does not consider reflection. As a result of this assumption, the factor $(1 - \epsilon_g)$ is equal to the gas transmissivity τ_g .

2.2 Temperature-dependent Emissivity

2.2.1 Factors Affecting the Radiative Properties of Metals

As established in Section 2.1, radiation in solids is a surface phenomenon. For metals, the emission of the generated radiant energy is due to the oscillations of the atoms/molecules located within a depth of 1000 Å in which the properties are influenced by the topographical, chemical and physical characteristics (Touloukian & DeWitt, 1970). Topographical characteristics describe the geometrical profile of the surface; chemical characteristics describe the surface layer composition such as inhomogeneities and contaminants; physical characteristics describe the surface structures such as crystal lattice orientation, particle size, and strain (Touloukian & DeWitt, 1970).

The topography of the surface, in simpler terms, corresponds to the surface roughness. The roughness, which can be visualized as irregular patterns of peaks and valleys, is commonly measured in terms of parameters such as root-mean-square height, centreline-average height, lay, average slope, and height distribution (Touloukian & DeWitt, 1970). A material surface is said to be optically smooth if the average length scale of surface roughness is less than the radiation wavelength (Modest, 2013). The root-mean-square height σ_h can be measured by using a profilometer which consists of a stylus that records the height fluctuations as it traverses across the surface (Modest, 2013). However, σ_h is an inadequate measure of surface roughness because it does not give information on other roughness parameter such as the average slope along the surface. This is illustrated in Fig. 2-5. Nonetheless, the effect of surface roughness to the radiative property has been studied based on the correlation between this parameter and the order of the wavelength λ . If σ_h is larger than λ , radiative interaction is governed by geometrical optics wherein the surface reflects radiation in various directions depending on the properties and orientation of the facets which can be described statistically

(Touloukian & DeWitt, 1970). Meanwhile, if σ_h is smaller than λ , the radiative interaction follows the diffraction phenomena leading to the assumption that the surface roughness has no effect on the total reflectance (Touloukian & DeWitt, 1970). Based on Eq. 2.2, it follows that for σ_h smaller than λ , the surface roughness has negligible effect on the total emittance and vice-versa.

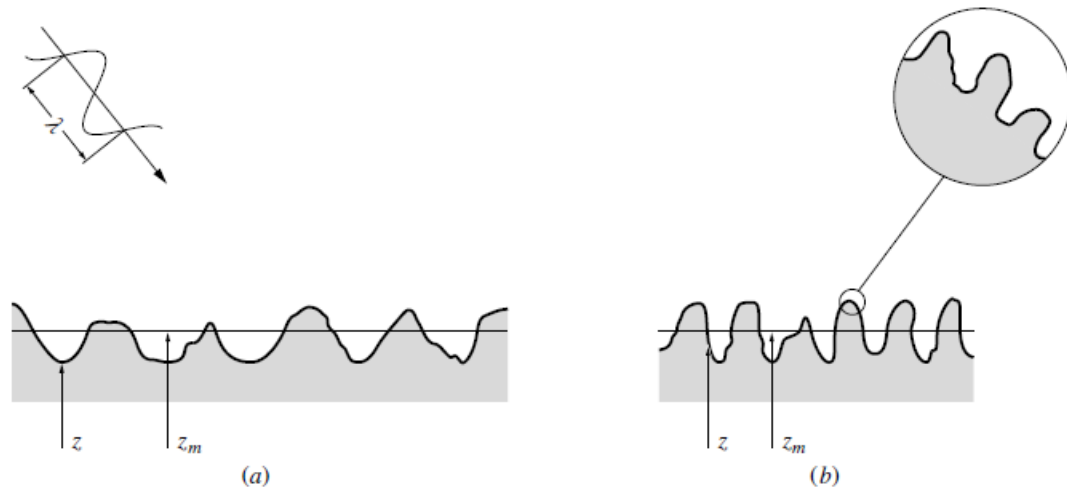


Figure 2-5. Topography differences in surfaces with equal σ_h : (a) gradual slopes, (b) steep slopes. Adapted from Modest (2013).

Chemical characteristics are based on the fact that any metal surface has a surface film which can either be deposits or oxides of the base metal (Touloukian & DeWitt, 1970). Examples of deposits are grease, dust, or soot. These thin films may be formed by chemical reaction such as oxidation, adsorption in the case of grease or water, and electrostatics in the case of dust particles (Modest, 2013). Metals, naturally, have high reflectance but the addition of a thin non-metallic film with low reflectance can significantly raise the emittance of the composite surface (Modest, 2013). In general, metals at room temperature forms an oxide film so thin that it has negligible effects on the radiative properties, but metals in high-temperature oxidizing environments have radiative properties similar to that of their oxide layer (Modest, 2013).

Physical characteristics corresponds to the structural feature of the surface layer. This feature may include adsorbed gas atoms, lattice imperfections, and crystallinity variations (Touloukian & DeWitt, 1970). Changes in the physical features are usually caused by surface damage during machining, heat-treating, cold-working, polishing, and other treatments for surface preparation (Modest, 2013; Touloukian & DeWitt, 1970). Because of this mechanical works, the properties of the surface differ from that of the bulk material. Evidence suggests that

a layer of supercooled fluid metal called Beilby layer fills the scratches due to abrasion, and that this layer is non-crystalline in the outermost portion and becomes more crystalline with increasing depth from the surface (Touloukian & DeWitt, 1970). Additionally, a polished layer is unstable and will eventually go back to the ordinary crystalline state (Touloukian & DeWitt, 1970).

2.2.2 Emissivity Models for Steel

Several studies had been performed which sought to find the emissivity value of steel. As discussed in Subsection 2.2.1, this value is not only a function of the material but also of the process and the environment in which it was exposed to. Despite of the huge variability, different emissivity models had been made to generalize this radiative property. These models can be categorized into two: spectral models and temperature-dependent models. Spectral models are usually given in terms of the wavelength and temperature. An example of a study about the spectral emissivity of different kinds of steel was done by Wen (2010). For elements exposed to fires, temperature-dependent models are more commonly used because of their convenience since the emissivity is given as the total emissivity and, therefore, is only a function of one variable which is temperature. Different temperature-dependent emissivity models are going to be discussed in the subsequent paragraphs.

Touloukian & DeWitt (1970) presented different constant and temperature-dependent emissivity values of iron. Although not the exact material, structural steel is almost entirely made up of iron with less than 0.25% carbon content (Subramanian, 2010). Therefore, it can be assumed that its properties are not going to differ a lot compared to iron. Touloukian & DeWitt (1970) performed a regression analysis on the different data that they presented for oxidized iron and the equation of the line of best fit is shown below.

$$\varepsilon = 0.173 + (68.6 \times 10^{-5})T - (25.6 \times 10^{-8})T^2 \quad (2.13)$$

where ε is the emissivity and T is the surface temperature in K.

Kay et al. (1996) calculated the heating of unprotected steel members in a standard fire resistance test. In their study, they enumerated and plotted several temperature-dependent emissivity values of dull oxidized mild steel from different studies. Due to the scatter in their plot, the author of this study removed outlier values based on the knowledge that emissivity of metals increases with increasing temperature. The final set of equations by Kay et al. (1996) as amended by the author is given as

$$\varepsilon = 0.79 \quad T < 260 \text{ } ^\circ\text{C} \quad (2.14)$$

$$\varepsilon = 0.0009T + 0.5579 \quad 260 \text{ } ^\circ\text{C} \leq T < 316 \text{ } ^\circ\text{C} \quad (2.15)$$

$$\varepsilon = 0.00005T + 0.8228 \quad 316 \text{ } ^\circ\text{C} \leq T < 500 \text{ } ^\circ\text{C} \quad (2.16)$$

$$\varepsilon = 0.0006T + 0.55 \quad 500 \text{ } ^\circ\text{C} \leq T < 650 \text{ } ^\circ\text{C} \quad (2.17)$$

$$\varepsilon = -0.0004T + 1.2289 \quad 650 \text{ } ^\circ\text{C} \leq T < 740 \text{ } ^\circ\text{C} \quad (2.18)$$

$$\varepsilon = -0.0001T + 0.9974 \quad 740 \text{ } ^\circ\text{C} \leq T < 816 \text{ } ^\circ\text{C} \quad (2.19)$$

$$\varepsilon = -0.0054T + 5.31 \quad 816 \text{ } ^\circ\text{C} \leq T \leq 840 \text{ } ^\circ\text{C} \quad (2.20)$$

$$\varepsilon = 0.76 \quad T > 840 \text{ } ^\circ\text{C} \quad (2.21)$$

Bentz et al. (2009) performed experiments on bare steel column sandblasted with silica to remove the oxide layer in the surface. Cube samples were taken from the column and the reflectance was measured at room temperature giving an emissivity of 0.85 which is in good agreement with the data provided by Kay et al. (1996). Further advanced testing was done to measure the emissivity by extracting cylindrical disks from the cubes and subjecting them to a Fourier transform spectrometer source. Measurements at room temperature were taken using Reference Infrared Integrating Sphere Reflectometer (RIISR) while measurements at elevated temperatures were taken using Infrared Spectral Emittance Measurement (ISEM) apparatus. The measured emissivity values as a function of the temperature is expressed as

$$\varepsilon = 0.32 \quad T < 200 \text{ } ^\circ\text{C} \quad (2.22)$$

$$\varepsilon = 0.0026T - 0.19 \quad 200 \text{ } ^\circ\text{C} \leq T < 400 \text{ } ^\circ\text{C} \quad (2.23)$$

$$\varepsilon = 0.0003T - 0.71 \quad 400 \text{ } ^\circ\text{C} \leq T \leq 800 \text{ } ^\circ\text{C} \quad (2.24)$$

$$\varepsilon = 0.95 \quad T > 800 \text{ } ^\circ\text{C} \quad (2.25)$$

It was found that, at a temperature equal to 400 °C, the measured emissivity agrees with the emissivity of oxidized steel. This means that the process of oxidation happens when steel is exposed to this temperature.

Drysdale (2011) provided a range of values for the emissivity of polished steel which is shown below.

$$\varepsilon = 0.14 \quad T < 425 \text{ } ^\circ\text{C} \quad (2.26)$$

$$\varepsilon = 0.0004T - 0.03 \quad 425 \text{ } ^\circ\text{C} \leq T \leq 1025 \text{ } ^\circ\text{C} \quad (2.27)$$

$$\varepsilon = 0.38 \quad T > 1025 \text{ } ^\circ\text{C} \quad (2.28)$$

The relatively low values of emissivity are noticeable. This is due to the high reflectance of polished steel. Therefore, this model can be used to represent steel which is shinier than normal oxidized steel.

Sadiq et al. (2013) determined the emissivity of carbon steel using a furnace and an infrared camera. This study is similar to a study done by Paloposki & Liedquist (2005) but with modifications and improvements in the test setup. In the older study, thermocouples were used to measure the temperature of the furnace walls, air around the specimen, and the specimen itself. The temperature inside the furnace was maintained first before swiftly inserting the samples. This caused a slight disturbance in the thermal equilibrium inside the furnace and because of this limitation, no reliable data could be taken at temperatures below 150 °C. This was improved in the newer study by placing the sample inside the furnace before the start of the experiment and simultaneously monitoring the evolution of the temperature inside the furnace and of the sample without disturbance. The temperature-dependent emissivity as reported by (Sadiq et al., 2013) is expressed as

$$\varepsilon = 0.28 \quad T < 380 \text{ } ^\circ\text{C} \quad (2.29)$$

$$\varepsilon = 0.0029T - 0.8329 \quad 380 \text{ } ^\circ\text{C} \leq T \leq 520 \text{ } ^\circ\text{C} \quad (2.30)$$

$$\varepsilon = 0.69 \quad T > 520 \text{ } ^\circ\text{C} \quad (2.31)$$

Note that Eq. 2.30 was slightly modified by the author of this study so that the formula agrees with the bounding values. Similar to the findings of Bentz et al., (2009), it was also found that there was a sudden change in the emissivity of the samples at 400 °C which they attributed to the oxidation and change in the surface roughness of the samples.

Jiang et al. (2018) investigated the thermal performance of composite slabs with steel deck exposed to fire. The emissivity model was from a modified version based on a study done by Hamerlinck et al. (1990). The modification was based on the result of the computer simulation performed by Jiang et al. (2018) which showed that changing the upper bound of the Hamerlinck et al. (1990) model gave better temperature values in comparison to experimental results. The major difference of this model compared to the previously discussed models is the material. Steel deck is made of galvanized steel which is a steel with a thin layer of zinc applied to prevent corrosion (Hamerlinck et al., 1990; Jiang et al., 2018). Because of this coating, the emissivity of galvanized steel is relatively low at low temperatures which is almost the same as that of polished steel. Despite that, it was deemed appropriate as a steel emissivity model because this zinc coating starts to crack and peel off the surface at temperatures higher than 250 °C (Duran, 2013) and melts at temperatures of around 400 to 500 °C (Hamerlinck et

al., 1990). This means that at temperatures that are characteristic of a fire, it can be assumed to behave in the same way as normal steel. The Jiang et al. (2018) model is given as

$$\varepsilon = 0.1 \quad T < 400 \text{ } ^\circ\text{C} \quad (2.32)$$

$$\varepsilon = 0.0015T - 0.5 \quad 400 \text{ } ^\circ\text{C} \leq T \leq 800 \text{ } ^\circ\text{C} \quad (2.33)$$

$$\varepsilon = 0.7 \quad T > 800 \text{ } ^\circ\text{C} \quad (2.34)$$

The emissivity models discussed above were put into one graph and shown in Fig. 2-6. These models will be used in further analyses to find the effect of varying the emissivity of steel as a function of temperature to the thermomechanical response of steel members.

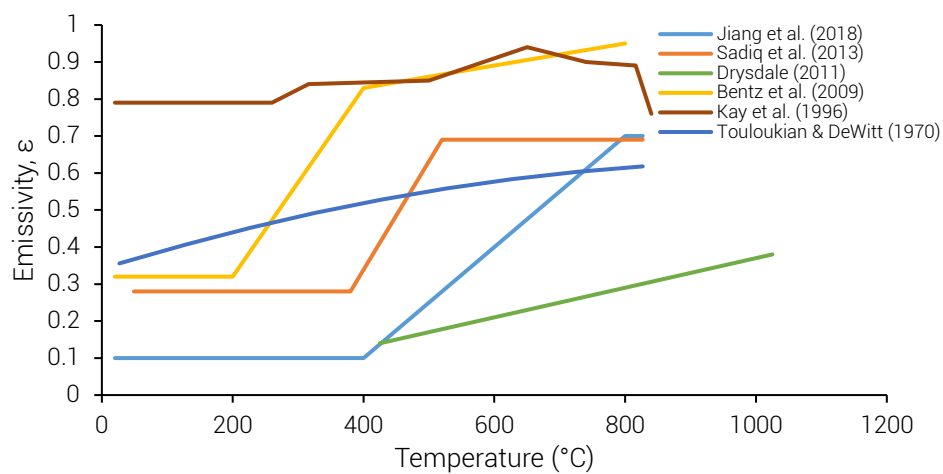


Figure 2-6. Temperature-dependent emissivity models.

2.3 Survey of Building Codes About Fire-Exposed Steel Structures

The procedure in designing structural elements for any type of load varies according to a country/region which has different sets of codes and guidelines. In structural fire engineering, despite the universally accepted physics of fire dynamics and heat transfer, the design approach still differs because of the complexity of the fire phenomenon. Nonetheless, these approaches are founded on the fundamental goals of fire safety engineering: safety of lives, properties and the environment. Because building codes guide engineers on proper fire safety solutions, it is but necessary to review their provisions. A similar but more extensive survey of building codes from selected countries/regions around the world was performed by Duthinh (2014) from which this section took inspiration from. However, this study focused more on provisions related to steel structures under fire exposure.

2.3.1 Europe: Eurocode

Inarguably the most comprehensive performance-based code in the world is the Eurocode. Eurocode 1 Part 1-2 (CEN, 2002b) consists of provisions related to the treatment of fire as a structural load. The following are the requirements to limit fire risks as stated by CEN (2002b):

The construction works must be designed and built in such a way, that in the event of an outbreak of fire

- the load bearing resistance of the construction can be assumed for a specified period of time,
- the generation and spread of fire and smoke within the works are limited,
- the spread of fire to neighbouring construction works is limited,
- the occupants can leave the works or can be rescued by other means,
- the safety of rescue teams is taken into consideration. (p. 7)

The design procedure is as follows: selection of the design fire scenarios through fire risk assessment, representation of the design fire using temperature-time and/or heat release rate curves, calculation of the time-based temperature of the structural member, and determination of the mechanical response as a result of the temperature changes in the member. The code has provisions for both nominal fire curves such as the ISO 834 standard curve, external fire curve, and hydrocarbon curve, and natural fire models which include the parametric temperature-time curve, localized fire model and advanced fire models. It also includes the calculation procedure for the heat flux to be imposed to the surface of the member.

For the purpose of this study, the net radiative heat flux $\dot{Q}''_{net,rad}$ as calculated using Eurocode 1 Part 1-2 is expressed as

$$\dot{Q}''_{net,rad} = F_f \varepsilon_s \varepsilon_f \sigma (T_r^4 - T_s^4) \quad (2.35)$$

where F_f is the view factor between the fire and the surface, ε_s is the surface emissivity of the member, ε_f is the fire emissivity, σ is the Stefan-Boltzmann constant ($5.67 \times 10^{-8} \text{ W/m}^2 \cdot \text{K}^4$), T_r is the effective radiation temperature of the fire environment in K, and T_s is the surface temperature of the member in K. For members engulfed by the fire, the gas temperature around the member can be used as T_r . However, no other suggestions are given for other heating scenarios such as a localized fire. Additionally, a generalized value of $\varepsilon_f = 1$ is suggested, and guidance is only provided for the calculation of ε_f for members external to the compartment.

Hostikka (2003b) pointed out that the above equation is inherently erroneous because of the following reasons: the view factor and the fire emissivity are multiplied to both the incoming and outgoing terms, and no instructions are provided to account for other radiation sources apart from the fire. It was stated that the more suitable form of Eurocode 1 Part 1-2 Eq. 3.3 where Eq. 2.35 was based should be

$$\dot{Q}''_{net,rad} = \varepsilon_s \sum_i F_{f,i} \varepsilon_{f,i} \sigma T_i^4 - \varepsilon_s \sigma T_s^4 \quad (2.36)$$

where $F_{f,i}$ is the view factor between source i and the surface, $\varepsilon_{f,i}$ is the emissivity of source i , and T_i is the effective radiation temperature of source i in K. Furthermore, for practical applications, a simplified version with the source term consisting of the 'fire' term and 'rest of the visible world' term was also given which is expressed as

$$\dot{Q}''_{net,rad} = F_f \varepsilon_s \varepsilon_f \sigma T_r^4 + (1 - F_f) \varepsilon_s \varepsilon_a \sigma T_a^4 - \varepsilon_s \sigma T_s^4 \quad (2.37)$$

where ε_a is the emissivity of the ambient surroundings and T_a is the ambient temperature in K. Assuming $\varepsilon_a = 1$ and $T_a = 293\text{ K}$ gives reasonable estimates of $\dot{Q}''_{net,rad}$ (Hostikka, 2003b). This study, however, suggests a modified version of Eq. 2.12 by removing the blackbody assumption and introducing the actual emissivity values of the different terms. This equation is as follows,

$$\dot{Q}''_{net,rad} = \varepsilon_s \varepsilon_g \sigma T_g^4 + (1 - \varepsilon_g) [F_f \varepsilon_s \varepsilon_f \sigma T_r^4 + (1 - F_f) \varepsilon_s \varepsilon_a \sigma T_a^4] - \varepsilon_s \sigma T_s^4 \quad (2.38)$$

where ε_g is the emissivity of the intervening medium such as smoke, and T_g is the smoke temperature in K. Although Eq. 2.38 is better than Eq. 2.37, both equations neglect reflection for simplicity.

On the other hand, Eurocode 3 Part 1-2 (CEN, 2005b) discusses the temperature-dependent material properties of steel and the procedure in designing steel structures exposed to fire. The only mention of a radiation-related concept is the emissivity value of steel which, unlike other material properties, stays constant throughout the duration of a fire. CEN (2005) reported that steel has an emissivity of 0.7.

2.3.2 USA: International Building Code 2018

The International Building Code or IBC was developed by the International Code Council which provides "minimum requirements to safeguard the public health, safety and general welfare of the occupants of new and existing building and structures" (ICC, 2017)*. In terms of

*Page unknown because the reference was taken from the 'Free View' version by ICC.

fire safety, the code provisions which can be found in IBC 2018 Chapter 7 details a prescriptive approach where the fire resistance rating of structural elements is determined using the procedures set by ASTM E119 (ASTM International, 2012). This rating is then compared to the code requirements depending on the construction classification and structural element type according to IBC 2018 Table 601.

IBC 2018 Section 721 also provides guidance for the minimum thickness of the insulation to structural elements depending on the type of insulating material and time period of fire resistance needed by the structural element. Conversely, IBC 2018 Section 722 details a guideline for the calculated fire resistance rating of structural elements depending on the material and thickness of the insulation. This is based on the ASCE 29-05 standard (ASCE, 2005). Meanwhile, IBC 2018 Chapter 16 does not provide any guidance on how to treat fire as a structural load.

Because of these reasons, the prescriptive method of IBC 2018 does not consider the phenomenon of heat transfer—even more so radiation—to compare the calculated rating to the experimental rating. However, IBC 2018 Section 104 stipulated the use of alternative methods approved by the building official which gives freedom to the designer.

2.3.3 New Zealand: New Zealand Building Code

The New Zealand Building Code or NZBC is stated in Schedule 1 of the Building Regulations 1992 (MBIE, 1992). It consists of clauses which state the objectives, functional requirements and performance indicators of buildings. Clauses B1 and B2 are for general building stability, while clauses C1 to C6 are for fire safety. These clauses have corresponding Acceptable Solutions (AS) and Verification Methods (VM) which are referenced standards used to guide the designer and fulfil the provisions of the code. These are also published by the same authority responsible for the NZBC. However, when the structure is complex and compliance to the code departs AS or VM, performance-based Alternative Solutions can be used.

Although explicitly for fire safety, especially C6 or the 'structural stability' clause, the AS for clauses C1 to C6 provide the fire resistance rating (FRR) depending only on the risk group (occupancy of the building). Meanwhile, clause B1 or the "structure" clause refers to the New Zealand Standard or NZS 3404: Part 1: 2009 for the design of steel structures (NZS, 2009). It was found that Part 5 of the said standard is still unavailable as of the writing which means that NZS 3404: Part 1: 1997 Section 11 (NZS, 1997) still applies.

NZS 3404: Part 1: 1997 Section 11 states that the period of structural adequacy (PSA) should be at least equal to the FRR. The PSA can be calculated using three methods. The first is by finding the limiting temperature of the steel using the ratio of the design capacity under fire conditions to the design capacity in room temperature, and then determining the time at which the limiting temperature is attained which depends on whether the structural member is protected or not. The second is by using the standard fire test. The third is by structural analysis with temperature-dependent material properties where the temperature of the steel is obtained using rational method of analysis. Only the temperature variation of the yield stress and modulus of elasticity are provided by the standard.

The discussion above shows that the NZBC also has provisions for both prescriptive and performance-based approach to structural fire design. Moreover, the last method for finding the PSA implicitly states the relevance of adequate modelling of heat transfer to the structural elements.

2.3.4 Australia: National Construction Code 2019

The National Construction Code or NCC is a performance-based code developed by the Australian Building Codes Board which "sets the minimum required level for the safety, health, amenity, accessibility and sustainability of certain buildings" (ABCB, 2019, p.9). Volumes 1 and 2 makes up the Building Code of Australia while Volume 3 is the Plumbing Code of Australia. Volume 1 is for multi-residential, commercial, industrial, and public buildings while Volume 2 is for residential and non-inhabitable structures. However, the two volumes have a similar approach. The code works by meeting the Performance Requirements (PR) using either a Performance Solution (PS) or a Deemed-to-Satisfy Solution (DTS).

NCC 2019 Volume 1 Section C details the PRs for the general fire resistance of buildings. Part C1 enumerates the conditions for which a DTS or PS satisfies these PRs. An appropriate DTS depends on the type of fire-resisting construction required which is based on the class of the buildings and the number of storeys. Then a structural element is given a fire resistance level (FRL), which is the amount of time in minutes corresponding to the fire resistance in terms of structural adequacy, integrity, and insulation, in accordance with Specification 1.1 based on the determined type of construction. Once the FRL is known, Schedule 5 of the code provides different methods to achieve it—either by using Table 1 of the Schedule which indicates the minimum required thickness of the insulation, subjecting the element to a standard fire test in accordance to Australian Standard or AS 1530.4:2014 (AS, 2014), designing the element in

accordance to AS 4100-1998 (AS, 1998), or calculating the FRL using the standard fire curve and an appropriate analysis method that takes into account the temperature reached by the element and its effect on the strength and elastic modulus, the support conditions, and the design load. It should be noted that the Australian Standards and the New Zealand Standards for steel structures are identical to each other.

On the contrary, although the code gives a guideline on how to use a PS, it is generic, and freedom is given to the designer as long as the PRs are met and it is at least equivalent to the DTS Provisions. For these reasons, it can be concluded that the NCC 2019 implicitly considers the heat transfer phenomenon which is largely dependent on the method of analysis used by the designer.

2.3.5 Japan: Building Standard Law

Because of the unavailability of the actual Building Standard Law or BSL, this section was based on the supplementary document to the BSL by Hasegawa (2013). Enacted in 1950, the BSL provides "minimum standards concerning the site, construction, equipment, and use of buildings...to contribute to the furtherance of the public welfare" (Hasegawa, 2013, p. 21). Buildings must be having fire-resistive principal building parts which are designed either by meeting the prescriptive performance criteria, fire resistance verification method or advanced verification method which needs the Minister's approval.

The first method of meeting the criteria of fire-resistive performance means that structural elements must not deform, melt, crack, or undergo damage that is detrimental to the structure during the heating time which is based on the storey number and the type of element. The second method is based on technical standards wherein the calculated heat-withstanding period must be longer than the fire duration. The last method makes use of any approach not issued by the government but evaluated by a designated body using a manual approved by the Minister. The BSL, therefore, implicitly considers heat transfer in its methods.

2.3.6 Hong Kong: Code of Practice for Fire Resisting Construction 1996

The Code of Practice for Fire Resisting Construction or CPFRC was developed by the Building Authority with the objective to state the "provisions for the protection of buildings from the effects of fire by inhibiting the spread of fire and ensuring the integrity of the structural elements of buildings" (Building Authority, 1996, p. 1). It has two approaches to fire safety. The

first is by using prescriptive provisions given by the code and the second is by using an alternative approach assessed by the Building Authority against a set of reference criteria.

All structural elements in the building should have a fire resistance period (FRP) based on the class and compartment volume as stipulated in CPFRC 1996 Table 3. Additionally, the FRP is deemed to satisfy the provisions if the minimum thickness of insulation is provided as required by CPFRC 1996 Tables A to F, or by testing in accordance to BS 476 (BSI, 2009) and comparing it to the required FRP. In conclusion, this code implicitly recognizes heat transfer in fire safety via its alternative approach.

2.3.7 India: National Building Code of India 2016

The National Building Code of India or NBCI was developed by the Bureau of Indian Standards (BIS, 2016). The provisions for structural fire design can be found in NBCI 2016 Section 6(s). The provisions of this code are the same as the AS 4100-1998 because this section of the code was taken from Indian Standard or IS 800:2007 (BIS, 2007) where the Australian standard was referenced. This means that the Indian approach to fire safety of steel structures is the same as the Australian or New Zealand approach where the heat transfer phenomenon is not explicitly stated.

2.3.8 Singapore: Code of Practice for Fire Precautions in Buildings 2018

The Code of Practice for Fire Precautions in Buildings or CPFPB was developed by the Singapore Civil Defence Force to "ensure that fire safety standards keep pace with Singapore's evolving urban landscape and national development" (SCDF, 2018, p. C). The code requires the structural elements to have a fire resistance rating not lower than those stated in CPFPB Table 3.3A which depends on the purpose of the building, the maximum dimensions, and the location of the compartment along the height of the building. CPFPB Annex 3A provides a deemed-to-satisfy solution to this based on the minimum thickness of the insulation applied to the steel member.

Additionally, the fire resistance rating can also be determined using BS 476 (BSI, 2009) which should not be less than the performance criteria of stability, integrity and insulation as required by CPFPB Table 3.4A. The two stated methods are prescriptive approaches. The performance-based approach is detailed in another supplementary document called the

Singapore Fire Safety Engineering Guidelines or SFEG developed to meet the objectives of the CPFPB (SCDF, 2015). This means that the code does not directly consider heat transfer.

2.3.9 Philippines: National Structural Code of the Philippines 2015

The National Structural Code of the Philippines or NSCP was developed by the Association of Structural Engineers of the Philippines to “provide minimum requirements for the design of buildings, towers and other vertical structures, and minimum standards and guidelines to safeguard life or limb, property and public welfare...” (ASEP, 2015, p. 1-2). The provisions for the design of steel buildings were adapted from the American Institute of Steel Construction Manual (AISC, 2005).

The code enumerated two methods of design: engineering analysis and qualification testing. Design by engineering analysis makes use of the design fires and temperature-dependent mechanical properties of steel such as elastic modulus, yield stress, and ultimate stress. The design fires can be localized fire, post-flashover compartment fire, and exterior but the code did not provide any method of modelling them. The National Building Code of the Philippines or NBCP (DPWH, 1972) and the Fire Code of the Philippines or FCP (BFP, 2003) also have no provisions for it. This means that the method is based on the discretion of the designer upon the approval of the building official. On the other hand, design by qualification testing uses the provisions of ASTM E119 (ASTM International, 2012).

The code, therefore, has provisions for both prescriptive and performance-based approach. However, a clearer but very simple prescriptive approach can be found in the NBCP in which the fire rating is based solely on the type of construction. In essence, the NSCP does not explicitly consider heat transfer in its provisions.

2.3.10 Summary

It was found that the Eurocode is the most advanced building code compared to the other selected codes. Despite a major error in one of its formulations and the lack of suggestions for cases other than for members fully-engulfed in a fire, it explicitly considers the phenomenon of heat transfer in its provisions which is one of the major steps in proper structural fire design. On the contrary, other codes failed to present methods on how to treat heat transfer and mostly rely on prescriptive approach of matching the required fire resistance rating based on at least one of the following criteria—usage or occupancy of the building,

dimensions of the building, type of element, number of storeys, and volume of the compartment—with deemed-to-satisfy solutions such as obtaining the rating based on standard fire tests, and applying insulation of a certain thickness to the member.

The prescriptive approach is problematic in the sense that designers are applying the same fire safety strategies for buildings that may fall within the same classification but completely different in terms of geometry, configuration, and complexity. It does not capture what structural members are actually exposed to in a fire. The building codes recognize this dilemma with play-safe provisions on the implementation of a performance-based design. Essentially, the job of finding a suitable technique is passed onto the designer. These codes, which should serve as ultimate guides to designers, should instead suggest and/or recognize even at least a method complete with models for the design fire, heat transfer, and structural response, albeit being open to other possible methods and thereby allowing designers to use their engineering judgments. This is where other codes fall short compared to the Eurocode.

3 METHODOLOGY

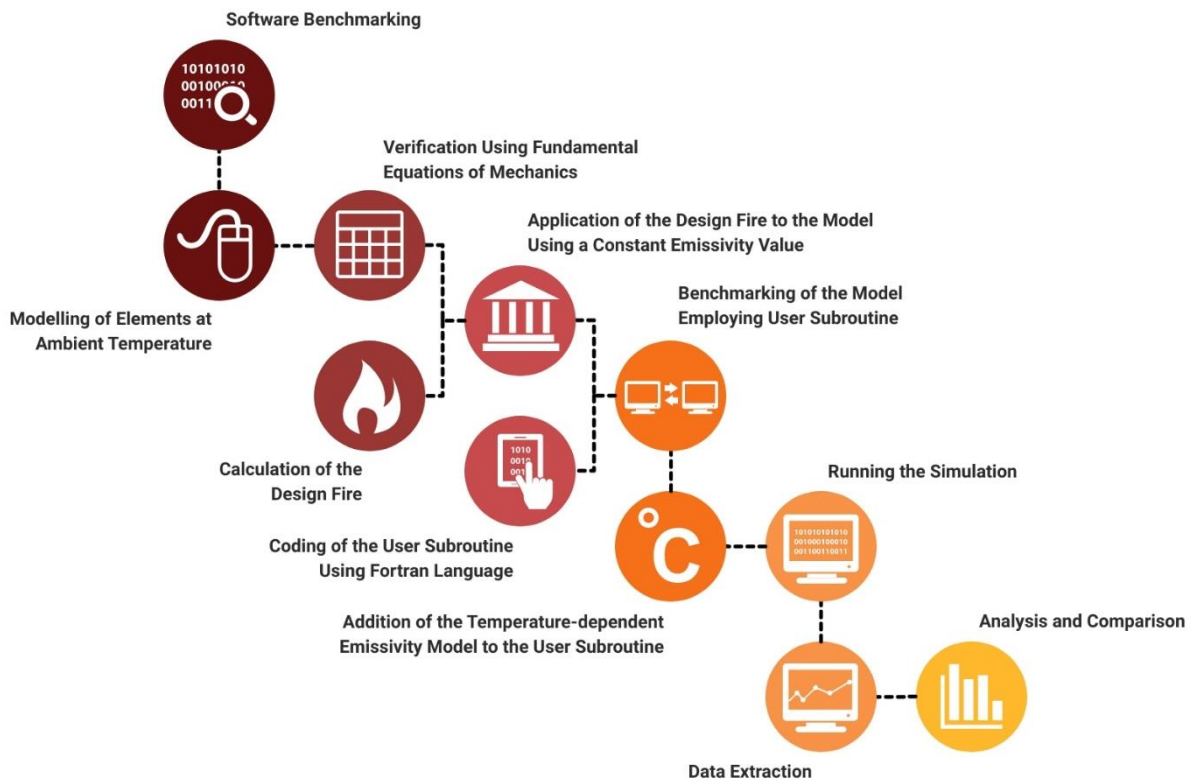


Figure 3-1. Methodological framework.

3.1 General Description

The methodological framework of this study is shown in Fig. 3-1. The methodology can be split into two major parts: manual calculation and computer simulation. All inputs to the finite element model were calculated from spreadsheets coded by the author. A compartment of arbitrary size and occupancy containing the structural elements, i.e., beams and columns, was selected. The mechanical and thermal loads according to the specifications of the compartment were calculated before a computer model of the structural elements with static loads referred here as 'static model' were made using the finite element analysis software Abaqus/CAE 2018.

Before modelling the elements, software verification was first done using the Gillie (2009) benchmark. After the simulation of the statically loaded members, manual calculation of loads and stresses was performed to verify the accuracy of the results. Thermal loads were then added to the static model, and simulation was done using a constant emissivity. This model was called the 'thermal benchmark model'. Because of the limitations of the software to

model temperature-dependent emissivity, user subroutines were coded using the Fortran language. A user subroutine is a code used to command a software to do specific tasks. To verify the equations used in the user subroutine, simulation of the structural elements was done by employing user subroutines with constant emissivity. The results for each structural element were then compared to their respective thermal benchmark model.

After verifying the user subroutine, the temperature-dependent emissivity models as discussed in Subsection 2.2.2 were added. The simulation was run and data points were extracted after the completion of the simulation. Analysis of the results was then performed which will be shown in Chapter 4.

3.2 Design Scenario

The compartment is at the ground floor of a two-storey concrete office building with two openings: a door and a window. The sketch of the perspective view and the framing plan of the compartment along with the dimensions can be seen in Fig. 3-2. The beam extensions were put to indicate that the compartment is part of a bigger structure and the slab on top of the frame was hidden on purpose. The total load in the slab including self-weight is 9.4 kPa; causing a 15-kN/m uniform load in the beam and an 85-kN concentrated load in the column. The compartment has a fuel load density of 450.8 MJ/m². Appendix A shows the calculation of the design loads based on Eurocode 0 and Eurocode 1 Part 1-1 (CEN, 2002a, 2002c).

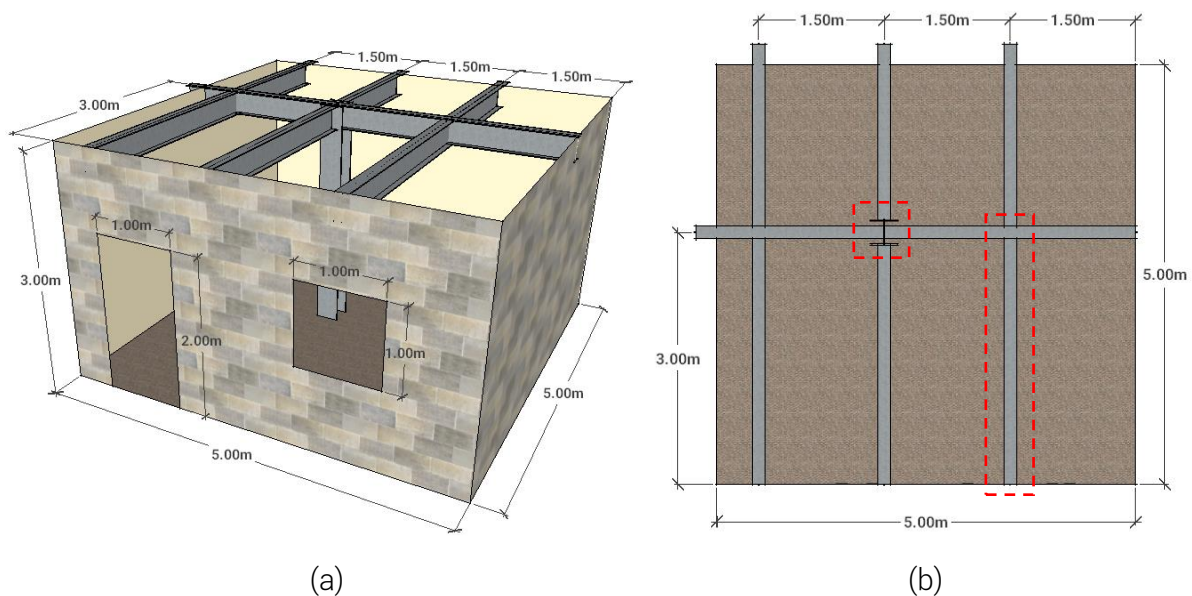


Figure 3-2. Sketch of the compartment: (a) perspective view and (b) framing plan. Highlighted in red are the structural elements being investigated.

3.3 Fire Curves

The structural members were subjected to two general cases of heating: uniform and localized. Uniform heating happens in a fully-developed fire where the gas temperature is the same throughout the compartment and, therefore, all exposed surfaces of the member are subjected to the same heat flux. Localized heating happens when there is varying heat flux throughout the member. For uniform heating, the parametric temperature-time curve and ISO 834 standard fire curve were used. For localized heating, the localized fire curve was used.

3.3.1 Case 1: Uniform Heating

Using the dimensions, boundary material properties, and fire load density of the compartment, the parametric temperature-time curve was determined based on Annex A of Eurocode 1 Part 1-2 (CEN, 2002b). To get the equivalent ISO 834 standard fire curve, Annex F of Eurocode 1 Part 1-2 was used. This method is similar to the time equivalence method discussed by Thomas, Buchanan, & Fleischmann (2008). It was stated that because of the dependence of radiation to the fourth power of the absolute temperature, a short-duration fire with a higher temperature is more severe than a long-duration fire with a lower temperature even if it has the same area as the temperature-time curve. The two temperature-time curves representative of a fully developed fire in the compartment is shown in Fig. 3-3. Appendix B shows parameters used to construct these curves using the material properties taken from Karlsson & Quintiere (2000).

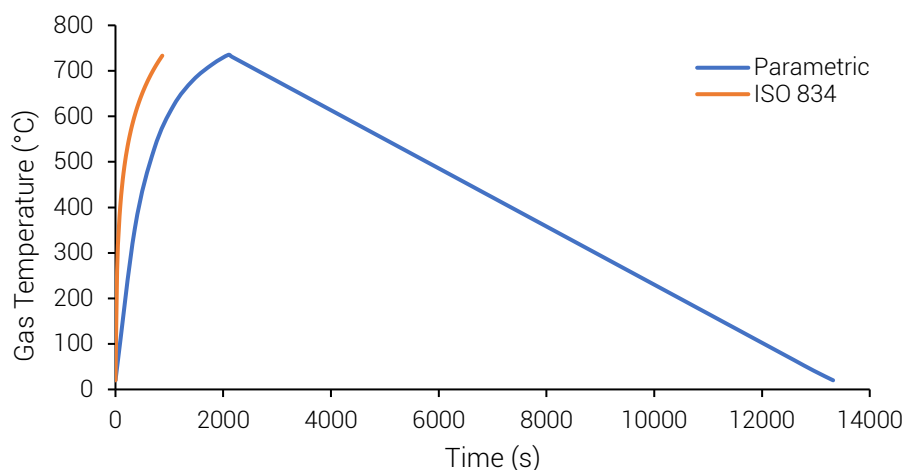


Figure 3-3. Temperature-time curves of a fully-developed fire in the compartment.

3.3.2 Case 2—Scenario 1: Column Fully Engulfed in the Localized Fire

In the case of a localized fire, instead of a temperature-time curve, a heat release rate curve was constructed based on Annex C of Eurocode 1 Part 1-2 using the same fire load density and assuming that the fuel has a diameter of 1 m. This curve superimposed with the flame height is shown in Fig. 3-4. Appendix C shows the design parameters for the calculation of the heat release rate and flame height.

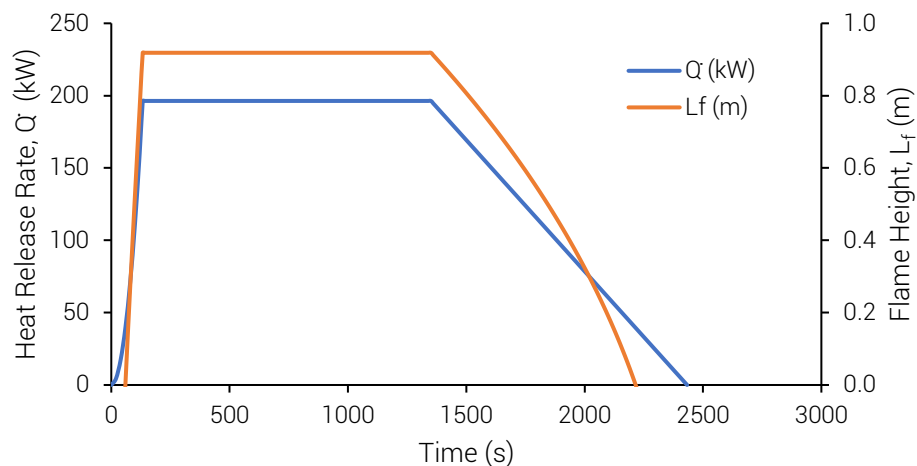


Figure 3-4. Heat release rate curve and flame height as a function of time for the localized fire.

This curve was used for three different localized fire scenarios. The first scenario is a column fully engulfed in the fire. The temperature along the plume corresponding to the mid-heights of the discretized column were calculated using Annex C of Eurocode 1 Part 1-2 and graphed in Fig. 3-5.

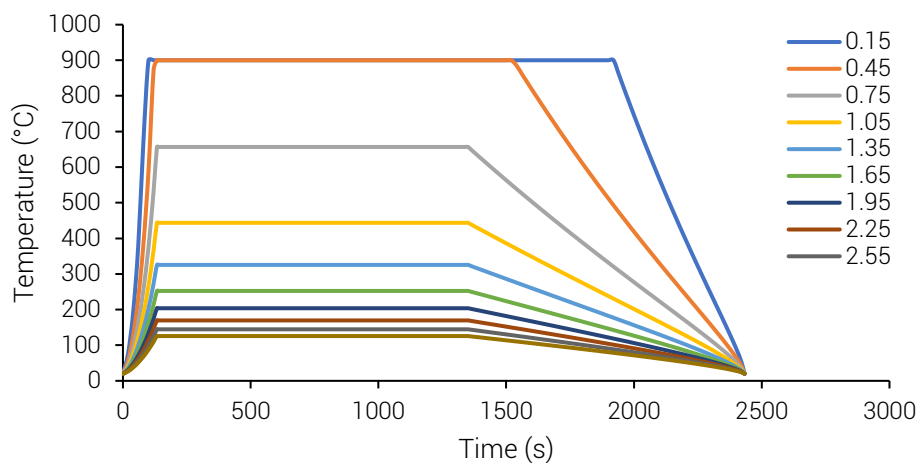


Figure 3-5. Temperature-time curve along the height of the column fully engulfed in the localized fire. The legend corresponds to the height from the floor in m.

3.3.3 Case 2—Scenario 2: Column at a Distance from the Localized Fire

The second scenario is a column at a distance from the fire. It does not include the effect of smoke accumulation in the ceiling to simplify the problem due to the difficulty of finding a model that considers the radiation to the surfaces not engulfed by the smoke. The distance from the centre of the fuel to the exposed flange of the column is 1 m. Because no guidance was provided by Eurocode 1 Part 1-2 for a fire away from the element, the method by Shokri & Beyler was used (Beyler, 2016). This method assumes that the fire is a “cylindrical, blackbody, homogenous radiator with an average emissive power” (Beyler, 2016, p. 2606). It uses a formula for finding the view factor of a differential area, which can either be horizontally or vertically oriented, located at a distance from the centre of the cylinder. For complex configurations, the view factor can be determined using view factor algebra. The incident radiant heat flux \dot{Q}''_{rad} in kW/m² is expressed as

$$\dot{Q}''_{rad} = 58 \cdot (10^{0.00823D}) \cdot F_f \quad (3.1)$$

where D is the fuel diameter in m, F_f is the view factor from the fire to the target surface. The calculated incident radiant heat flux to the target surfaces in the column is shown in Fig. 3-6.

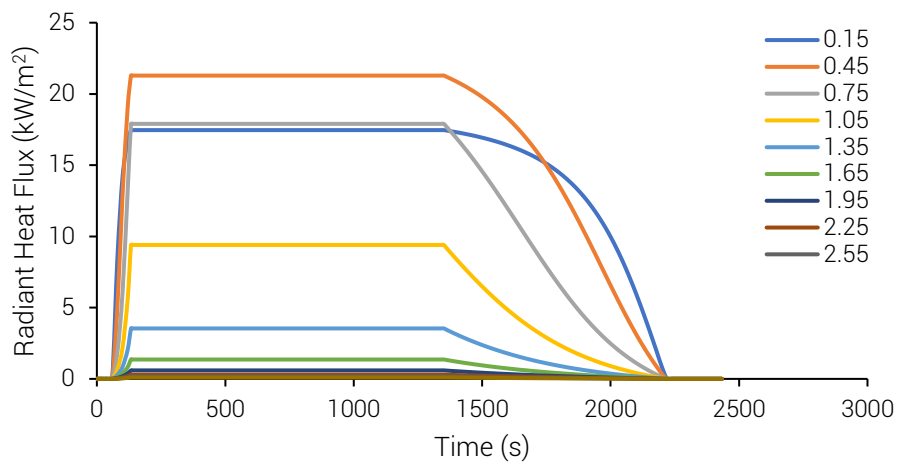


Figure 3-6. Incident radiant heat flux to the target surfaces of the column at a distance of 1 m from the fire. The legend corresponds to the height from the floor in m.

3.3.4 Case 2—Scenario 3: Beam Directly Above the Localized Fire

The third scenario is a fire directly below the midspan of the beam. The distance between the ceiling and the centre of the fuel is 2 m. This distance was chosen to represent a fire elevated from the ground and also to get higher heat flux to the beam surfaces. The incident

radiant heat flux in kW/m² from the fire was calculated using the Point Source Method as discussed by Beyler (2016) which is expressed as

$$\dot{Q}''_{rad} = \frac{(0.21 - 0.0034D)\dot{Q} \cos \theta}{4\pi R^2} \quad (3.2)$$

where \dot{Q} is the total heat release rate in kW, θ is the angle between the normal of the target surface and the line of sight from the source to the target in radians, and R is the distance from the mid-height of the flame to the target surface in m. This method was chosen because the Shokri & Beyler Method cannot be used to calculate the view factor of surfaces within the area of the fuel. Figure 3-7 shows the incident radiant heat flux along the length of the beam.

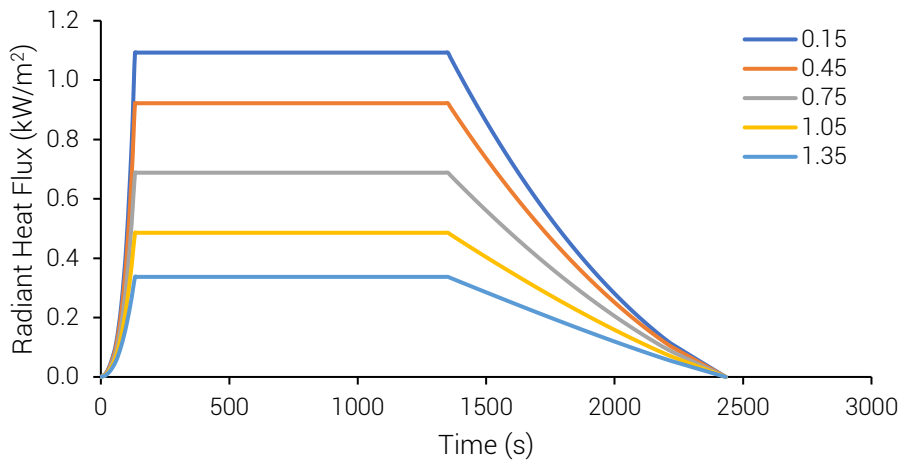


Figure 3-7. Incident radiant heat flux to the target surfaces of the beam 2 m above the fire. The legend corresponds to the distance from the beam midspan in m.

In this scenario, due to the availability of a model for smoke accumulation in the ceiling, its contribution was considered. It was assumed that the beam was completely covered with smoke. The temperature of the smoke which varies according to the distance from the plume centreline was calculated using the Alpert's ceiling jet correlation as discussed by Karlsson & Quintiere (2000). For this to be applicable, the room was assumed to have a large area which makes it practically unconfined. The correlation is given by

$$T_g - T_a = \frac{16.9\dot{Q}^{2/3}}{H^{5/3}} \quad \frac{r}{H} \leq 0.18 \quad (3.3)$$

$$T_g - T_a = \frac{5.38(\dot{Q}/r)^{2/3}}{H} \quad \frac{r}{H} > 0.18 \quad (3.4)$$

where T_g is the gas temperature in °C, T_a is the ambient temperature in °C, H is the distance from the centre of the fuel to the ceiling in m, and r is the distance from the plume centreline in m. Figure 3-8 shows the temperature of the gas around the beam.

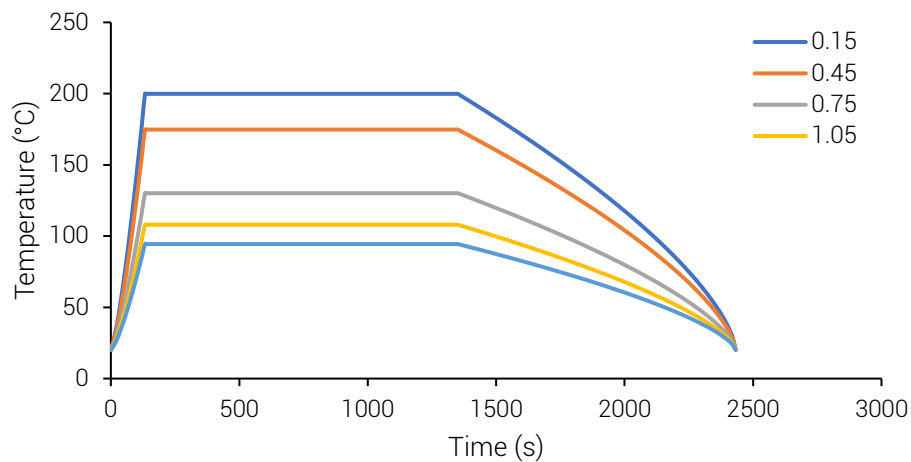


Figure 3-8. Ceiling jet temperature along the length of the beam. The legend corresponds to the distance from the beam midspan in m.

3.4 Software and Model Preparation

Before using the software Abaqus/CAE 2018, it was first verified using the Gillie (2009) benchmark. The benchmarking procedure can be found in Appendix D. Then, arbitrary sizes were chosen for the structural members: IPE 300 for the beam and UC 305 x 305 x 97 for the column. The structural elements were modelled with static loads only and these were called static models.

Figure 3-9 shows the models of the column and the beam. The column bottom and top cross-sections were constrained to reference points RP-1 and RP-2 respectively. RP-1 was then assigned a fixed support boundary condition. The 85-kN concentrated load was applied to RP-2. On the other hand, the beam was considered to be simply supported. The pin and roller support, on the left and right side respectively, were assigned to the whole line of the bottom part of the section. The 15-kN/m uniform line load was assigned by constraining the top surface of the web to reference point RP-3 and applying a concentrated load equal to the uniform load multiplied by the length of the beam. In this case, the concentrated load was 45 kN. Distributing the uniform load to the web was done to prevent local buckling of the top flange. Also, it was initially observed that there was stress concentration near the supports causing local buckling. This was resolved by putting 10-mm-thick web stiffeners at both ends which had negligible effects to the overall structural behaviour. Using manual calculations, the

reaction forces, stresses and deflections were determined and compared to the results of the static models. This comparison can be found in Appendix E.

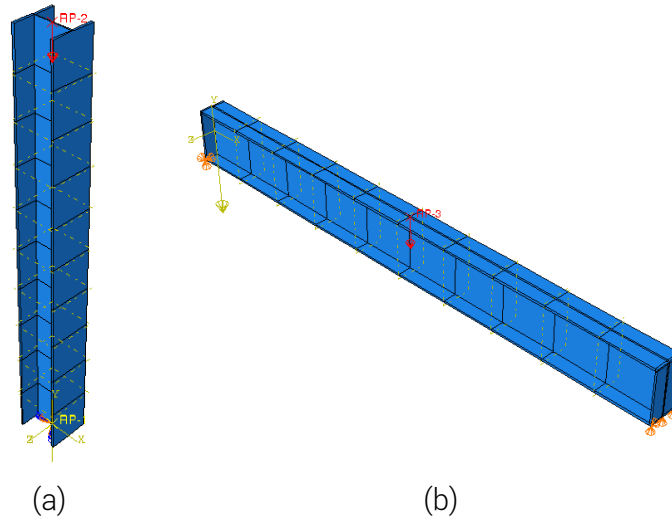


Figure 3-9. Abaqus model of the structural members: (a) column and (b) beam.

3.5 Heat Transfer Modelling

After the verification of the static models, the fire curves were applied to the static models. These models were called thermal benchmark models. Five models were prepared: two for uniform heating using the parametric temperature-time curve (beam and column), and three for each of the localized fire scenarios. In actual, not all surfaces of the structural members are exposed to the fire because some are in contact with other materials. The heat losses by conduction to these boundaries were assumed to be one-dimensional and that the boundaries are semi-infinite in thickness. This was done using the general heat conduction equation as given by Karlsson & Quintiere (2000) expressed as

$$\dot{Q}''_{cond} = \frac{1}{\sqrt{\pi}} \sqrt{\frac{k\rho c}{t}} (T_s - T_{bo}) \quad (3.5)$$

where \dot{Q}''_{cond} is the conductive heat flux, $k\rho c$ is the thermal inertia of the material, t is the time, T_s is the surface temperature of the member in contact with the boundary surface, and T_{bo} is the temperature of the boundary. The boundary was assumed to have a constant temperature of 20 °C for simplification.

In most real constructions, the beam is carrying a concrete slab and is supported on both ends by other steel members. On the other hand, since the column is assumed to be in the ground floor, it is in contact with concrete at the bottom and steel at the top. This was done

in the model by calculating the effective heat transfer coefficient and treating the conductive heat transfer like convection. Note the similarity between Eq. 3.5 and Eq. 3.7 below. The effective heat transfer coefficient h_{eff} is given by

$$h_{eff} = \sqrt{\frac{k\rho c}{\pi t}} \quad (3.6)$$

Based on Karlsson & Quintiere (2000), the values of the thermal inertia of concrete and steel are $2 \times 10^6 \text{ W}^2\cdot\text{s}/\text{m}^4\cdot\text{K}^2$ and $1.6 \times 10^8 \text{ W}^2\cdot\text{s}/\text{m}^4\cdot\text{K}^2$, respectively.

The net radiative heat flux was modelled based on Eq. 2.39 using a constant emissivity of 0.7 as suggested by Eurocode 1 Part 1-2. Additionally, the exposed surfaces are also experiencing heat transfer by convection apart from radiation. In this study, the temperature dependency of the convective heat transfer coefficient h_{conv} was not considered as discussed in Section 1.4. Instead, the values of h_{conv} were taken from the Eurocode 1 Part 1-2. For simplified fire models such as parametric temperature-time curve and localized fire curve, h_{conv} for exposed surfaces can be taken as $35 \text{ W}/\text{m}^2\cdot\text{K}$. For standard fire curves, h_{conv} can be taken as $25 \text{ W}/\text{m}^2\cdot\text{K}$. The net convective heat flux $\dot{Q}''_{net,conv}$ is given by

$$\dot{Q}''_{net,conv} = h_{conv}(T_g - T_s) \quad (3.7)$$

For Case 1 and Case 2—Scenario 1, the temperature-time curves were applied to the software both as surface radiation and surface film condition for the radiative and convective heat transfer, respectively, treating them as ambient temperature that changes with time. For Case 2—Scenario 2, the heat flux from the fire was applied only to the column flange surface directly facing the fire. It was assumed that the other surfaces were not receiving radiation from the fire and only radiating and convecting heat with the ambient surroundings ($T_a = 20 \text{ }^\circ\text{C}$). The h_{conv} used was $4 \text{ W}/\text{m}^2\cdot\text{K}$ which was suggested by Eurocode 1 Part 1-2 for unexposed side of members. For Case 2—Scenario 3, the heat flux from the fire was applied only to the bottom flange of the beam. Other surfaces were assumed to be not receiving radiation from the fire same as with Case 2—Scenario 2. However, the main difference between the two cases is that Case 2—Scenario 3 was engulfed by the ceiling jet. This means that heat transfer by radiation and convection was considered in the same way as for Case 1 and Case 2—Scenario 1 using the temperature of the ceiling jet as the ambient temperature. In all cases, the emissivity of the fire was taken as 1.0 as suggested by Eurocode 1 Part 1-2. However, for the three scenarios of Case 2 where it was possible to calculate the height of the flame, the emissivity of the smoke was considered using Eq. 2.12.

3.6 Material Properties of Steel

Steel has a density of 7850 kg/m^3 , a Poisson's ratio of 0.3, a coefficient of linear thermal expansion of $1.2 \times 10^{-5}/\text{K}$ (CEN, 2002c, 2005a). Other properties of steel that was input in the software were taken from Eurocode 3 Part 1-2 (CEN, 2002b). Majority of the material properties such as effective yield stress, elastic modulus, specific heat, thermal conductivity, and stress-strain relationship are given as a function of temperature as shown in the next figures.

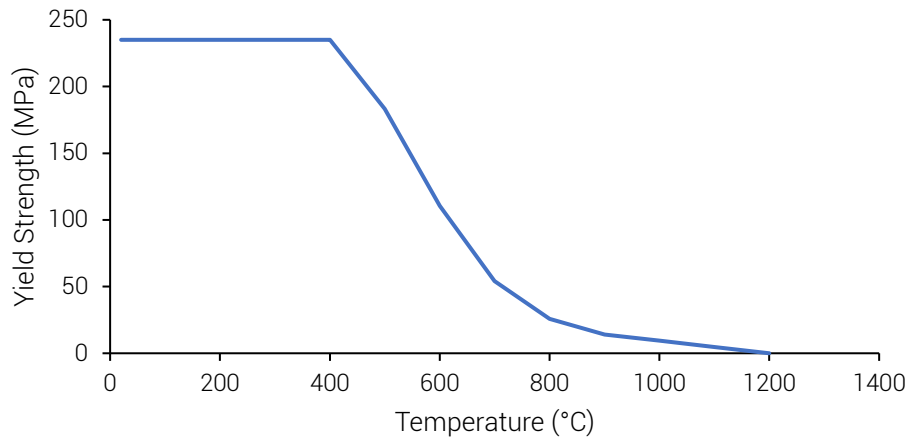


Figure 3-10. Yield strength of steel.

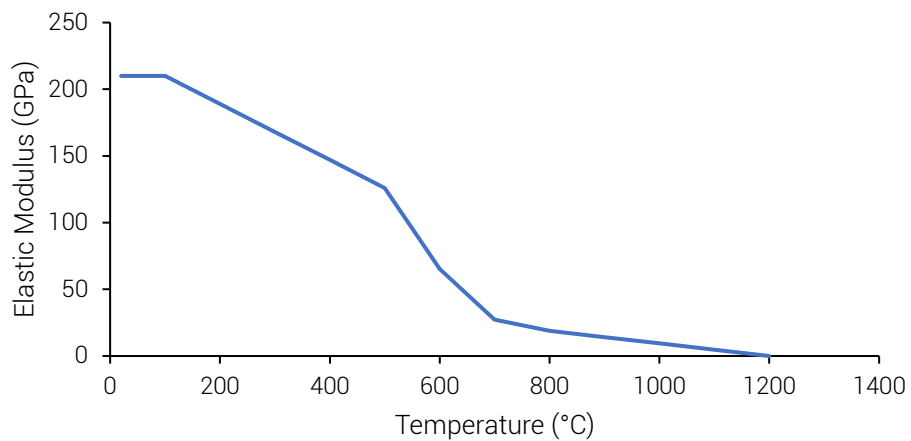


Figure 3-11. Elastic modulus of steel.

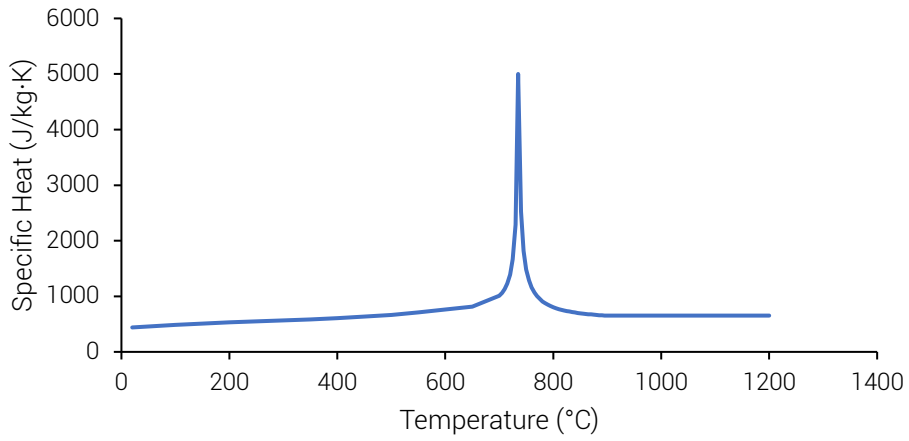


Figure 3-12. Specific heat of steel.

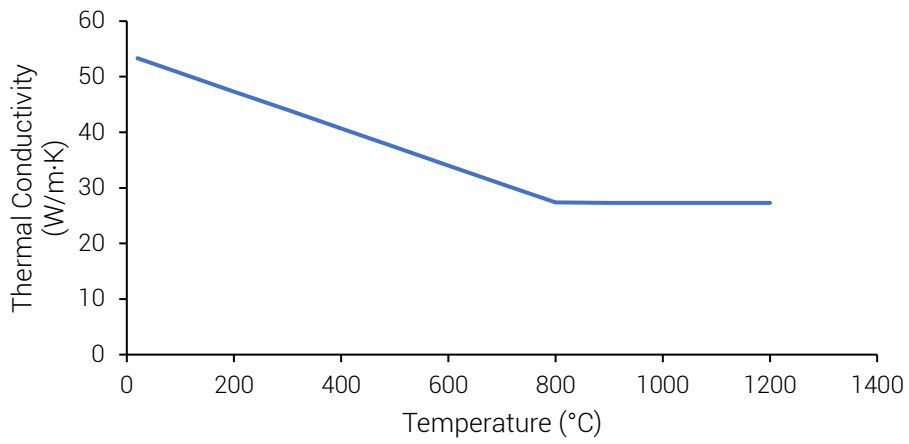


Figure 3-13. Thermal conductivity of steel.

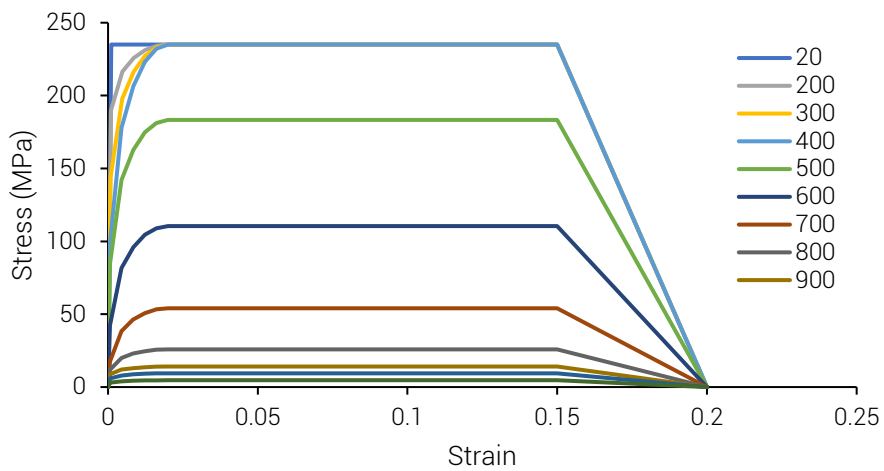


Figure 3-14. Stress-strain relationship of steel at elevated temperatures. The legend is in °C.

3.7 Verification of the User Subroutines

In most computer modelling software, user subroutines are used to instruct them to perform simulations which are beyond their default capabilities. In Abaqus/CAE 2018, the user can only input a single emissivity value for surface radiation. To apply the temperature-dependent emissivity models in Subsection 2.2.2, the user subroutine DFLUX was utilized. An initial set of user subroutines applying a constant emissivity value corresponding to the thermal benchmark models was coded in Fortran language. This was done to verify the code before applying the temperature-dependent emissivity models. The verification process along with samples of the coded user subroutines can be seen in Appendix F. In total, there were seven sets of simulations—four for Case 1 and one for each scenarios of Case 2—each employing seven emissivity models which summed up to 49 user subroutines.

4 RESULTS AND DISCUSSION

4.1 Temperature

4.1.1 Case 1: Uniform Heating

Under uniform heating, the beam can be crudely divided into two regions where the cross sections have almost the same temperature profile: near-support and middle regions. The near-support region has a temperature significantly lower than the rest of the beam due to the heat losses by conduction to the boundaries. The temperature distribution along the beam using constant emissivity can be seen in Fig. 4-1. The time steps were chosen based on when the maximum temperature in the beam occurred. The web stiffener plates were hidden for clarity.

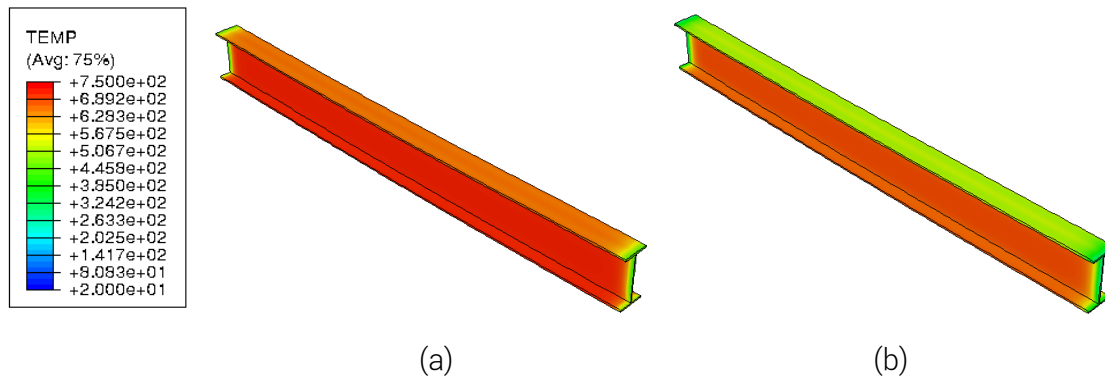


Figure 4-1. Temperature distribution along the beam: (a) parametric curve at $t = 2200$ s and (b) ISO 834 standard curve at $t = 870$ s. The legend is in $^{\circ}\text{C}$.

Comparing the two beams, it can be seen that the one subjected to the ISO 834 standard curve had a higher temperature gradient along its cross section than the one subjected to the parametric curve. This is further attested by the temperature profiles in the cross section of the beam at different time steps which is shown in Fig. 4-2. This can be attributed to the steep temperature-time curve of the ISO 834 standard curve. At early stages of the fire, the effective heat transfer coefficient is high as can be deduced in Eq. 3.6. A huge difference between the surface temperatures of the member and the boundary coupled with a high effective heat transfer coefficient means that the heat loss by conduction was greater in the beam exposed to the ISO 834 standard curve than that exposed to the parametric curve, as can be confirmed using Eq. 3.5.

Moreover, because of the steep curve, less time per change in temperature was given to the section which resulted to a difficulty reaching thermal equilibrium. This should not be construed as saying that the beam exposed to the parametric curve had the same temperature all throughout its section and, therefore, reached thermal equilibrium. It just means that the beam exposed to the parametric curve had a more uniform temperature distribution than that exposed to the ISO 834 curve. In summary, it was found that the time equivalence concept used to equate the two curves was unable to capture the actual thermal response of the beam which has a huge effect on its overall performance.

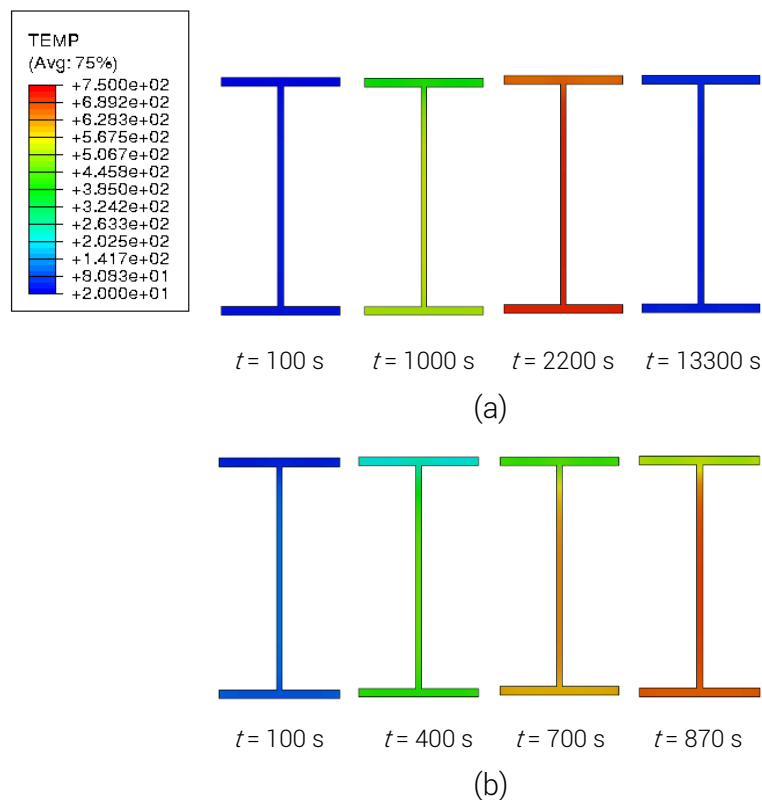


Figure 4-2. Temperature profile across the beam midspan cross section: (a) parametric curve and (b) ISO 834 standard curve. The legend is in °C.

Additionally, Fig. 4-2 also shows that the maximum surface temperature occurred at the point below the centroid. This part of the beam has a thinner width making it more thermally thin than other parts and is far from the boundary where high heat losses were occurring. Because of that, it heated up faster than other portions of the beam. The temperature at this point was taken for all emissivity models and is shown in Fig. 4-3 and Fig. 4-4 using parametric curve and ISO 834 standard curve, respectively. Both figures show significant differences between the temperatures which reached the order of hundreds. All emissivity models except

for Kay et al. (1996) and Bentz et al. (2009) had lower temperature than that of the Eurocode throughout the whole duration of the fire. The reason is because the former uses higher emissivity than the Eurocode at all temperatures while the latter starts to become higher than the Eurocode at a temperature of around 340 °C. At a temperature of around 470 °C, Bentz et al. (2009) started to surpass the Eurocode. The delay can be attributed to the low heat absorption by this model at lower temperatures as a result of its emissivity being lower, a direct consequence of Kirchhoff's Law.

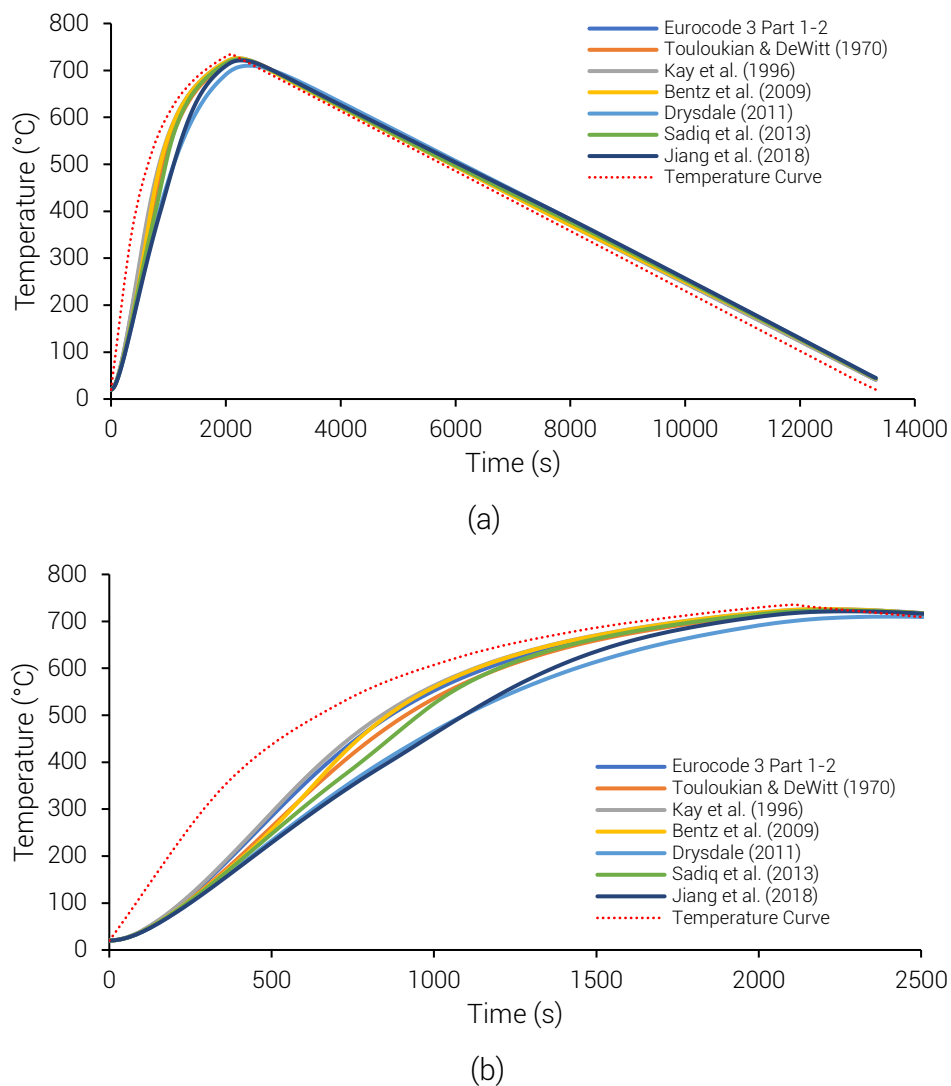


Figure 4-3. Temperature evolution of the specified point in the beam under parametric curve heating: (a) whole duration and (b) heating period.

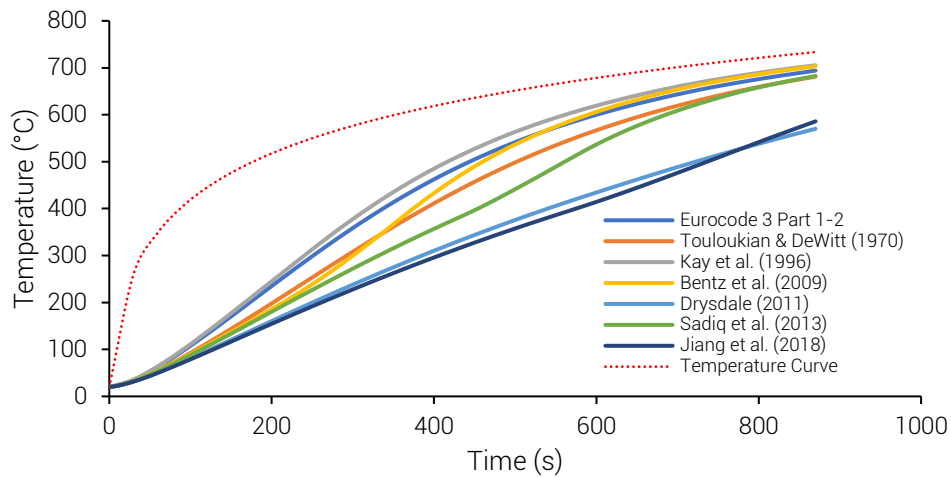


Figure 4-4. Temperature evolution of the specified point in the beam under ISO 834 standard curve heating.

The main difference between a beam and a column subjected to a fully-developed fire is that in a column, heat losses occur only in the ends to which it is being supported. However, same with the beam, there is a portion along its length which has roughly similar temperatures. The temperature profile along the column modelled using constant emissivity be seen in Fig. 4-5. It can be seen that there was a significant temperature difference between the lower and upper support in both scenarios. This is due to the assumption in modelling the heat losses to the boundaries. The upper portion lost heat through conduction with steel while the lower portion with concrete. Since steel has higher conductivity, heat was transmitted faster to the boundary, thereby, lowering the temperature in that portion.

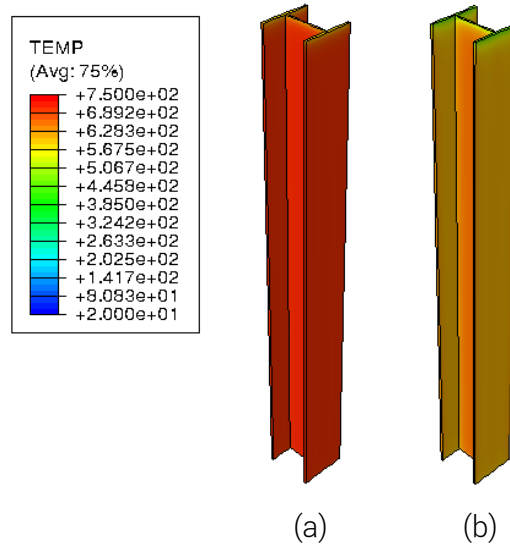


Figure 4-5. Temperature distribution along the column: (a) parametric curve at $t = 2300$ s and (b) ISO 834 standard curve at $t = 870$ s. The legend is in °C.

Similar to the observation for the beam, Fig. 4-6 shows that the ISO 834 standard curve caused higher temperature gradient along the column cross section than the parametric curve. However, the temperature gradient in the column was observed to be less than that of the beam. This is because the column was exposed to the same heat flux and not in contact to a boundary surface where it could lose heat. Even so, the thermal response to the two scenarios had significant differences, especially the maximum surface temperature which is directly related to the main criteria of equivalency—gas temperature. This proves again that the time equivalence concept does not really represent the severity of an equivalent compartment fire.

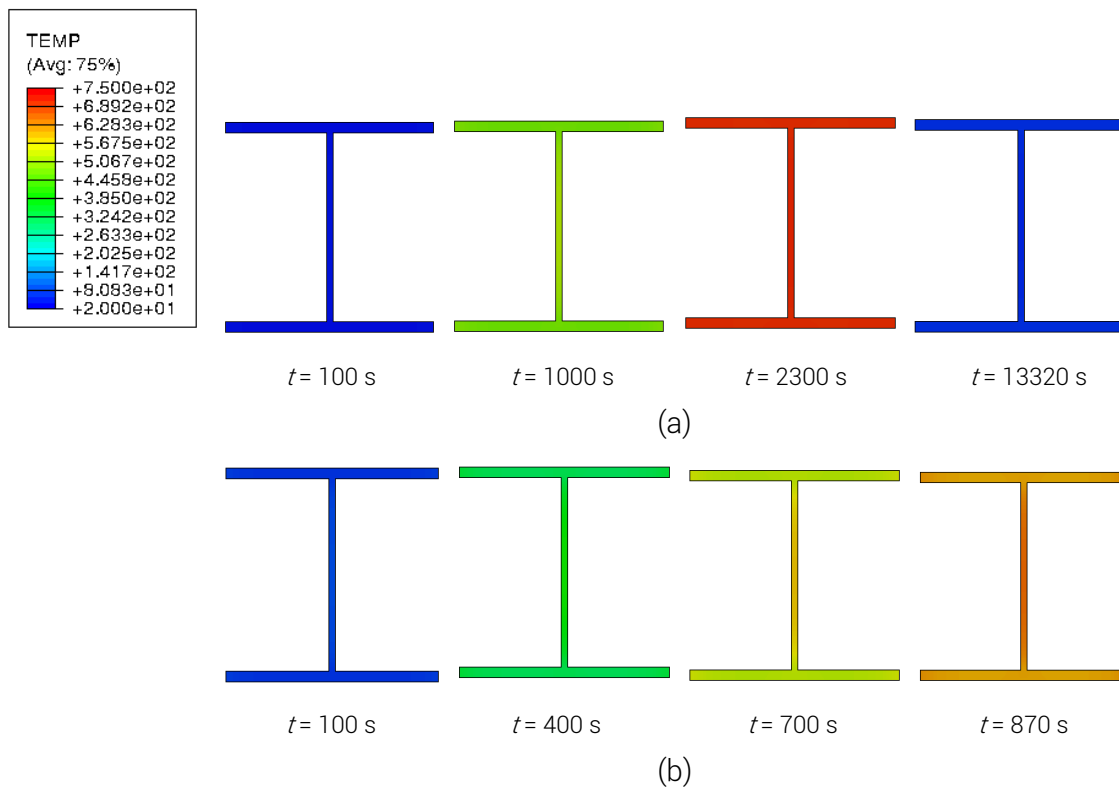


Figure 4-6. Temperature profile across the column cross section at a height of 2.425 m above the floor: (a) parametric curve and (b) ISO 834 standard curve. The legend is in °C.

Due to the thin width of the web, the maximum surface temperature was observed at this part midway between the flanges. The surface temperature of this point is shown in Fig. 4-7 and Fig. 4-8 for the parametric curve and ISO 834 standard curve, respectively. The same response as with the beam was observed in the column exposed to the two uniform heating scenarios. Huge temperature differences relative to that of the Eurocode were observed as a result of using different temperature-dependent emissivity models. The explanation provided for the beam regarding the surface temperature is also applicable for the column.

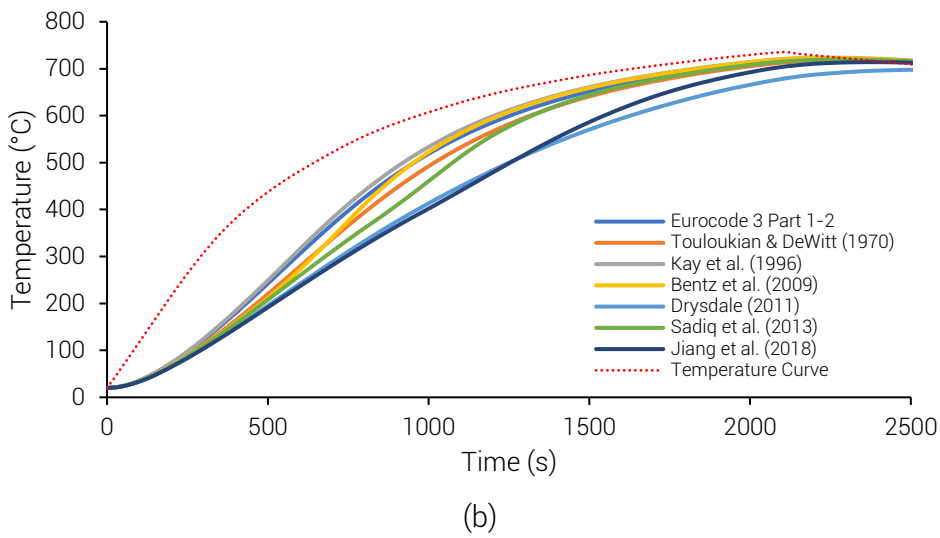
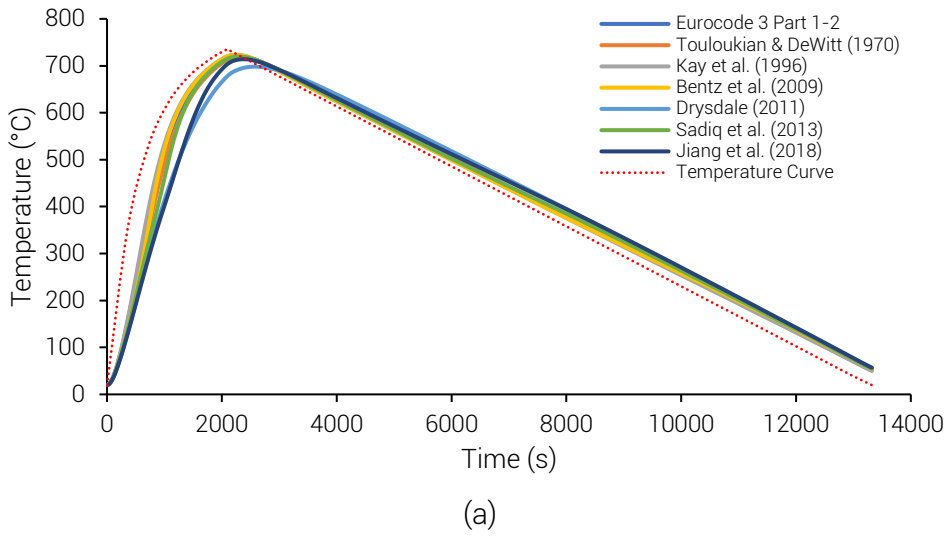


Figure 4-7. Temperature evolution of the specified point in the column under parametric curve heating: (a) whole duration and (b) heating period.

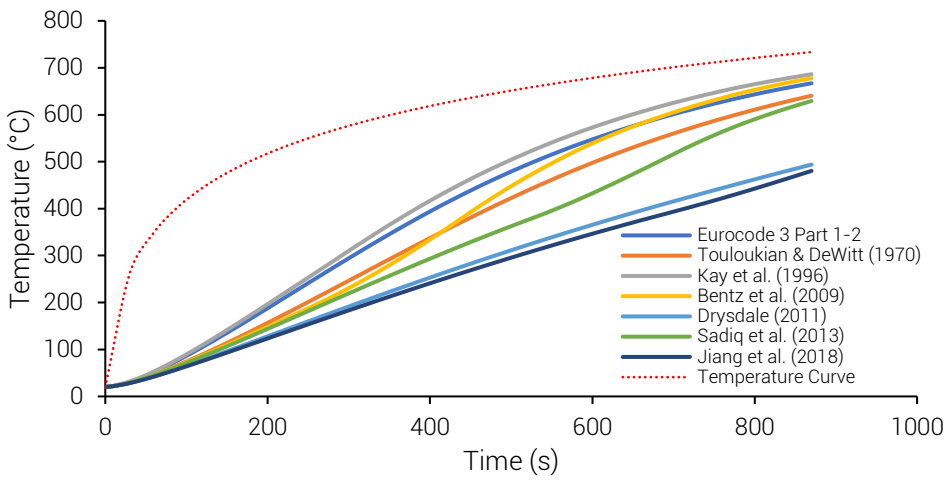


Figure 4-8. Temperature evolution of the specified point in the column under ISO 834 standard curve heating.

Generally, for uniform heating, the graphs show that temperature-dependent emissivity had a huge impact on the thermal response of structural steel members. This is consistent with the claims of Ghojel & Wong (2005) and Wang & Tan (2008). Emissivity models which started at values lower than the Eurocode resulted into lower member temperatures due to the lower rate of absorption as a result of the lower emissivity. This can be explained by Kirchhoff's Law.

At early stages of the fire, when the gas temperature is lower than 200 °C, temperature-dependent emissivity had negligible effects to the temperature. This means that, indeed, convection dominates the early stages of the fire. During the growth phase, as the gas temperature increased from 200 °C until the maximum of around 735 °C, the effect of temperature-dependent emissivity started to become prominent as shown by the large difference between the surface temperatures at any given time within that period. This is because the emissivity of steel starts to vary at this range of temperatures. Additionally, because the temperature changes rapidly in this region, the difference between the thermal response is more pronounced than in the region during which there was gradual decrease in the gas temperature as the fire started to decay. This means that although radiation—which is greatly affected by the surface emissivity—is the dominant heat transfer mechanism at higher temperatures, time is also a major factor to determine the overall thermal response of a member.

4.1.2 Case 2: Localized Heating

The temperature distribution along the column engulfed in the localized fire (Case 2—Scenario 1) with the steel surfaces at constant emissivity is shown in Fig. 4-9. Since the column was exposed to a fire with the temperature decreasing with flame height, the bottom part of the column was observed to be the hottest. Unlike the uniform curve scenarios, there was a long period in the localized fire curve when the heat release rate is constant causing the temperature of the flame region to be constant also at 900 °C. As a result, the temperature at the bottom part of the column reached the temperature of the fire around it.

Due to the heat loss to the boundary at the bottom support, the location of the maximum temperature was found to be at the web midway between the flanges and above the bottom support. The temperature profile of the section containing this point is shown in Fig. 4-10. Initially, there was a huge temperature gradient in the section but when the heat release rate reached the plateau, the whole section started to have an approximately uniform distribution.

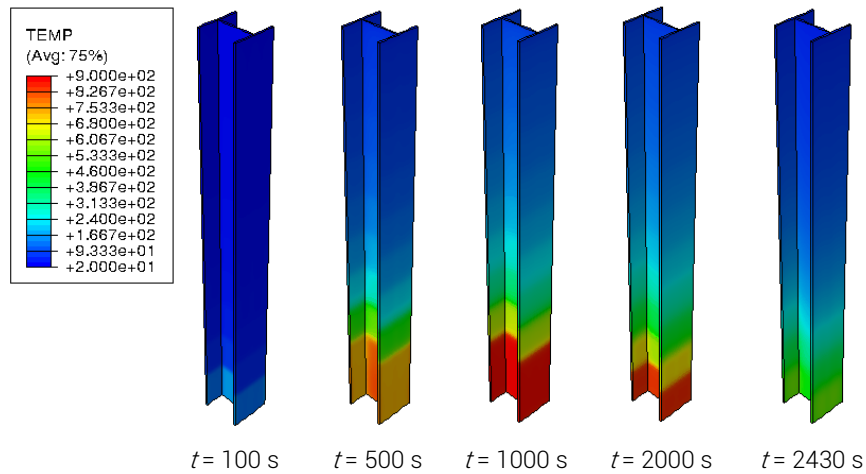


Figure 4-9. Temperature distribution along the column (Case 2—Scenario 1). The legend is in °C.

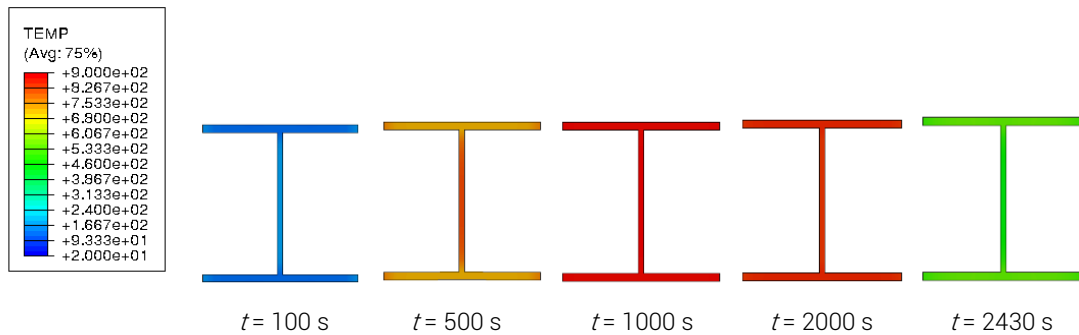


Figure 4-10. Temperature profile across the column (Case 2—Scenario 1) cross section at a height of 0.175 m above the floor. The legend is in °C.

Figure 4-11 shows the evolution of the temperature of the point where the maximum was observed. Because it is located at the bottom portion of the column, this point was exposed to the flame region most of the time. This explains why even after the heat release rate started to decrease, the temperature of the specified point continued to increase. During this instance, it was still within the flame region. After the flame height became lower than the location of the specified point, its temperature started to decrease.

Additionally, it is also noticeable that before and after the steady-state condition of the fire, the temperature increase slowed down for a short period of time before it started to increase rapidly again. This can be related to the delay in the application of the heat flux as the fire grew as a result of a coarse discretization of the column. The segment containing the specified point rapidly heated up and lost heat through conduction to the unheated portion until it reached steady state. Then, in a short period, the fire grew and reached the next segment

which supplied additional energy to the lower segment allowing the temperature to rapidly reach the temperature of the flame surrounding it. With respect to the effect of the temperature-dependent emissivity, the same behaviour as with that of the members exposed to the uniform heating was observed.

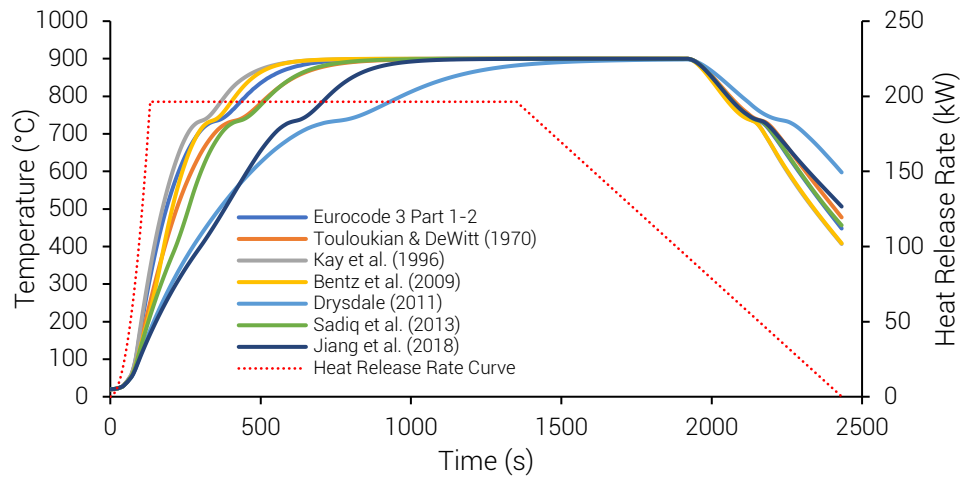


Figure 4-11. Temperature evolution of the specified point in the column (Case 2–Scenario 1).

Unlike the column engulfed in the fire, the surface temperature of the column 1 m away from the centre of the fuel is lower. For constant emissivity, this is illustrated in Fig. 4-12. Moreover, the time step $t = 1600$ s clearly shows that even if two or more segments are within the flame length, they are not going to be exposed to the same heat flux according to this fire model. This is due to the view factor calculation which, in essence, is directly related to the distance from the centroid of the cylinder to the target surface. This is the reason why at $t = 1600$ s, the maximum temperature occurred at the middle portion of the exposed surface.

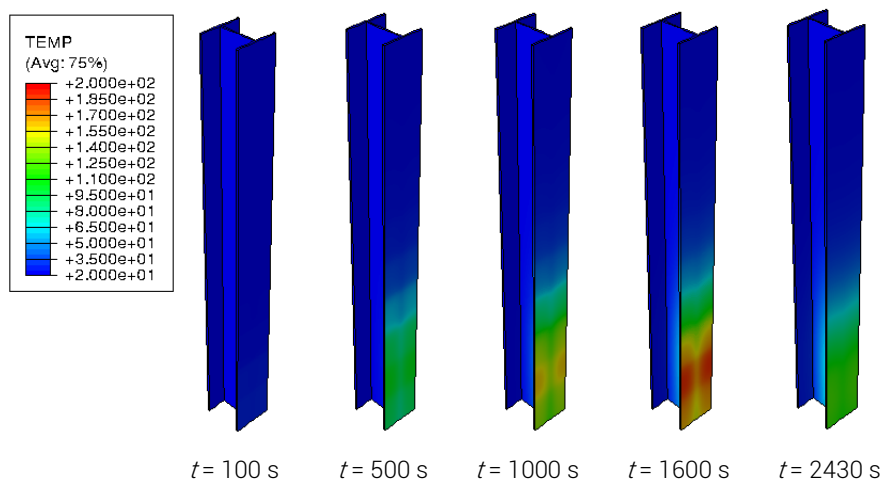


Figure 4-12. Temperature distribution along the column (Case 2–Scenario 2). The legend is in °C.

Figure 4-13 shows the temperature distribution across the column cross section where the maximum temperature was observed for Case 2—Scenario 2. In this scenario, it can be seen that the maximum temperature was found to be at the lower corners of the exposed flange. This is because this point is farthest away from the cooler steel portions which served as a heat sink.

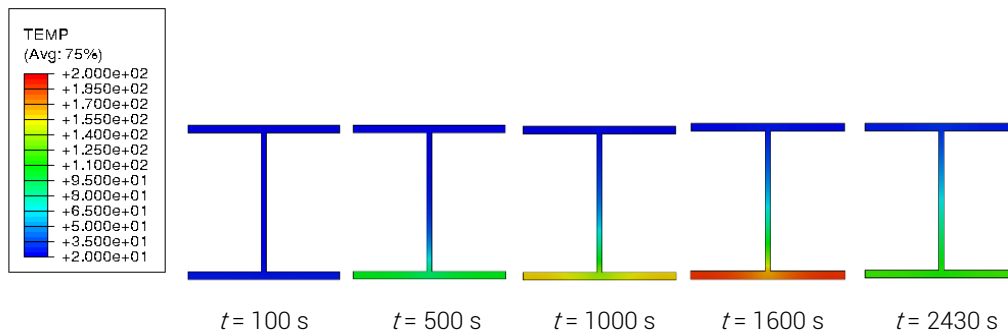


Figure 4-13. Temperature profile across the column (Case 2—Scenario 2) cross section at a height of 0.45 m above the floor. The legend is in °C.

Figure 4-14 shows how the temperature of the specified point in the column for Case 2—Scenario 2 changed over time. The impact of temperature-dependent emissivity is also significant in this case as evidenced by the large temperature variations. The graph shows that only the Kay et al. (1996) model has higher temperature compared to the Eurocode. In previous scenarios, Bentz et al. (2009) surpassed the Eurocode at some point but since the surface temperature in this scenario is lower, the emissivity did not reach the value higher than that of the Eurocode.

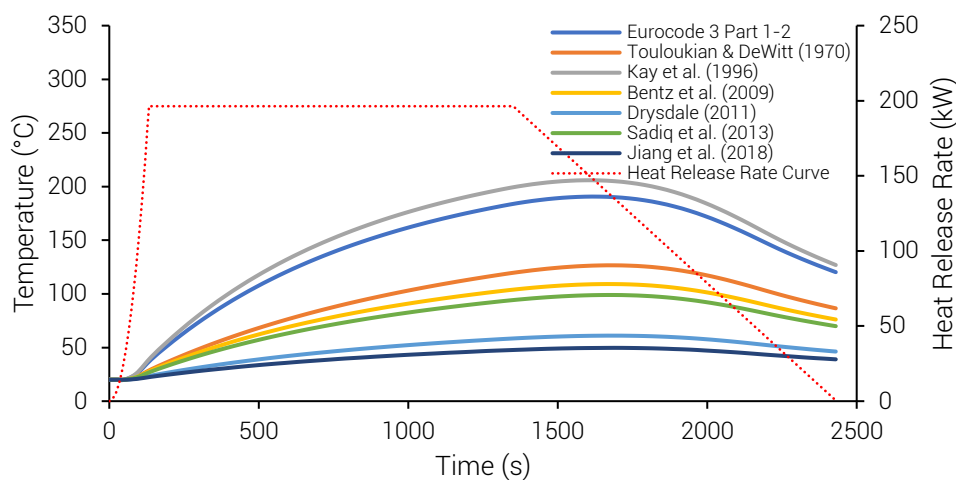


Figure 4-14. Temperature evolution of the specified point in the column (Case 2—Scenario 2).

In Case 2—Scenario 3 wherein the beam was exposed to radiation from the fire and the ceiling jet, the temperature of the whole member increased. The midspan segment had the highest temperature due to its proximity to the plume centreline which means higher smoke temperature and shorter distance from the point source. The temperature distribution along the beam with constant emissivity is illustrated in Fig. 4-15.

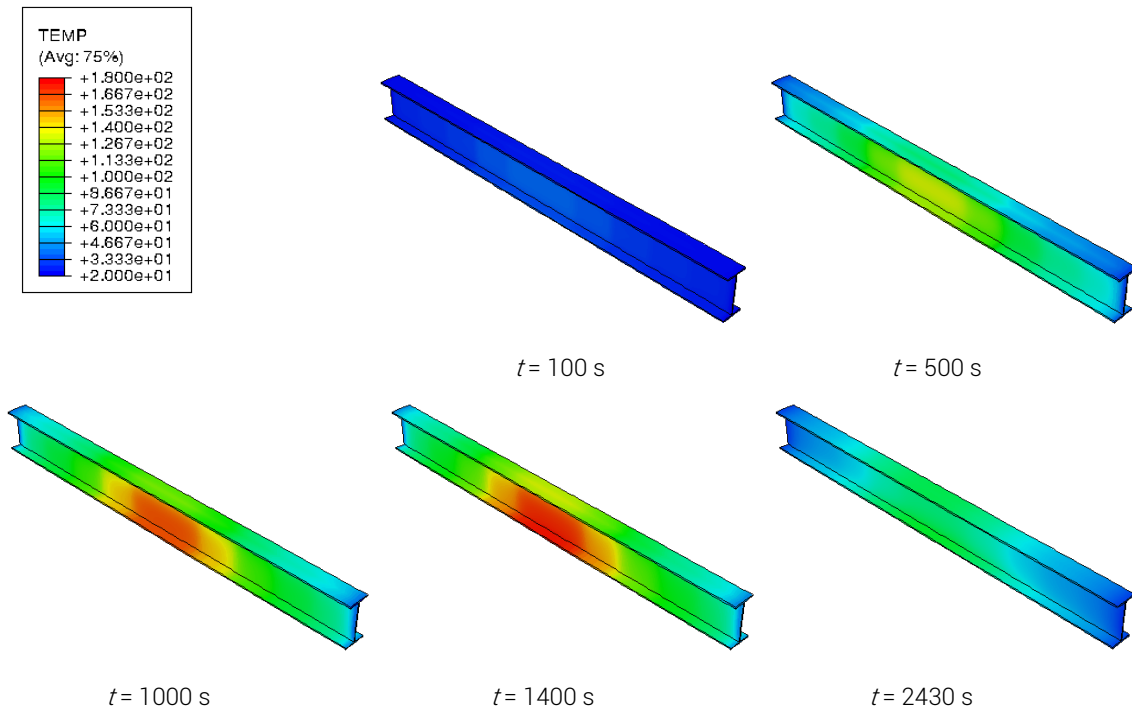


Figure 4-15. Temperature distribution along the beam (Case 2—Scenario 3). The legend is in °C.

The temperature profile across the midspan cross section of the beam is presented in Fig. 4-16. Initially, the point with the maximum temperature was found in the web because the heat transfer was dominated by the radiation and convection from the smoke. However, after the fire grew and the radiation from it increased, the point shifted to the surface of the bottom flange. This point was then chosen to compare the effect of temperature-dependent emissivity as shown in Fig. 4-17. Despite being within the same range of temperatures compared to Case 2—Scenario 2, the effect of temperature-dependent emissivity was considerably lower. This can be attributed to the minimizing effect of including the smoke emissivity. It lowered the incident heat flux to the surface, making radiation less dominant. Additionally, the impact of steel's temperature-dependent emissivity did not follow the expected trend observed in the previous scenarios. At the later stages of the fire, it was found that those with higher emissivity values got lower surface temperatures. This is because the low incident heat flux could not compensate for the high emission of the surface as a result of its high emissivity.

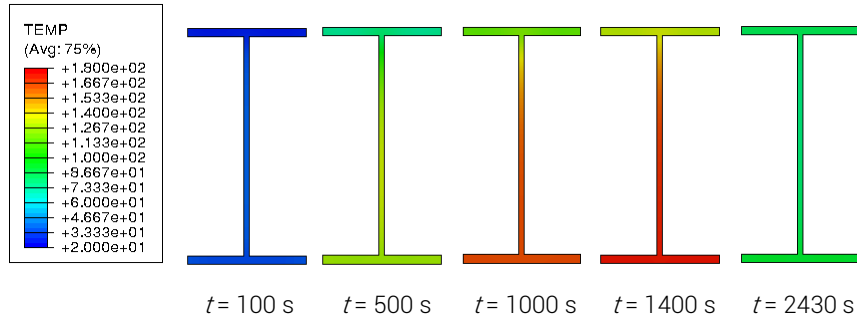


Figure 4-16. Temperature profile across the beam midspan cross section (Case 2–Scenario 3). The legend is in °C.

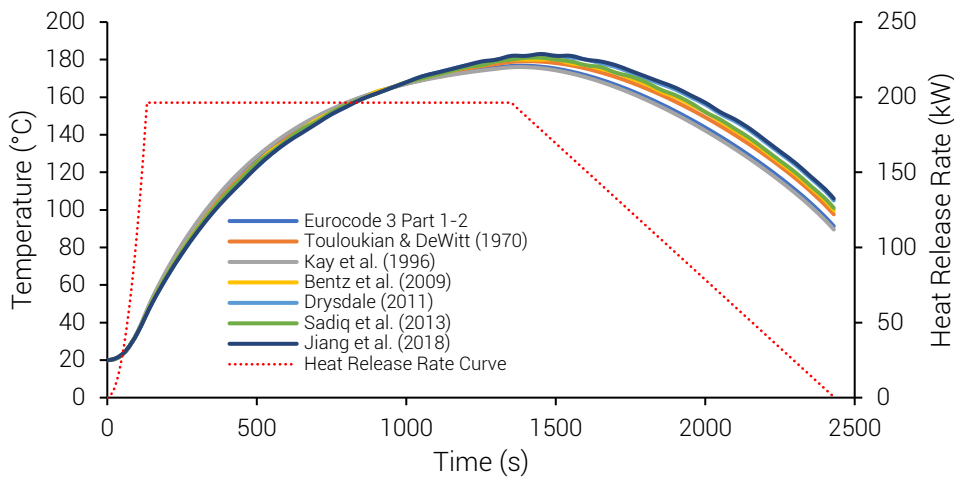


Figure 4-17. Temperature evolution of the specified point in the beam (Case 2–Scenario 3).

In summary, the temperature-dependent emissivity of steel has a significant impact on members exposed to localized fires. However, this impact depends on how the fire was treated. In all scenarios, varying the emissivity had a negligible effect in the surface temperature at the early growth stages of the fire. In both column scenarios, the effect was the same in trend and magnitude as with the uniform heating because of high heat fluxes from the high gas temperatures for the engulfed scenario and because of the inherently large variation in the emissivity models at low temperatures which compensates for the lower heat fluxes for the distant scenario. However, for the beam exposed to radiation from the fire and the smoke engulfing it, the effect of temperature-dependent emissivity was minimized by the low emissivity of the smoke. Additionally, in the later stage of the fire, the high emission due to high emissivity compensated for the minimizing effect of the smoke. This led to a lower surface temperature which was not consistent with the previous scenarios. Therefore, unlike the

uniform heating with an already established method for modelling the fire, the effect of temperature-dependent emissivity on localized heating varies according to the fire model used.

4.2 Stress

Most of the discussions related to the effect of temperature-dependent emissivity of the steel have been presented in the previous section. Its effect on stress is a direct implication of the thermal response of the member. There are many types of stress being experienced by a member. However, for the purpose of this section, the stress in which a structural member is usually designed for will be used for comparison: normal stress due to bending for beam and normal stress due to axial forces for column. As a convention, a positive value means tension while a negative value means compression.

4.2.1 Case 1: Uniform Heating

For a simply supported beam in ambient temperature, the maximum bending stress is expected to be in the extreme fibres of the flanges at the midspan—with the stresses in the top and bottom flanges in opposite directions. However, for a beam under the uniform heating of a parametric curve, the maximum stress was found to shift to the centroid as shown in Fig. 4-18. As discussed in Subsection 4.1.1, the thermal gradient across the cross section for this scenario was high only at the initial stage as shown in Fig. 4-19.

The stress induced in the web can be attributed to the differential thermal stresses. Since the web is thinner, initially, it had a higher temperature than the flanges which made it want to expand more. However, because it was constrained by the stiffer flanges, it was being compressed while subsequently causing the flanges to be stretched. As the fire continued to grow until it reached the maximum temperature, the whole section tried to expand. Since the support is a roller, the expansion was not restrained which relieved the stress. At the same time, the lower portion of the beam became hotter which caused strength reduction and, in effect, shifted the neutral axis upwards. This caused tension to the web. During the decay stage, the gradual decrease of the gas temperature caused minimal stress to the flanges. On the contrary, since the web is thinner, it wanted to contract faster than the rest of the section but was being constrained by the flanges. This, again, caused tension to the web. This was balanced by the compression in the flange which explains the minimal stress decrease.

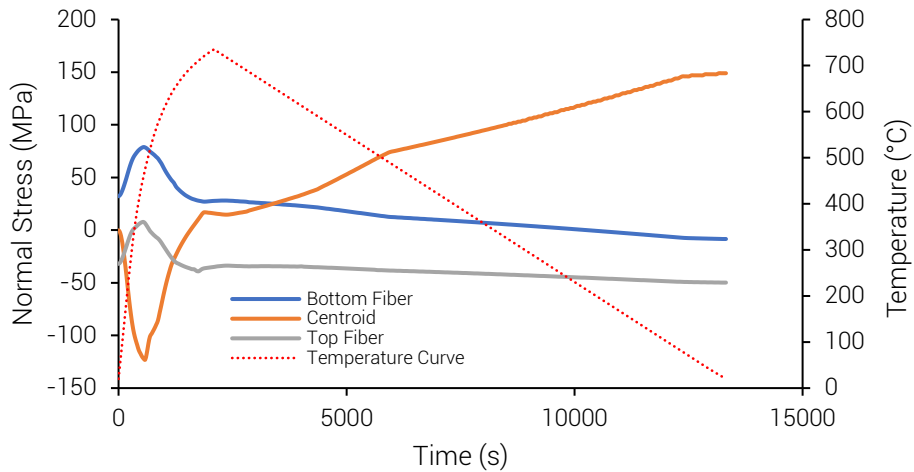


Figure 4-18. Normal stress at different points across the beam midspan cross section under parametric curve heating.

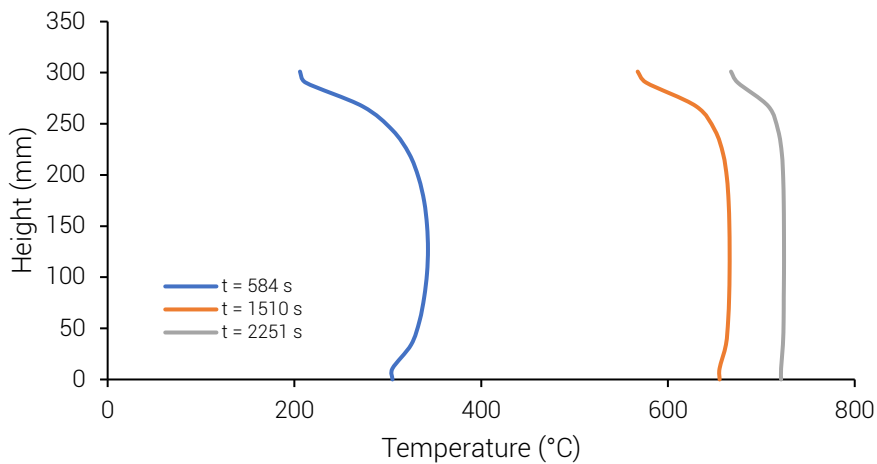


Figure 4-19. Temperature variation along the height of the beam cross section under parametric curve heating at chosen timesteps.

The maximum stress was found in the centroid and this was used as the point for comparison of the normal stress in the beam which is shown in Fig. 4-20. Comparing the maximum tension and compression, it can be seen that the stress based on the Eurocode was lower and higher, respectively, than those based on most temperature-dependent emissivity models. Members are designed on the maximum stress they experience, tension in this case, which means that using a constant emissivity can actually lead to under-designing the member.

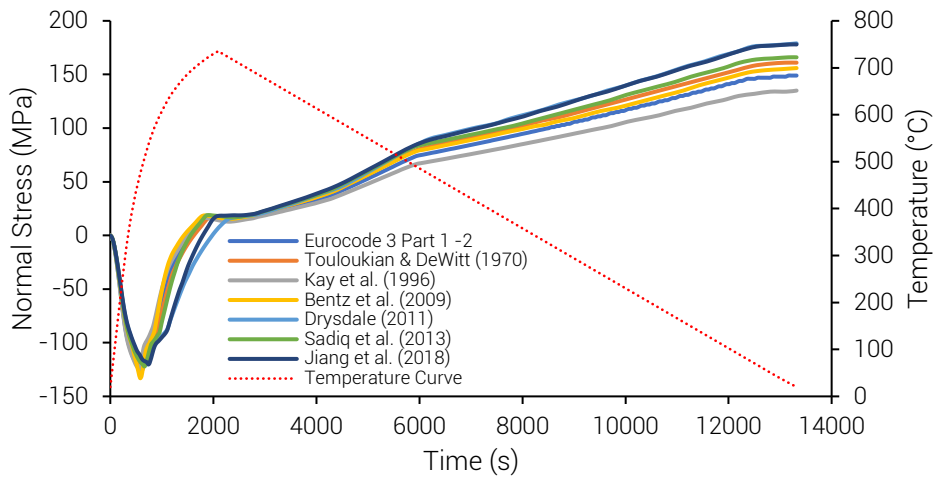


Figure 4-20. Evolution of the normal stress in the specified point of the beam under parametric curve heating.

In the case of the beam heated by the ISO 834 standard curve, the same behaviour as that of the beam in the initial stage of the parametric curve was observed. The point of maximum stress was found to be above the centroid. This is due to the higher temperature of the bottom part of the beam causing reduction in the stiffness. In structural mechanics, the stiffer an element, the more stress it attracts. This explains why the upper portions of the web had higher stresses. This was also observed in the beam exposed to parametric curve but the observations in the later stage of the fire overcame those of the initial stage. Back to the ISO 834 standard curve, the stress evolution of the specified point is presented in Fig. 4-21. Similar to what was found in parametric curve case, the maximum stress corresponding to the Eurocode was higher than that of the other emissivity models before the relaxation of stress where the Eurocode had lower values than most models.

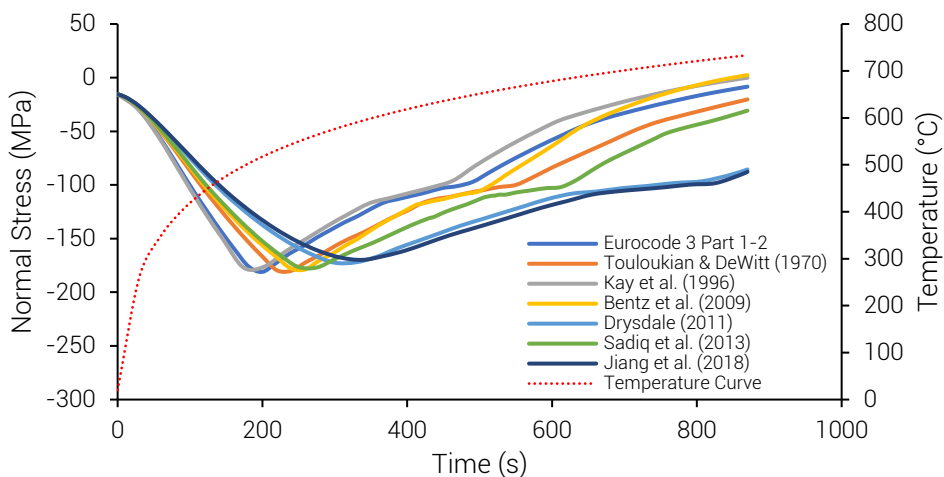


Figure 4-21. Evolution of the normal stress in the specified point of the beam under parametric curve heating.

For the column subjected to both parametric and ISO 834 standard curves, the location of the maximum stress is straightforward due to less complicated loading and heat loss. It behaved in the same way as the beam. The thermal gradient caused differential stresses across the section initially which was then relieved when the whole section started to cope with the changes in the temperature. This is illustrated in Fig. 4-22. This cross section can be taken anywhere in the portion of the column, which has the same temperature distribution, away from the boundaries.

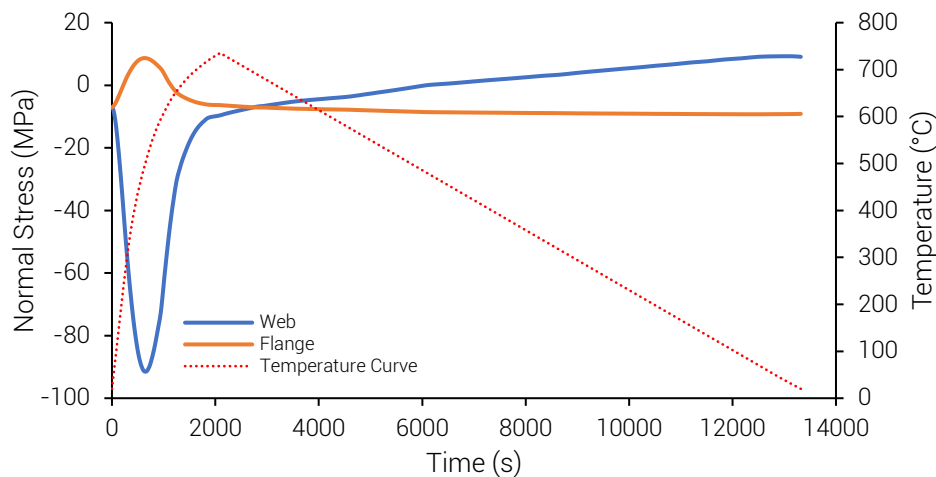


Figure 4-22. Normal stress at different points across the column cross section under parametric curve heating.

The stress evolution in this section can be seen in Fig. 4-23 and Fig. 4-24 corresponding to the parametric curve and ISO 834 standard curve, respectively. Figure 4-23 shows that, in the initial stage of the parametric curve, the Eurocode either underestimated or overestimated the stress depending on the emissivity model used. In the later stage, the Eurocode underestimated the stress. Similarly, the behaviour of the column at the initial stage of the parametric curve is the same as that of the ISO 834 standard curve as shown in Fig. 4-24. However, since this column should be designed for the maximum stress which is compression in the initial stage of the fire in this case, the impact of the temperature-dependent emissivity is inconclusive and, therefore, the choice of the emissivity model is important to get the column's realistic response.

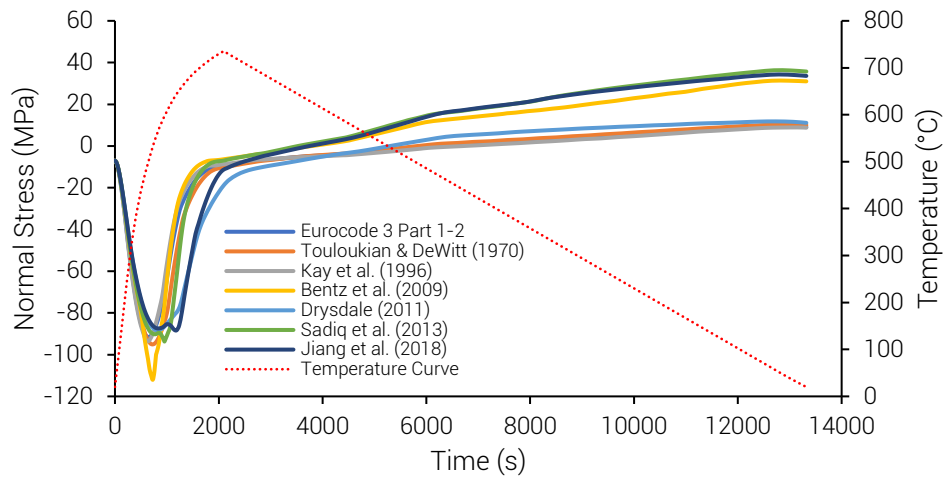


Figure 4-23. Evolution of the normal stress in the specified point of the column under parametric curve heating.

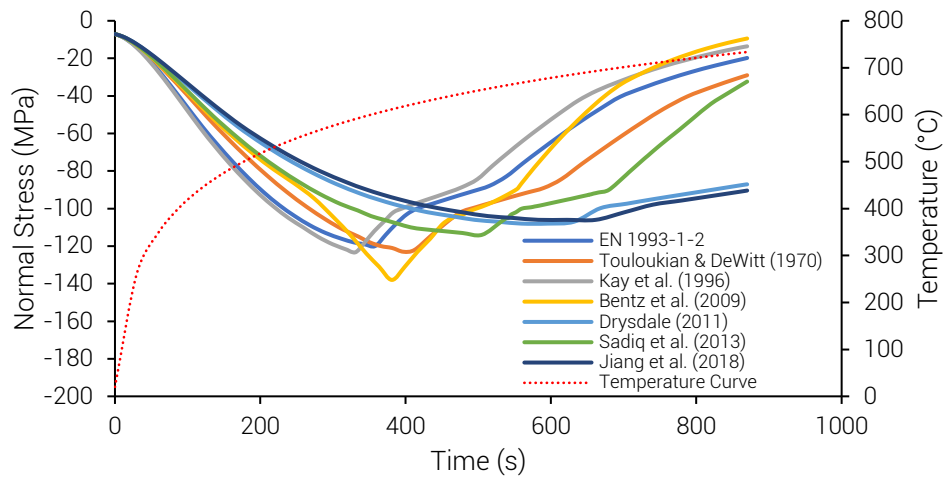


Figure 4-24. Evolution of the normal stress in the specified point of the column under ISO 834 standard curve heating.

Generally, for uniform heating, the impact of temperature-dependent emissivity on the mechanical response of structural members, although clearly significant, varied. For the beam under parametric curve heating, the Eurocode underestimated the maximum stress. For the beam under ISO 834 standard curve heating, the maximum stress did not vary that much but Eurocode produced the highest stress. For the column exposed to both curves, the effect of temperature-dependent emissivity varied according to the model used. Unlike the temperature where it was clear that using temperature-dependent emissivity gives lower surface temperatures, its effect on the mechanical response cannot be generalized especially because other material properties also play a major role.

4.2.2 Case 2: Localized Heating

The behaviour of a column engulfed in a localized fire (Case 1—Scenario 1) is the same as that of a column exposed to uniform heating except that it has no portion along its length which has same temperature distribution. The point of comparison was taken above the support where the heat loss was at its minimum. The stress evolution at this point is presented in Fig. 4-25. During the growth phase, the maximum values did not vary that much and most emissivity models produced higher stress compared to the Eurocode. This is in contrary to what happened in the decay phase where the Eurocode produced a higher stress.

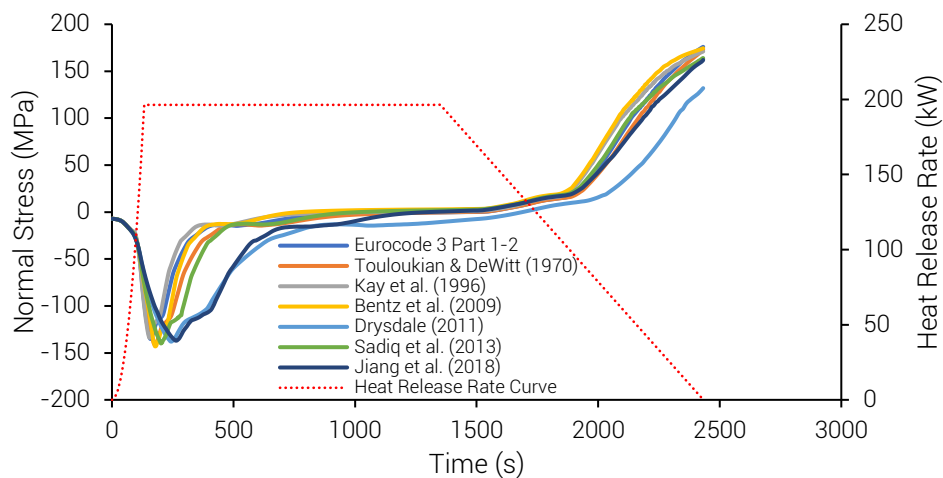


Figure 4-25. Evolution of the normal stress in the specified point of the column (Case 2—Scenario 1).

For the column distant from the fire (Case 2—Scenario 2), the location of the maximum stress was found at the web, between the column axis and the exposed flange. The cross section containing that point was found at the same level where the maximum surface temperature was recorded. The stress evolution of parts of this section can be seen in Fig. 4-26. Generally, the whole flange was free to expand due to its high temperature which barely changed the stress in the middle point of the exposed flange. However, as described in the previous section, the high temperature was recorded at the edge of the flange. Because of that, this part wanted to expand more but is being restrained by the rest of the flange, hence, the compression. The effect of this expansion in the flange caused the web, with a lower temperature to be stretched, hence, the tension. This point in the flange was chosen for comparison and its stress evolution is presented in Fig. 4-27. The graph shows that, except for the Kay et al. (1996) model, temperature-dependent emissivity resulted to lower stress.

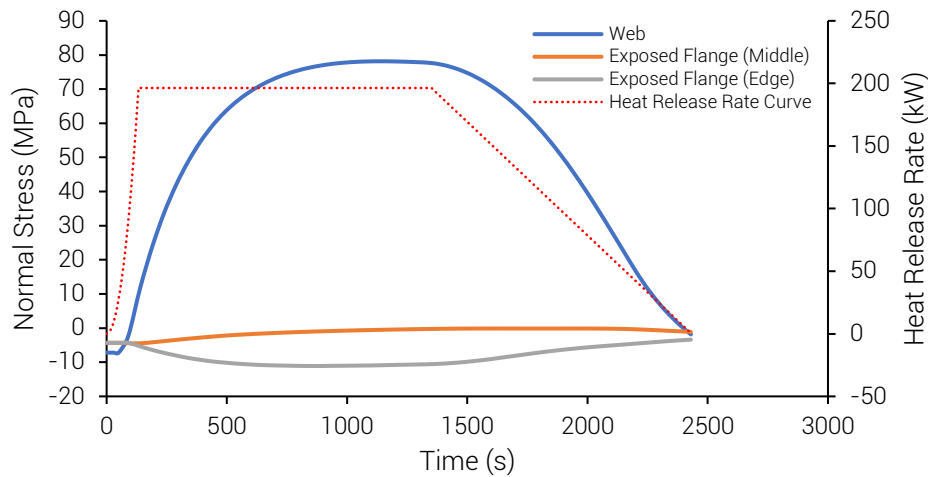


Figure 4-26. Normal stress at different points across the cross section of the column (Case 2–Scenario 2).

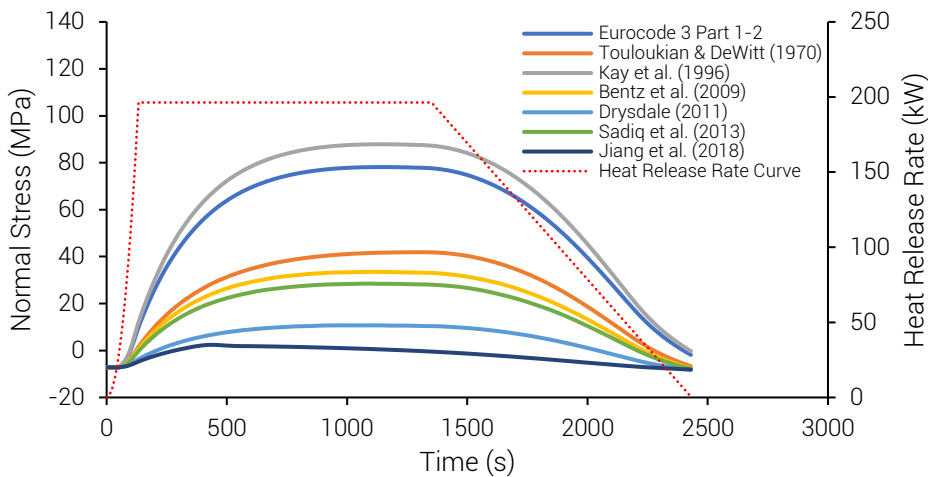


Figure 4-27. Evolution of the normal stress in the specified point of the column (Case 2–Scenario 2).

In the case of the beam directly above the localized fire (Case 2–Scenario 3), the point of maximum stress was found at the web. The explanation for this, during the initial stage, is the same as that of the beam exposed to the ISO 834 standard curve. During the decay stage, it did not undergo the development of tension experienced by the beam under parametric curve heating because it was exposed to much lower temperatures and shorter fire duration. The evolution of the stress at this point is shown in Fig. 4-28. It can be seen that the Eurocode underestimated the stress compared to most emissivity models after the stress reversal. However, the maximum stress in compression were approximately the same for all models.

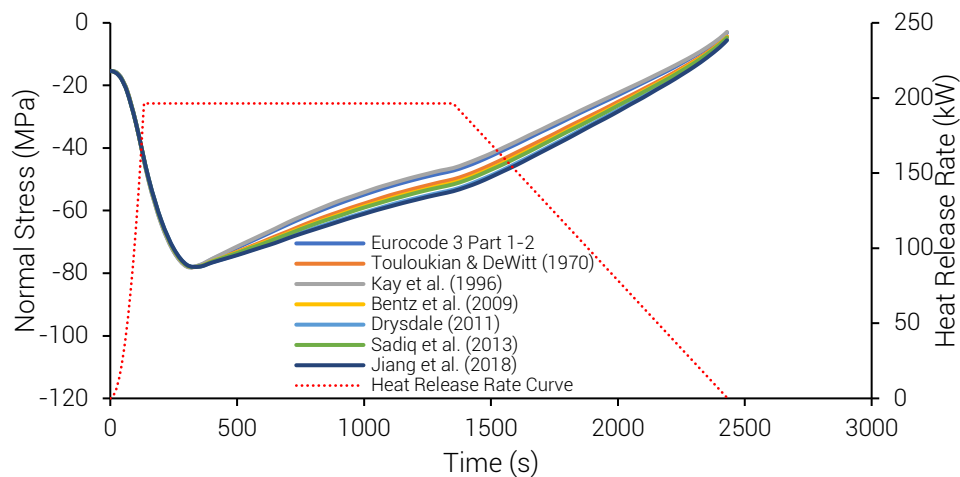


Figure 4-28. Evolution of the normal stress in the specified point of the beam (Case 2–Scenario 3).

In general, the impact of temperature-dependent emissivity on the stress of structural members exposed to a localized fire is significant but varied. For the column engulfed in the localized fire, Eurocode overestimated the tension stress while it underestimated the compression stress. For the column distant from the fire, the Eurocode overestimated the stress throughout the whole duration of the fire. For the beam directly above the fire, the maximum stress was approximately the same for all models but during the steady state and decay phases of the fire, the Eurocode underestimated the stress. Same as with the uniform heating, the impact of temperature-dependent emissivity on the mechanical response of structural members exposed to localized heating cannot be generalized.

4.3 Deflection

Same with the stress, the impact of temperature-dependent emissivity on the deflection is also a direct implication of the member's temperature. In the design of a structural member, the deflection is used as a measure of the serviceability. For the purpose of this section, the deflection along the vertical direction will be assessed except for the column distant from the fire because this case deformed more horizontally than vertically.

4.3.1 Case 1: Uniform Heating

The deformed shape of the beam exposed to both parametric and ISO 834 standard curve during the timestep when the resultant deformation was as its maximum superimposed

with the undeformed shape is presented in Fig. 4-29. Because the beam is simply supported, it was able to expand laterally. Additionally, the temperature increase reduced the strength of the material which made it deflect more vertically.

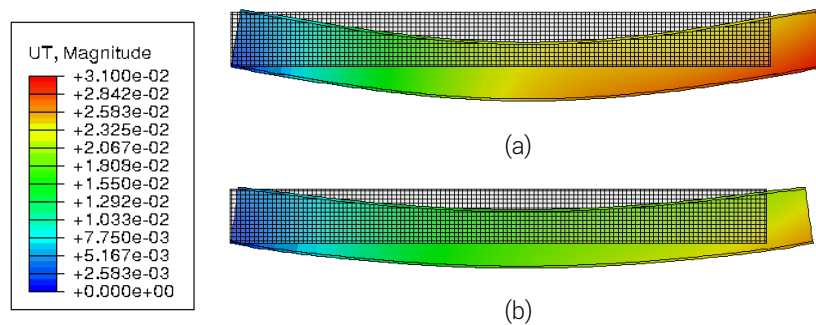


Figure 4-29. Deformed shape of the beam (scaled 10×): (a) parametric curve at $t = 2212$ s and (b) ISO 834 standard curve at $t = 870$ s. The legend is in m.

The midspan deflection was taken and presented in Fig. 4-30. The graphs reveal that the impact of temperature-dependent emissivity was not consistent along the duration of the fire. In the case of the parametric curve, during the growth phase of the fire characterized by sudden increase in temperature, the effect was inconsistent. However, during the gradual temperature decrease during the decay phase, it was found that deflection based on the Eurocode is higher than most of the emissivity models except for Kay et al. (1996) and Bentz et al. (2009) models. This was also the case for the maximum deflection. On the other hand, in the case of the ISO 834 standard curve, it was also inconsistent throughout the whole duration. In terms of the maximum deflection, the Eurocode had a lower value except for Drysdale (2011) and Jiang et al. (2018) models.

In the case of the column under uniform heating, it was only expanding along the vertical direction because both static and thermal loads were applied symmetrically. The deformed shape of the column at the timestep when the maximum deflection was recorded is shown in Fig. 4-31. The deflection evolution of the section on top of the column can be seen in Fig. 4-32. In the case of the parametric curve, the effect was not consistent throughout the whole duration. However, in terms of the maximum deflection, the Eurocode slightly overestimated it except when compared to the Kay et al. (1996) and Bentz et al. (2009) models. In case of the ISO 834 standard curve, the same with the parametric curve was observed.

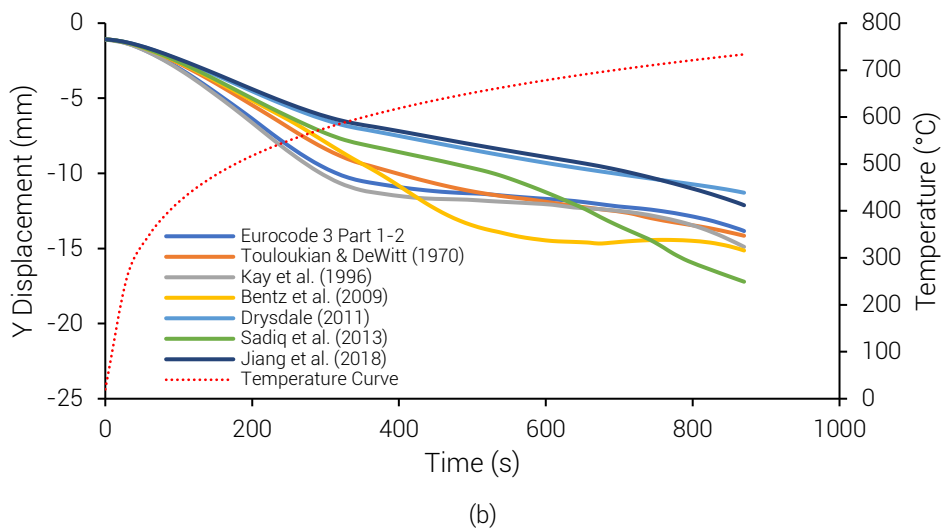
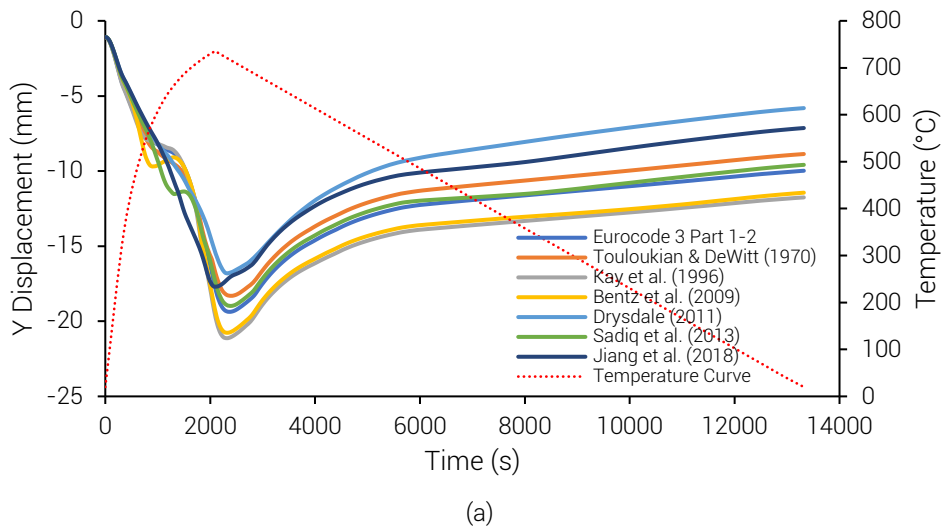


Figure 4-30. Evolution of the vertical deflection of the beam midspan: (a) parametric curve and (b) ISO 834 standard curve.

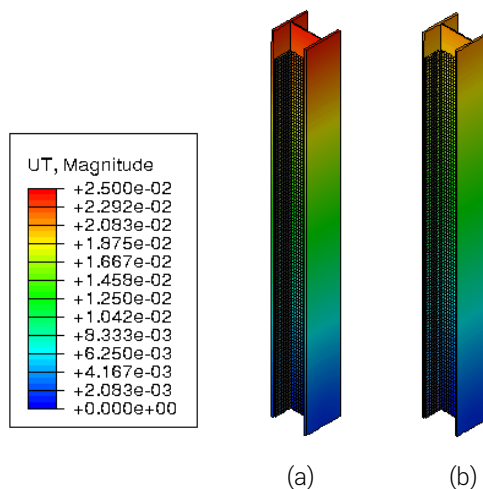


Figure 4-31. Deformed shape of the column (scaled 10x): (a) parametric curve at $t = 2292$ s and (b) ISO 834 standard curve at $t = 870$ s. The legend is in m.

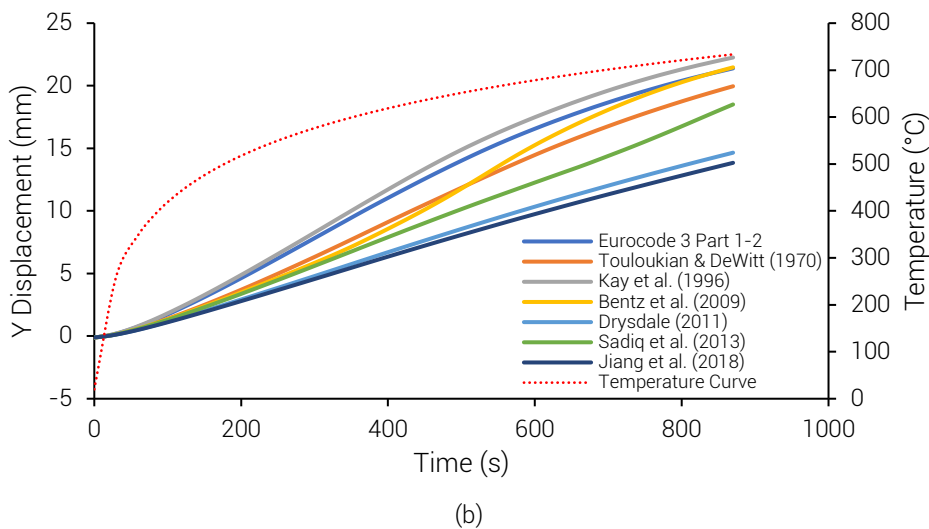
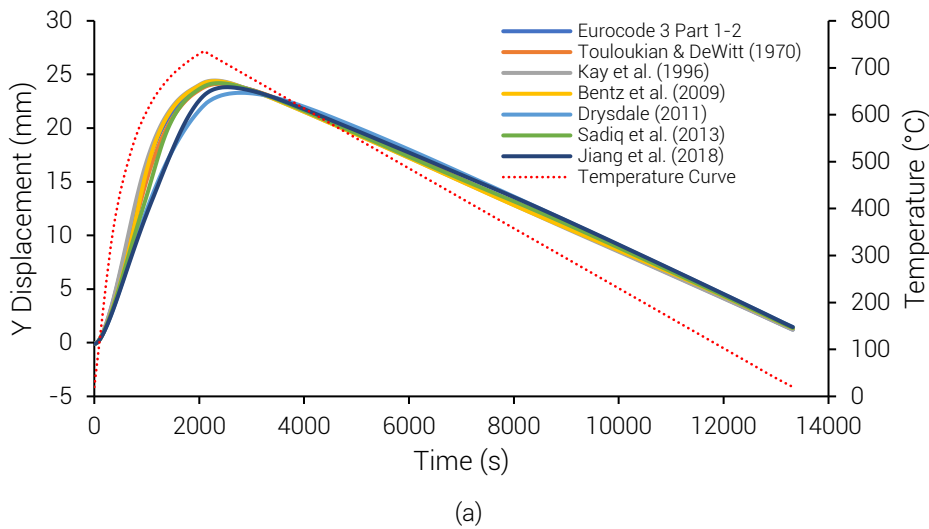


Figure 4-32. Evolution of the vertical deflection of the column top section: (a) parametric curve and (b) ISO 834 standard curve.

The impact of temperature-dependent emissivity on members exposed to uniform heating cannot be generalized. However, it was clear that it is significant. In most of the scenarios, the Eurocode overestimated the value of the maximum deflection.

4.3.2 Case 2: Localized Heating

The deformed shape of the column engulfed by the fire and distant from the fire is shown in Fig. 4-33. The timesteps were chosen as the time when the maximum resultant deflections were recorded. It can be noticed that the lower part of the engulfed column expanded, which made it appear bigger than the rest of the column, due to the high heat flux. On the other hand, due to the high heat flux on one portion of the column distant from the fire, it bent away from the fire as a result of the expansion of that portion. However, despite the fire-

engulfed column being exposed to higher heat fluxes, it can be seen that the column distant from the fire deflected more. This indicates that even if distant fires produce lower heat fluxes, the asymmetrical application of these heat fluxes can result to higher deflections which can be detrimental to the structure.

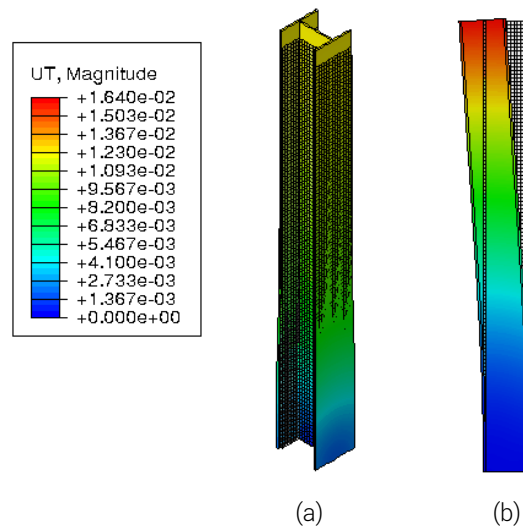


Figure 4-33. Deformed shape of the column (scaled 10×): (a) engulfed by the fire at $t = 1396$ s and (b) distant from the fire at $t = 1590$ s. The legend is in m.

The deflection evolution of the fire-engulfed column top surface can be seen in Fig. 4-34. The maximum deflection was almost the same for all models. However, the Eurocode overestimated, with the exception of Kay et al. (1996) and Bentz et al. (2009) models, the deflection during the growth phase and steady state burning but the final deflection was underestimated.

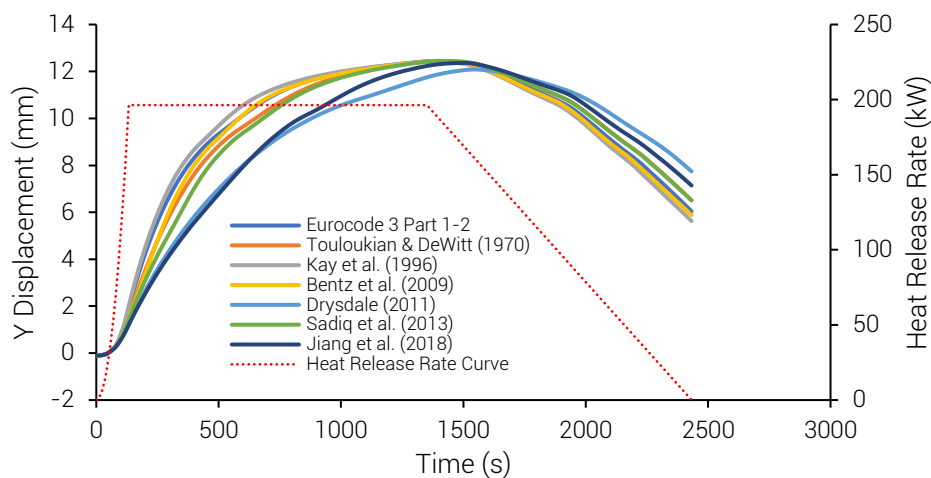


Figure 4-34. Evolution of the vertical deflection of the column top section (Case 2—Scenario 1).

For the column distant from the fire, the deflection evolution is shown in Fig. 4-35. With the exception of the Kay et al. (1996) model, the Eurocode overestimated the deflection throughout the whole duration of the fire.

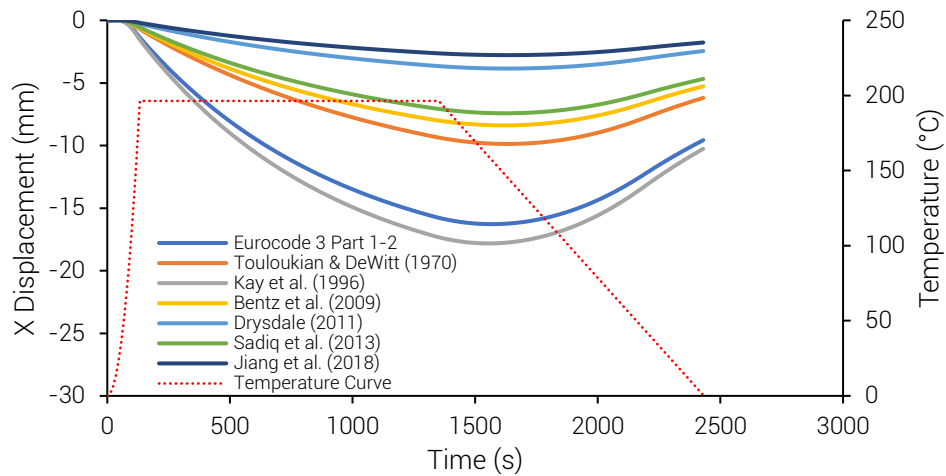


Figure 4-35. Evolution of the horizontal deflection of the column top section (Case 2—Scenario 2).

The deformed shape of the beam above the fire is presented in Fig. 4-36. The vertical deflection of the midspan was compared for all models and shown in Fig. 4-37. It can be seen that maximum deflection was approximately the same for all models but the final deflection was underestimated by the Eurocode except for the Kay et al. (1996) model.

Same as with the uniform heating, the effect of temperature-dependent emissivity, however significant, cannot be generalized for a localized fire. In the cases of the column engulfed by the fire and the beam engulfed by the smoke, it was observed that the maximum deflection was almost the same for all models while the final deflection was underestimated by the Eurocode for most models. In the case of the column distant from the fire, the Eurocode overestimated the deflection.

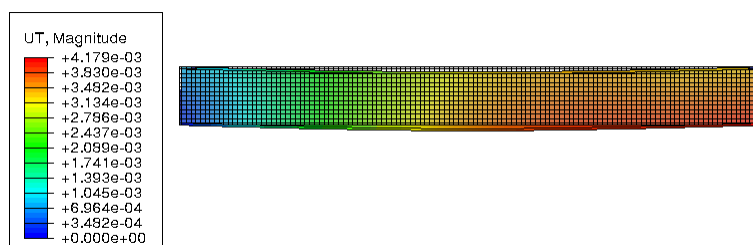


Figure 4-36. Deformed shape of the beam above the localized fire (scaled 10 \times) at $t = 1401$ s.

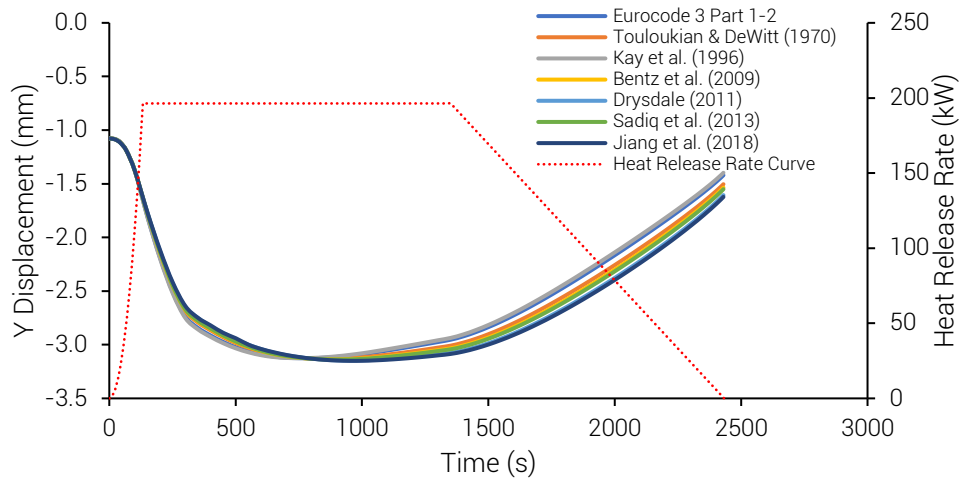


Figure 4-37. Evolution of the vertical deflection of the beam midspan (Case 2—Scenario 3).

4.4 Quantitative Comparison of the Impact of Temperature-dependent Emissivity

4.4.1 Temperature

As shown in the previous sections, the time when the maximum temperature occurs does not necessarily mean that that time is the same as when other parameters is at their extremum. To quantify the effect of the emissivity models in the temperature, the timestep when the huge variation happened was taken using visual estimation. The results of the models were then averaged and compared to the result obtained using the Eurocode. With the Eurocode as the control variable, the percent error was calculated and is shown in Table 4-1.

It can be seen that, on average, the surface temperature based on temperature-dependent emissivity is lower than that of the Eurocode. The difference was found to be as high as 43.09%. However, there was also an instance when the temperature was higher than that of the Eurocode at 9.33%. This observation belongs to the case when the effect of an intervening medium was considered. Although not enough evidence can be used to draw a conclusion from this, based on the results, the case when there is no intervening medium between the radiation source and the surface yields lower surface temperatures relative to that of the Eurocode. Therefore, same as with temperature-dependent emissivity, the proper treatment of heat transfer should also be accounted.

Table 4-1. Comparison of the effect of temperature-dependent emissivity on the surface temperature.

Case	Time (s)	Temperature (°C)		% Error
		Eurocode	Temperature-dependent	
Case 1: Beam—Parametric	870	501.80	461.80	-7.97%
Case 1: Beam—ISO 834	500	541.42	462.15	-14.64%
Case 1: Column—Parametric	1000	518.60	470.44	-9.29%
Case 1: Column—ISO 834	600	547.35	458.95	-16.15%
Case 2—Scenario 1	250	641.77	509.90	-20.55%
Case 2—Scenario 2	1640	190.63	108.49	-43.09%
Case 2—Scenario 3	2430	91.30	99.82	9.33%

*Negative percentage means the value is lower than the hypothesized value.

4.4.2 Stress

As mentioned in Section 4.2, structural members are designed based on the maximum stress they experience. It was seen throughout the duration of the fire that huge stress variations could be observed at different timesteps. However, stress variation at the same timestep has little significance compared to maximum stress throughout the fire duration because the member will ultimately be designed for the latter. The average maximum stress recorded in each case can be seen in Table 4-2.

Table 4-2. Comparison of the effect of temperature-dependent emissivity on the maximum stress.

Case	Maximum Stress (MPa)		% Error
	Eurocode	Temperature-dependent	
Case 1: Beam—Parametric	149.00	162.50	-9.06%
Case 1: Beam—ISO 834	-181.00	-175.88	2.83%
Case 1: Column—Parametric	-91.50	-95.13	-3.97%
Case 1: Column—ISO 834	-120.00	-118.67	1.11%
Case 2—Scenario 1	176.00	162.75	7.53%
Case 2—Scenario 2	78.15	34.14	56.31%
Case 2—Scenario 3	-77.80	-77.85	-0.06%

*Negative percentage means the value is lower than the hypothesized value.

The data reveals that no generalization can be drawn about the effect of temperature-dependent emissivity on the maximum stress of a member. Despite an overestimation by the Eurocode as high as 56.31%, there is also an underestimation as low as 9.06%. Had the results just favoured the overestimation by the Eurocode, it can be seen as just overdesign and, therefore, is not detrimental to the structural integrity. However, the results also show that using a constant emissivity could also lead to under-design. This reiterates more the importance of using temperature-dependent emissivity as its impact on the determination of stress varies immensely according to the structural system and the heating scenario.

4.4.3 Deflection

Two deflection parameters were used to compare the impact of temperature-dependent emissivity. The first one is the maximum deflection as this is related to the maximum stress and the subsequent damage that this can induce into other members connected to the exposed member. The second one is the final deflection as this is related to the permanent deformation of the structure after the fire which can affect its serviceability. The average maximum deflection and final deflection are tabulated in Table 4-3 and Table 4-4, respectively.

Table 4-3. Comparison of the effect of temperature-dependent emissivity on the maximum deflection.

Case	Maximum Deflection (mm)		% Error
	Eurocode	Temperature-dependent	
Case 1: Beam—Parametric	-19.37	-18.94	2.25%
Case 1: Beam—ISO 834	-13.84	-14.13	-2.11%
Case 1: Column—Parametric	24.25	24.04	0.87%
Case 1: Column—ISO 834	21.39	18.45	13.75%
Case 2—Scenario 1	12.43	12.36	0.55%
Case 2—Scenario 2	-16.27	-8.36	48.65%
Case 2—Scenario 3	-3.12	-3.14	-0.64%

Table 4-4. Comparison of the effect of temperature-dependent emissivity on the final deflection.

Case	Final Deflection (mm)		% Error
	Eurocode	Temperature-dependent	
Case 1: Beam—Parametric	-9.98	-9.10	8.82%
Case 1: Beam—ISO 834	-13.84	-14.13	-2.11%
Case 1: Column—Parametric	1.23	1.36	-10.43%
Case 1: Column—ISO 834	21.39	18.45	13.75%
Case 2—Scenario 1	6.04	6.57	-8.75%
Case 2—Scenario 2	-9.57	-5.10	46.67%
Case 2—Scenario 3	-1.42	-1.54	-8.10%

The results generally favoured the trend that the Eurocode overestimated the maximum deflection to as high as 48.65%. On the other hand, no generalization can be made for the final deflection as the results varied from an overestimation of 46.67% to an underestimation by 10.43%. This fluctuation of results stresses again the importance of temperature-dependent emissivity.

5 CONCLUSIONS

In the event of a fire, the effect of radiation dominates the heat transfer. Most building codes around the world does not properly account for this except for the Eurocode which was found to use a wrong formulation. Several studies had been done to properly model the most important property in radiant heat transfer—emissivity. This property differs according to the topographical, chemical, and physical characteristics of the material surface. The different temperature-dependent emissivity models exhibit huge variation relative to each other which captured a wide range of possible results. Employing these models to determine the thermomechanical response of steel members under uniform and localized heating led to the following conclusions:

- Using a constant value of emissivity from the Eurocode overestimated the surface temperature by as high as 43.09%. This is because a higher portion of the incident heat flux was absorbed by the surface as a result of a higher emissivity throughout the duration of the fire. However, when an intervening medium is present such as smoke, the portion of the incident heat flux to the surface was minimized by the emissivity and transmissivity of the smoke while the heat emitted by the surface remained large due to the high emissivity. This led to the Eurocode underestimating the surface temperature by 9.33%.
- In terms of maximum normal stress, the prediction by the Eurocode ranged from an overestimation of 56.31% to an underestimation of 9.06%. Therefore, it cannot be generalized that using a temperature-dependent emissivity would always mean savings in overall construction costs. However, this variability of results stresses the importance of using a more accurate value of this material property.
- The points of maximum temperature did not necessarily coincide with the points of maximum stress. Majority of the cases showed that relaxation of occurred at these points. However, the relaxation was possible only because, in this study, the support conditions are unrestrained such that the members are free to move. In real life structures, this is not always the case.
- For maximum deflection, the results generally showed that the Eurocode overestimated it by as much as 48.65%. On the other hand, the final deflection results revealed a varying effect ranging from an overestimation of 46.67% to an underestimation of 10.43%.

- Despite the possibility of underestimation of the different parameters by the Eurocode, more instances of overestimation were observed characterized by higher discrepancy compared to the hypothesized value from the Eurocode.

Unlike yield strength or elastic modulus, emissivity is one of the material properties with a disaster-specific application. However, it was found that its effect on the thermomechanical response of steel members is huge. An appropriate treatment of this property by the use of equations that more accurately model its behaviour translates into better design and assessment of structures exposed to fire.

6 RECOMMENDATIONS

Due to the large differences in the models found in literature, further research about temperature-dependent steel emissivity should be done using a wide range of samples taken from different manufacturers. Additionally, since emissivity is largely affected by the characteristics of the steel surface, models differentiated according to the degree of polish, oxidation, and roughness should be made so that it would be easy for the user to choose the appropriate model.

A huge part of structural fire safety engineering lies on proper treatment of the heat transfer phenomenon. It is, therefore, highly recommended to improve the simplifications done in this study. For instance, the effect of temperature-dependent convective heat transfer coefficient could also be done. Similarly, heat transfer is also affected by the geometry of the member and the configuration of the compartment. This study can be further improved by using a coupled computational fluid dynamics and structural analysis software to more accurately model heat transfer especially the complex radiation transport equation.

The use of an unprotected steel's emissivity is used in the initial design of the member to determine the amount of passive fire protection to be applied. Usually, steel members, if not insulated, are painted with anti-rust or intumescent paint and remain in that condition for the rest of their service lives. The effect of the temperature-dependent emissivity of these materials could also be investigated. However, the author recognizes that paints come in different colours which is a major factor in their radiative behaviour. Additionally, elevated temperatures could burn paints causing them to be chipped off from the surface and this could also be looked into.

Regarding the structural members, this study made use of beams and columns in isolation and relatively simpler support conditions. Application of temperature-dependent emissivity and determination of the response of members as part of an actual frame structure is also recommended. Moreover, a structural member is only as strong as its support. Investigating the effect of temperature-dependent emissivity on steel connections could also be studied.

REFERENCES

- ABCB. (2019). *National Construction Code* (Vol. 1). Canberra: Australian Building Codes Board.
- AISC. (2005). *AISC 325-05 Steel construction manual* (13th ed.). American Institute of Steel Construction.
- AS. (1998). *AS 4100-1998 Steel structures*. Sydney: Standards Australia.
- AS. (2014). *AS 1530.4:2014 Methods for fire tests on building materials, components and structures - Part 4: Fire-resistance tests for elements of construction*. Sydney: Standards Australia.
- ASCE. (2005). *Standard calculation methods for structural fire protection*. Reston: American Society of Civil Engineers.
- ASEP. (2015). *National Structural Code of the Philippines 2015* (7th ed.). Quezon City: Association of Structural Engineers of the Philippines.
- ASTM International. (2012). *E119-12a: Standard test methods for fire tests of building construction and materials*. ASTM International. <https://doi.org/10.1520/E0119-18CE01>. These
- Bentz, D. P., Hanssen, L. M., & Wilthan, B. (2009). Thermal performance of fire resistive materials III. Fire test on a bare steel column. *NISTIR 7576*. <https://doi.org/10.6028/NIST.IR.7576>
- Beyler, C. L. (2016). Fire hazard calculations for large, open hydrocarbon fires. In M. J. Hurley (Ed.), *SFPE Handbook of Fire Protection Engineering* (5th ed., pp. 2591–2663). New York: Springer.
- BFP. (2003). *Fire Code of the Philippines*. Manila: Bureau of Fire Protection.
- BIS. (2007). *IS 800:2007 General construction in steel - Code of practice*. New Delhi: Bureau of Indian Standards.
- BIS. (2016). *National Building Code of India 2016*. New Delhi: Bureau of Indian Standards.
- BSI. (1999). *BS EN 1363-1:1999 Fire resistance tests - Part 1: General requirements*. London: British Standard Institution.
- BSI. (2009). *BS 476-10:2009 Fire tests on building materials and structures –*
- Buchanan, A. H., & Abu, A. K. (2017). *Structural design for fire safety* (2nd ed.). Chichester: John Wiley & Sons, Inc.
- Building Authority. (1996). *Code of Practice for Fire Resisting Construction 1996*. Hong Kong: Building Authority.
- CEN. (2002a). *Eurocode - Basis of structural design*. Brussels: European Committee for Standardization.
- CEN. (2002b). *Eurocode 1: Actions on structures - Part 1-2: General actions – Actions on structures exposed to fire*. Brussels: European Committee for Standardization.
- CEN. (2002c). *Eurocode 1 - Actions on structures - Part 1-1: General actions – Densities, self-weight, imposed loads for buildings*. Brussels: European Committee for Standardization.
- CEN. (2005a). *Eurocode 3: Design of steel structures - Part 1-1: General rules and rules for buildings*. Brussels: European Committee for Standardization. [https://doi.org/\[Authority: The European Union Per Regulation 305/2011, Directive 98/34/EC, Directive 2004/18/EC\]](https://doi.org/[Authority: The European Union Per Regulation 305/2011, Directive 98/34/EC, Directive 2004/18/EC])

- CEN. (2005b). *Eurocode 3: Design of steel structures - Part 1-2: General rules – Structural fire design*. Brussels: European Committee for Standardization.
- de Ris, J. (1979). Fire radiation—a review. *Symposium (International) on Combustion*.
[https://doi.org/10.1016/S0082-0784\(79\)80097-1](https://doi.org/10.1016/S0082-0784(79)80097-1)
- DPWH. (1972). *The National Building Code*. Manila: Department of Public Works and Highways. Retrieved from
http://www.dpwh.gov.ph/dpwh/sites/default/files/laws_codes_orders/PD_1096_BASIC_LAW_%28book%20format%29.pdf
- Drysdale, D. (2011). *An introduction to fire dynamics* (3rd ed.). West Sussex: John Wiley & Sons, Ltd.
- Duran, B. I. A. (2013). Galvanized steel's performance in extreme temperatures. Retrieved April 9, 2019, from <https://galvanizeit.org/education-and-resources/resources/technical-faq-dr-galv/galvanized-steels-performance-in-extreme-temperatures>
- Duthinh, D. (2014). Structural design for fire : A Survey of building codes and standards. *NIST Technical Note 1842*. <https://doi.org/http://dx.doi.org/10.6028/NIST.TN.1842>
- Edwards, D. K., & Matavosian, R. (2009). Scaling rules for total absorptivity and emissivity of gases. *Journal of Heat Transfer*, *106*(4), 684. <https://doi.org/10.1115/1.3246739>
- Gardner, L., & Ng, K. T. (2006). Temperature development in structural stainless steel sections exposed to fire. *Fire Safety Journal*, *41*(3), 185–203.
<https://doi.org/10.1016/j.firesaf.2005.11.009>
- Ghojel, J. I., & Wong, M. B. (2005). Heat transfer model for unprotected steel members in a standard compartment fire with participating medium. *Journal of Constructional Steel Research*, *61*(6), 825–833. <https://doi.org/10.1016/j.jcsr.2004.11.003>
- Gillie, M. (2009). Analysis of heated structures: Nature and modelling benchmarks. *Fire Safety Journal*, *44*(5), 673–680. <https://doi.org/10.1016/j.firesaf.2009.01.003>
- Guo-wei, Z., Guo-qing, Z., & Li-li, H. (2014). Temperature development in steel members exposed to localized fire in large enclosure. *Safety Science*, *62*, 319–325.
<https://doi.org/10.1016/j.ssci.2013.09.006>
- Halliday, D., Resnick, R., & Walker, J. (2011). *Fundamentals of physics* (9th ed.). Hoboken: John Wiley & Sons, Inc.
- Hamerlinck, R., Twilt, L., & Stark, J. W. B. (1990). A numerical model for fire-exposed composite steel/concrete slabs. *10th International Specialty Conference on Cold-Formed Steel Structures - International Specialty Conference on Cold-Formed Steel Structures*. *5*, 115–130.
- Hasegawa, T. (2013). *Introduction to the Building Standard Law*. Tokyo: Ministry of Land, Transport, Infrastructure, and Tourism.
- Hostikka, S. (2003a). Computation of fire emissivity for Eurocode heat transfer equations. *VTT Project Report 10.1.2003*.
- Hostikka, S. (2003b). Computation of net radiative heat flux. *VTT Project Report 10.1.2003*.
- ICC. (2017). *International Building Code*. Country Club Hills: International Code Council.
- Incropera, F. P., Dewitt, D. P., Bergman, T. L., & Lavine, A. S. (2007). *Fundamentals of heat and mass transfer* (6th ed.). Hoboken: John Wiley & Sons, Inc.
- Jiang, J., Main, J. A., Weigand, J. M., & Sadek, F. H. (2018). Thermal performance of composite slabs with profiled steel decking exposed to fire effects. *Fire Safety Journal*, *95*(2018),

25–41. <https://doi.org/10.1016/j.firesaf.2017.10.003>

- Karlsson, B., & Quintiere, J. G. (2000). *Enclosure fire dynamics*. Boca Raton: CRC Press LLC.
- Kay, T. R., Kirby, B. R., & Preston, R. R. (1996). Calculation of the heating rate of an unprotected steel member in a standard fire resistance test. *Fire Safety Journal*, *26*(4), 327–350. [https://doi.org/10.1016/s0379-7112\(96\)00016-1](https://doi.org/10.1016/s0379-7112(96)00016-1)
- Kim, Y., & Worrell, E. (2002). International comparison of CO₂ emission trends in the iron and steel industry. *Energy Policy*, *30*(2002), 827–838. [https://doi.org/10.1016/S0301-4215\(01\)00130-6](https://doi.org/10.1016/S0301-4215(01)00130-6)
- Kloos, M. (2017). Tutorial: Structural fire engineering analysis with Abaqus, using the Gillie benchmark - YouTube. Retrieved February 5, 2019, from <https://www.youtube.com/watch?v=yDJ0mzRLXvQ&t=1456s>
- MBIE. (1992). Building Regulations. New Zealand: Ministry of Business, Innovation, and Employment.
- Modest, M. F. (2013). *Radiative heat transfer* (3rd ed.). New York: Academic Press. <https://doi.org/10.1016/B978-1-85617-635-4.00003-0>
- Mooney, J. (1992). Surface radiant-energy balance for structural thermal analysis. *Fire and Materials*, *16*, 61–66. <https://doi.org/https://doi.org/10.1002/fam.810160203>
- Morfeldt, J., Nijs, W., & Silveira, S. (2015). The impact of climate targets on future steel production - An analysis based on a global energy system model. *Journal of Cleaner Production*, *103*, 469–482. <https://doi.org/10.1016/j.jclepro.2014.04.045>
- Müller, D. B., Wang, T., & Duval, B. (2011). Patterns of iron use in societal evolution. *Environmental Science & Technology*, *45*(1), 182–188. <https://doi.org/10.1021/es102273t>
- Norgate, T. E., Jahanshahi, S., & Rankin, W. J. (2007). Assessing the environmental impact of metal production processes. *Journal of Cleaner Production*, *15*(8–9), 838–848. <https://doi.org/10.1016/j.jclepro.2006.06.018>
- NZS. (1997). *NZS 3404:Part 1:1997 Steel structures standard*. Wellington: Standards New Zealand.
- NZS. (2009). *NZS 3404:Part 1:2009 Steel structures standard - Part 1: Materials, fabrication, and construction*. Wellington: Standards New Zealand.
- Paloposki, T., & Liedquist, L. (2005). Steel emissivity at high temperatures. *VTT - Research Notes 2299*. Retrieved from <http://www.vtt.fi/inf/pdf/>
- Pettersson, O., Magnusson, S. E., & Thor, J. (1976). *Fire engineering design of steel structures. Bulletin 52 of the Division of Structural Mechanics and Concrete Construction, Lund Institute of Technology*. Stockholm: Swedish Institute of Steel Construction. <https://doi.org/10.1002/pse.2260010104>
- Rush, D. (2013). *Fire performance of unprotected and protected concrete filled steel hollow structural sections*. (Doctoral dissertation). The University of Edinburgh.
- Sadiq, H., Wong, M. B., Tashan, J., Al-Mahaidi, R., & Zhao, X.-L. (2013). Determination of steel emissivity for the temperature prediction of structural steel members in fire. *Journal of Materials in Civil Engineering*, *25*(2), 167–173. [https://doi.org/10.1061/\(ASCE\)MT.1943-5533.0000607](https://doi.org/10.1061/(ASCE)MT.1943-5533.0000607)
- SCDF. (2015). *Singapore Fire Safety Engineering Guidelines 2015*. Singapore: Singapore Civil Defence Force. <https://doi.org/10.1161/CIRCIMAGING.112.000277>

- SCDF. (2018). *Code of Practice for Fire Precautions in Buildings 2018*. Singapore: Singapore Civil Defence Force. Retrieved from <http://www.scdf.gov.sg>
- Siegel, R., & Howell, J. R. (1992). *Thermal radiation heat transfer* (3rd ed.). Washington: Hemisphere Publishing Corporation.
- Subramanian, N. (2010). *Steel structures - design and practice*. New Delhi: Oxford University Press.
- Thomas, G., Buchanan, A., & Fleischmann, C. (2008). Structural fire design: The role of time equivalence. *Fire Safety Science*, 5, 607–618. <https://doi.org/10.3801/iafss.fss.5-607>
- Touloukian, Y. S., & DeWitt, D. P. (1970). *Thermal radiative properties: Metallic elements and alloys. Thermophysical Properties of Matter: The TPRC Data Series* (Vol. 7). New York: IFI/Plenum Data Corporation.
- Wang, Z. H., & Tan, K. H. (2008). Radiative heat transfer for structural members exposed to fire: An analytical approach. *Journal of Fire Sciences*, 26(2), 133–152. <https://doi.org/10.1177/0734904107085746>
- Wen, C. Da. (2010). Investigation of steel emissivity behaviors: Examination of Multispectral Radiation Thermometry (MRT) emissivity models. *International Journal of Heat and Mass Transfer*, 53(9–10), 2035–2043. <https://doi.org/10.1016/j.ijheatmasstransfer.2009.12.053>
- Wickström, U. (2016). Methods in predicting temperatures in fire-exposed structures.pdf. In M. J. Hurley (Ed.), *SFPE Handbook of Fire Protection Engineering* (5th ed., pp. 1102–1130). New York: Springer.

APPENDICES

A Design Load

Static Load

The design static loads were determined based on the provisions of Eurocode 1 Part 1-1 (CEN, 2002c). The frame is supporting a variable load of 3.0 kPa corresponding to a Category B occupancy and a permanent load of 3.6 kPa due to the weight of the 150-mm concrete slab with a density of 24 kN/m³. Using the ultimate limit state load combination for structural members based on the provisions of Eurocode 0 (CEN, 2002a),

$$E_d = 1.35G + 1.5Q \quad (\text{A.1})$$

where E_d is the design load, G is the permanent load, and Q is the variable load, the total load to be supported by the frame is approximately 9.4 kPa. It must be noted that for the fire limit state in an office occupancy, the load combination is given as

$$E_d = G + 0.5Q + A_d \quad (\text{A.2})$$

where A_d is the accidental load, i.e., fire. However, to capture the effect of a higher static load, the load calculated using Eq. A.1 equal 9.4 kPa was used. Based on the tributary area, the beam is being subjected to approximately 15 kN/m uniformly distributed load while the column is subjected to 85 kN concentrated load.

Fire Load Density

The fire load density inside the compartment was determined using Annex E of Eurocode 1 Part 1-1. It was calculated using the equation

$$q_{f,d} = q_{f,k} \cdot m \cdot \delta_{q1} \cdot \delta_{q2} \cdot \delta_n \quad (\text{A.3})$$

where $q_{f,d}$ is the design fire load density (MJ/m²), $q_{f,k}$ is the characteristic fire load density per unit floor area (MJ/m²), m is the combustion factor, δ_{q1} is a factor related to fire activation risk due to the size of the compartment, δ_{q2} is a factor related to fire activation risk due to the type of occupancy, and δ_n is a factor related to different active firefighting measures generally imposed for life safety. Table A-1 shows the values of these parameters. The calculated fire load density is equal to 450.8 MJ/m².

Table A-1. Parameters for the calculation of the fire load density.

Parameter	Value	Remarks
q_{fk}	511	80% fractile for office
m	0.8	cellulosic materials
δ_{q1}	1.10	25 m ² compartment
δ_{q2}	1	office occupancy
δ_n	1	no active firefighting measure

B Temperature-time Curves: Parametric and Equivalent ISO 834

Table B-1. Design parameters for the parametric temperature-time curve and equivalent ISO 834 standard curve.

Parameter	Value	Conditions and Remarks	
Enclosure Dimensions (1 Door + 1 Window)			
Length, L [m]	5		
Width, W [m]	5		
Height, H [m]	3		
Floor area, A_f [m ²]	25		
Total area of enclosure including openings, A_t [m ²]	110		
Door height, h_d [m]	2		
Door width, w_d [m]	1		
Window height, h_w [m]	1		
Window width, w_w [m]	1		
Total area of vertical openings, A_v [m ²]	3		
Weighted average of opening heights, h_{eq} [m]	1.67		
Opening factor, O [m ^{1/2}]	0.04	$0.02 \leq O \leq 0.2$	OK
Material Properties of the Enclosure Boundary			
Density, ρ [kg/m ³]	2300		
Specific heat, c [J/kg·K]	880		
Thermal conductivity, λ [W/m·K]	1.40		
$b = \sqrt{\rho c \lambda}$, [J/m ² ·s ^{1/2} ·K]	1683.33	$100 \leq b \leq 2200$	OK
Fire Load			
Density per floor area, $q_{f,d}$ [MJ/m ²]	450.80		
Density per enclosure area, $q_{t,d}$ [MJ/m ²]	102.45	$50 \leq q_{t,d} \leq 1000$	OK
	Reached limit?	NO	
Other Parameters			
$\Gamma = (O/b)^2 / (0.04/1160)^2$	0.37		
Fire Growth Rate	Medium		
t_{lim} [hr]	0.33		
$t_{max} = \max(0.2 \cdot 10^{-3} \cdot q_{t,d} / O; t_{lim})$, [hr]	0.58	Vent-controlled	
$t_{max}^* = t_{max} \cdot \Gamma$, [hr]	0.21		
T_{max} [°C]	735.17		

$t_{max} = t_{lim}?$	NO
$O_{lim} = 0.1 \cdot 10^{-3} \cdot q_{t,d} / t_{lim}$	N/A
$\Gamma_{lim} = (O_{lim} / b)^2 / (0.04 / 1160)^2$	N/A
Apply k multiplier?	NO
Time Step [hr]	0.10
$x = 1.0$ if $t_{max} > t_{lim}$, or $x = t_{lim} \cdot \Gamma / t_{max}$ if $t_{max} = t_{lim}$	1.00

Equivalent Time of Exposure Parameters

Correction factor (enclosure properties), k_b	0.06	
Correction factor (structural properties), k_c	0.48	
$a_v = A_v / A_f$	0.12	OK
$a_h = A_h / A_f$	0	
$b_v = 12.5(1 + 10a_v - a_v^2)$	27.32	OK
Ventilation factor, w_f	1.21	
Equivalent time of exposure, $t_{e,d}$ [s]	869.14	

Conduction to Solid Boundaries

k_{pc} of steel [$W^2 \cdot s / m^4 \cdot K^2$]	1.60E+08
k_{pc} of concrete [$W^2 \cdot s / m^4 \cdot K^2$]	2.00E+06

C Localized Fire Curve

Table C-1. Design parameters for the localized fire curve.

Parameter	Value	Unit
Occupancy	Office	-
Fire Growth Rate	Medium	-
Time to reach HRR of 1 MW, t_a	300	s
Maximum HRR produced by 1 m ² of fire, RHR_f	250	kW/m ²
Fire Diameter, D	1	m
Area of the fire, A_{fi}	0.7854	m ²
Maximum HRR, Q_{max}	196349.5408	W
Time to reach maximum HRR, $t_{Q,max}$	132.9340	s
Time increment, Δt	20	s
Design fire load density, $q_{f,d}$	450.8	MJ/m ²
Total fire load, E_{total}	354.0575	MJ
70% of the total fire load	247.8402	MJ
Time to reach decay, t_{decay}	1350.8627	s
30% of the total fire load	106.2172	MJ
Time to reach burnout, t_{bo}	2432.7827	s
Room height, H_{room}	3	m
Height increment, Δz	0.3	m
Distance from fuel centre to face of column, r	1	m
Beam length, L_{beam}	3	m
Length increment, Δx	0.3	m
R value such that $r/H = 0.18$	0.54	m
<i>Conduction to Solid Boundaries</i>		
$k\rho c$ of steel [W ² ·s/m ⁴ ·K ²]	1.60E+08	[W ² ·s/m ⁴ ·K ²]
$k\rho c$ of concrete [W ² ·s/m ⁴ ·K ²]	2.00E+06	[W ² ·s/m ⁴ ·K ²]

D Benchmarking Procedure for the Software

Gillie (2009) presented the results of the simulation of a simple structure that can be used to verify a software. The structure is a beam with a length of 1 m and dimensions of 35 mm x 35 mm. It is made of elasto-plastic steel with an elastic modulus equal to 207 GPa, coefficient of thermal expansion equal to $1.2 \times 10^{-5} \text{ } ^\circ\text{C}$, and a yield strength which varies linearly from 250 MPa at 0 °C to 0 MPa at 1000 °C. It has a uniformly distributed load of 4250 N/m, and is heated uniformly in a linear manner from 0 °C to 800 °C until half of the time duration and then cooled back in a linear manner to 0 °C until the total time duration. Additionally, the stiffness of the support is equal to 75% of the axial stiffness of the beam. The problem is illustrated in Fig. D-1.

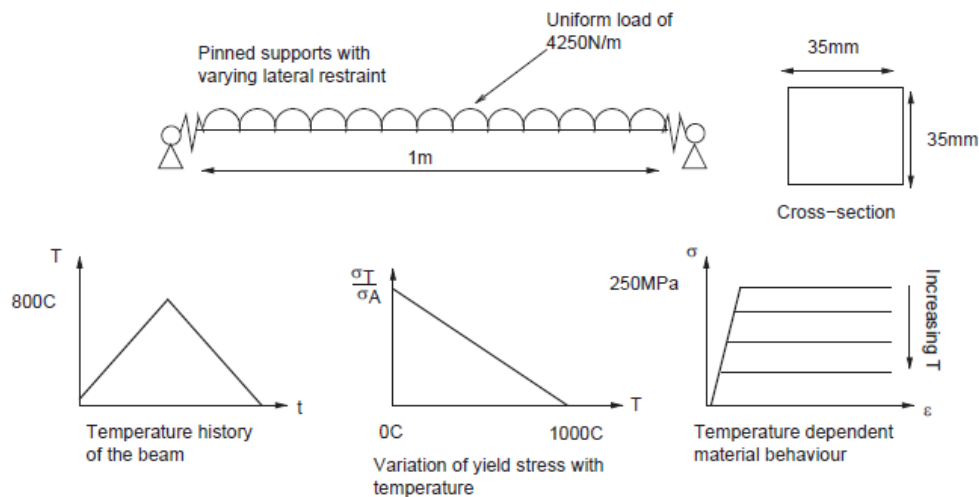
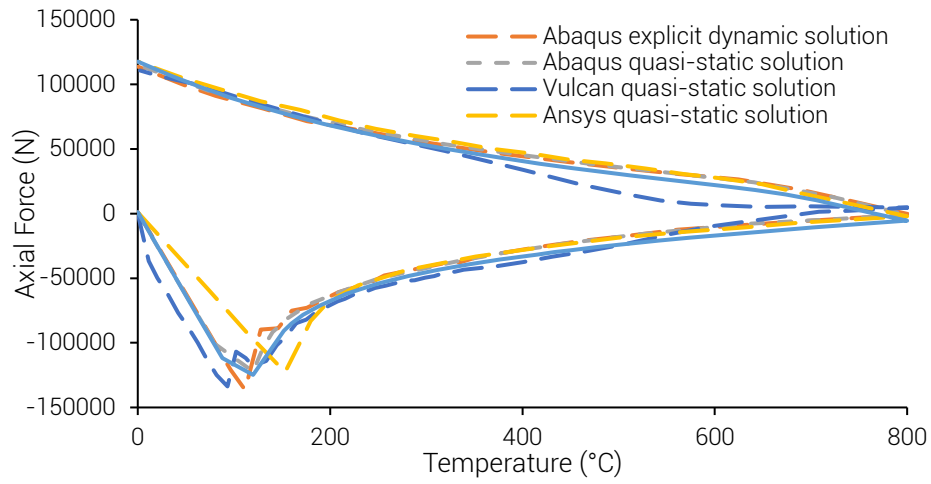
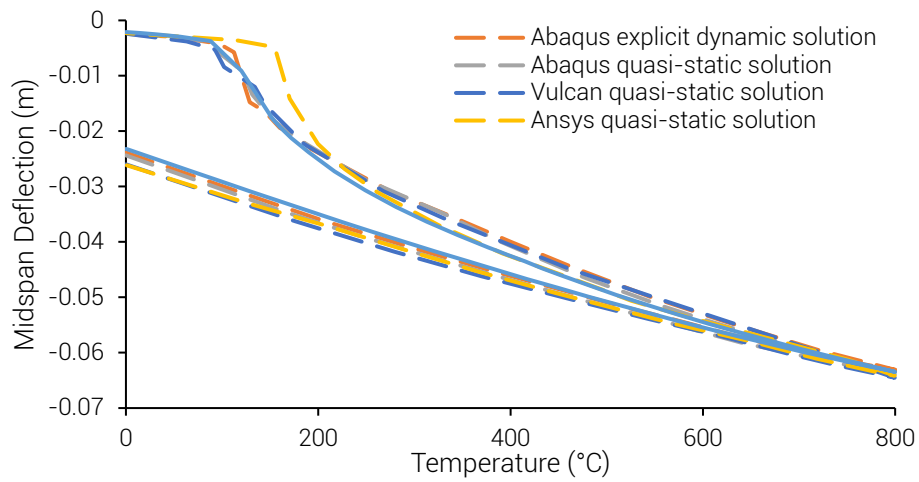


Figure D-1. Problem definition. Adapted from Gillie (2009).

There are several ways to model this problem but this verification was based on a video tutorial by Kloos (2017). The beam was modelled in Abaqus/CAE 2018 as a shell with a thickness of 35 mm. The support condition was achieved by constraining the left and right-hand edges of the shell to two reference points, pinning both supports, and applying a spring to the right support with a stiffness in the direction of the length of the beam. The result of the model benchmarking is shown in Fig. D-2.



(a)



(b)

Figure D-2. Benchmarking results: (a) axial force and (b) midspan deflection.

Figure D-2 shows the axial force and midspan deflection of the model using Abaqus/CAE 2018 in comparison with the results of other software as provided by Gillie (2009). It can be seen that it is in good agreement with other results. This means that the study could proceed with the chosen version of the software.

E Static Model Verification

Simply Supported Beam with 15 kN/m Uniform Load

Properties of IPE 300

Height, $h = 300$ mm

Width, $b = 150$ mm

Flange thickness, $t_f = 10.7$ mm

Web thickness, $t_w = 7.1$ mm

Area, $A = 5188.06$ mm²

Moment of inertia about the neutral axis, $I_{x-x} = 8.00 \times 10^7$ mm⁴

Distance from the extreme fiber to the neutral axis, $c = 150$ mm

Self-weight, $SW = 40.73$ kg/m (based on a 7850 kg/m³ density of steel)

Modulus of elasticity of steel, $E_a = 210$ GPa

Calculation of the Reaction Force

$$w = 15 \times 10^3 \text{ N/m} + (40.73 \text{ kg/m} \times 9.81 \text{ m/s}^2) \\ = 15399.56 \text{ N/m}$$

$$R_y = 15399.56 \text{ N/m} \times (3 \text{ m})/2 \\ = 23099.34 \text{ N}$$

Model: 23129.98 N (OK)

Calculation of the Maximum Bending Stress

$$M = wL^2/8 \\ = [15399.56 \text{ N/m} \times (3 \text{ m})^2]/8 \\ = 17324.51 \text{ N}\cdot\text{m}$$

$$\sigma = Mc/I_{x-x} \\ = (17324.51 \text{ N}\cdot\text{m} \times 0.15 \text{ m})/[(8.00 \times 10^7 \text{ mm}^4) \times (1 \text{ m}/1000 \text{ mm})^4] \\ = 32.48 \times 10^6 \text{ Pa}$$

Model: 32.23×10^6 Pa (OK)

Calculation of the Midspan Deflection

$$\delta = 5wL^4/384E_aI \\ = [5 \times 15399.56 \text{ N/m} \times (3 \text{ m})^4]/[384 \times (210 \times 10^9 \text{ Pa}) \times (8.00 \times 10^7 \text{ mm}^4) \times (1 \text{ m}/1000 \text{ mm})^4] \\ = 9.67 \times 10^{-4} \text{ m}$$

Model: 10.81×10^{-4} m (OK)

Column Fixed at the Base with 85 kN Concentrated Load

Properties of UC 305 × 305 × 97

Height, $h = 307.9$ mm

Width, $b = 305.3$ mm

Flange thickness, $t_f = 15.4$ mm

Web thickness, $t_w = 9.9$ mm

Area, $A = 12146.53$ mm²

Self-weight, $SW = 95.35$ kg/m (based on a 7850 kg/m³ density of steel)

Modulus of elasticity of steel, $E_a = 210$ GPa

Calculation of the Reaction Force

$$R_y = 85 \times 10^3 \text{ N} + (95.35 \text{ kg/m} \times 9.81 \text{ m/s}^2 \times 3 \text{ m}) \\ = 87806.15 \text{ N}$$

Model: 87806.20 N (OK)

Calculation of Maximum Axial Stress

$$\begin{aligned}\sigma &= R_y/A \\ &= 87806.15 \text{ N}/[12146.53 \text{ mm}^2 \times (1 \text{ m}/1000 \text{ mm})^2] \\ &= 72.29 \times 10^5 \text{ Pa}\end{aligned}$$

Model: $72.28 \times 10^5 \text{ Pa}$ (OK)

Calculation of Deflection

$$\begin{aligned}\delta &= PL/AE \\ &= (85000 \text{ N} \times 3 \text{ m})/[12146.53 \text{ mm}^2 \times (1 \text{ m}/1000 \text{ mm})^2 \times (210 \times 10^9 \text{ Pa})] \\ &= 1.00 \times 10^{-4} \text{ m}\end{aligned}$$

Model: $1.02 \times 10^{-4} \text{ m}$ (OK)

F Benchmarking Procedure for the User Subroutines

Case 1: Uniform Heating

The benchmarking of the user subroutine for Case 1 was done only in the beam exposed to the parametric temperature-time curve. This is because all the equations, whether applied to the beam or column, are the same except for the equation of the gas temperature for the scenarios using the ISO 834 standard curve. A sample parametric temperature-time curve user subroutine is shown below followed by a comparison between the results of the Abaqus/CAE 2018 built-in function and the user subroutine in Fig. F-1 for several chosen nodes. It can be seen that the two models have identical results which means that the user subroutine passed the verification.

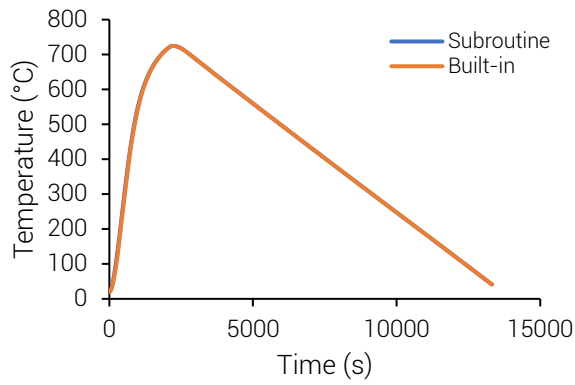
```

SUBROUTINE DFLUX(FLUX,SOL,KSTEP,KINC,TIME,NOEL,NPT,COORDS,
1 JLTYP,TEMP,PRESS,SNAME)
C
C   INCLUDE 'ABA_PARAM.INC'
C
C   DIMENSION FLUX(2), TIME(2), COORDS(3)
C   CHARACTER*80 SNAME
C
C   JLTYP=0
C
C   PARAMETRIC TEMPERATURE-TIME CURVE (EN 1999-1-2 Annex A)
C   !Important parameters are already pre-calculated to simplify this code.
C
C   TG = instantaneous gas temperature in degrees C
C   Tgmax = maximum gas temperature in degrees C
C   t = time in hours
C   tmax = time when Tgmax occurs in hours
C   G = uppercase gamma
C   x = tsmax multiplier in the cooling phase
C
C   !Manually input the value of these parameters.
C       Tmax=0.5820
C       G=0.3679
C       x=1.0
C
C       t=TIME(1)/3600.0
C       ts=t*G
C       tsmax=tmax*G
C
C       Tgmax=20.0+1325.0*(1.0-0.324*EXP(-0.2*tsmax)-0.204*EXP(-1.7*tsmax)-
0.472*EXP(-19.0*tsmax))
C
C       IF (t .LE. tmax) THEN
```

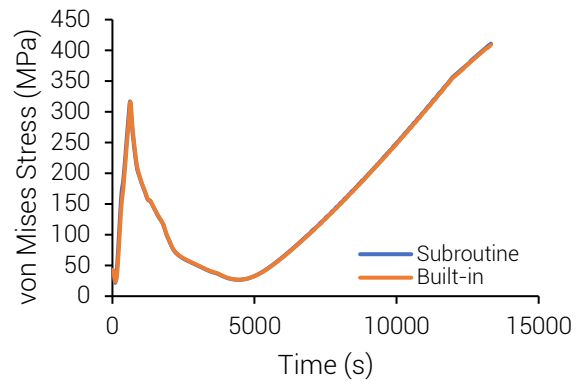
```

TG=20.0+1325.0*(1.0-0.324*EXP(-0.2*ts)-0.204*EXP(-1.7*ts)-0.472*EXP(-19.0*ts))
  ELSE IF (tsmax .LE. 0.5) THEN
    TG=Tgmax-625.0*(ts-tsmax*x)
      ELSE IF (tsmax .GT. 0.5 .AND. tsmax .LT. 2.0) THEN
        TG=Tgmax-250.*(3.0-tsmax)*(ts-tsmax*x)
      ELSE
        TG=Tgmax-250.0*(ts-tsmax*x)
      END IF
  END IF
C
  IF (TG .LT. 20.0) THEN
    TG=20.0
  END IF
C
C TEMPERATURE-DEPENDENT EMISSIVITY MODEL (EN 1993-1-2)
C
C TS = surface temperature in degrees C
C Em = surface emissivity
C
  TS=SOL
  Em=0.7
C
C NET SURFACE HEAT FLUX (Improved EN 1991-1-2 Section 3.1 Formulation by Hostikka
(2003))
C
C hnet = net surface heat flux in W/m^2
C hnetc = net convective heat flux in W/m^2
C hnetr = net radiative heat flux in W/m^2
C Ac = convective heat transfer coefficient = 35 W/m^2/K (EN 1991-1-2 Section 3.3.1.1)
C F = configuration factor = 1 (EN 1991-1-2 Section 3.1(7))
C Em = surface emissivity as defined above
C Ef = emissivity of the fire = 1 (EN 1991-1-2 Section 3.1(6))
C Ea = emissivity of the ambient surroundings
C Ta = temperature of the ambient surroundings
C SBC = Stefan-Boltzmann constant = 5.67*10^-8 W/m^2/K^4
C
  Ac=35.0
  F=1.0
  Ef=1.0
  Ea=1.0
  TA=20.0
  SBC=5.67*(10.0**-8.0)
C
  hnetc=Ac*(TG-TS)
  hnetr=F*Em*Ef*SBC*((TG+273.15)**4.0)+(1.0-F)*Em*Ea*SBC*((TA+273.15)**4.0)-
Em*SBC*((TS+273.15)**4.0)
  hnet=hnetc+hnetr
  FLUX(1)=hnet
C
  RETURN
  END

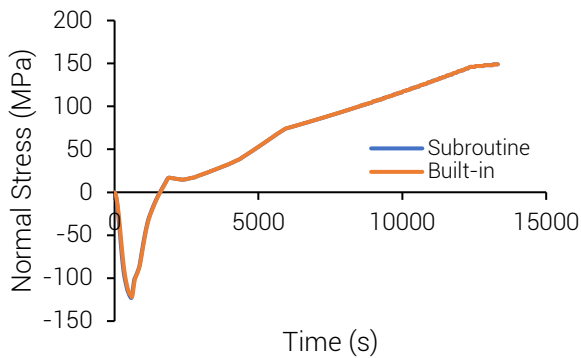
```



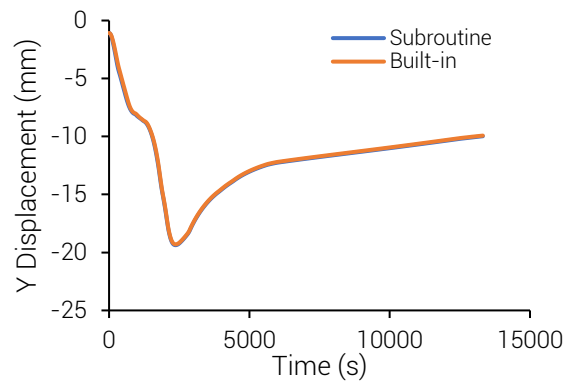
(a)



(b)



(c)



(d)

Figure F-1. Comparison of results for Case 1: (a) temperature, (b) von Mises stress, (c) normal stress, and (d) displacement along y-direction.

Case 2—Scenario 1: Column Fully Engulfed in the Localized Fire

The user subroutine for this scenario is almost the same as with that of Case 1 except for the equations used and that there are multiple heat fluxes. The user subroutine is shown below followed by the comparison of results in Fig. F-2 for several chosen nodes. The identical results signify that the user subroutine passed the verification.

```

SUBROUTINE DFLUX(FLUX,SOL,KSTEP,KINC,TIME,NOEL,NPT,COORDS,
1 JLTYP,TEMP,PRESS,SNAME)
C
C   INCLUDE 'ABA_PARAM.INC'
C
C   DIMENSION FLUX(2), TIME(2), COORDS(3)
C   CHARACTER*80 SNAME
C
C   JLTYP=0
C

```



```

C LOCALIZED FIRE CURVE (EN 1999-1-2 Annex C)
C !Important parameters are already pre-calculated to simplify this code.
C
C D = fuel diameter in m
C Qmax = maximum HRR in W
C Q = instantaneous total HRR in W
C Qc = convective portion of HRR in W
C t = time in s
C ta = time to reach HRR of 1 MW in s
C tQmax = time to reach maximum HRR in s
C tdecay = time to reach decay in s
C tbo = time to reach burnout in s
C fl = length of fire in m
C TG = instantaneous gas temperature in degrees C
C z = height along the flame axis in m
C z0 = virtual origin in m
C H = room height in m
C
C !Manually input the value of these parameters.
C D=1.0
C Qmax=196349.5408
C ta=300.0
C tQmax=132.9340
C tdecay=1350.8627
C tbo=2432.7827
C H=3.0
C
C t=TIME(1)
C
C IF (t .LT. tQmax) THEN
C Q=10.0**6.0*((t/ta)**2.0)
C ELSE IF (t .GE. tQmax .AND. t .LT. tdecay) THEN
C Q=Qmax
C ELSE IF (t .GE. tdecay .AND. t .LT. tbo) THEN
C Q=Qmax*((t-tbo)/(tdecay-tbo))
C ELSE
C Q=0.0
C END IF
C
C Qc=0.8*Q
C fl=-1.02*D+0.0148*(Q**(2.0/5.0))
C z0=-1.02*D+0.00524*(Q**(2.0/5.0))
C
C IF (SNAME .EQ. 'ASSEMBLY_EXPOSED_Y150') THEN
C Z=0.15
C ELSE IF (SNAME .EQ. 'ASSEMBLY_EXPOSED_Y450') THEN
C Z=0.45
C ELSE IF (SNAME .EQ. 'ASSEMBLY_EXPOSED_Y750') THEN
C Z=0.75
C ELSE IF (SNAME .EQ. 'ASSEMBLY_EXPOSED_Y1050') THEN
C Z=1.05
C ELSE IF (SNAME .EQ. 'ASSEMBLY_EXPOSED_Y1350') THEN

```

```

Z=1.35
ELSE IF (SNAME .EQ. 'ASSEMBLY_EXPOSED_Y1650') THEN
Z=1.65
ELSE IF (SNAME .EQ. 'ASSEMBLY_EXPOSED_Y1950') THEN
Z=1.95
ELSE IF (SNAME .EQ. 'ASSEMBLY_EXPOSED_Y2250') THEN
Z=2.25
ELSE IF (SNAME .EQ. 'ASSEMBLY_EXPOSED_Y2550') THEN
Z=2.55
ELSE IF (SNAME .EQ. 'ASSEMBLY_EXPOSED_Y2850') THEN
Z=2.85
END IF

C
TG=20.0+0.25*(Qc**(2.0/3.0))*((Z-z0)**(-5.0/3.0))
C
IF (TG .GT. 900.0) THEN
TG=900.0
END IF

C
C TEMPERATURE-DEPENDENT EMISSIVITY MODEL (EN 1993-1-2)
C
C TS = surface temperature in degrees C
C Em = surface emissivity
C
TS=SOL
Em=0.7

C
C NET SURFACE HEAT FLUX (Improved EN 1991-1-2 Section 3.1 Formulation by Hostikka
(2003))
C
C hnet = net surface heat flux in W/m^2
C hnetc = net convective heat flux in W/m^2
C hnetr = net radiative heat flux in W/m^2
C Ac = convective heat transfer coefficient = 35 W/m^2/K (EN 1991-1-2 Section 3.3.1.1)
C F = configuration factor = 1 (EN 1991-1-2 Section 3.1(7))
C Em = surface emissivity as defined above
C Ef = emissivity of the fire = 1 (EN 1991-1-2 Section 3.1(6))
C Ea = emissivity of the ambient surroundings
C Ta = temperature of the ambient surroundings
C SBC = Stefan-Boltzmann constant = 5.67*10^-8 W/m^2/K^4
C
Ac=35.0
F=1.0
Ea=1.0
TA=20.0
SBC=5.67*(10.0**-8.0)

C
C TEMPERATURE-DEPENDENT EMISSIVITY OF THE SMOKE LAYER (Gou-wei et al.,
2014)
C
IF (Z .GT. fl) THEN
Ef=0.458-1.29*(10.0**-4.0)*TG

```

```

ELSE
Ef=1.0
END IF

```

C

```

hnetc=Ac*(TG-TS)
hnetr=F*Em*Ef*SBC*((TG+273.15)**4.0)+(1.0-F)*Em*Ea*SBC*((TA+273.15)**4.0)-
Em*SBC*((TS+273.15)**4.0)
hnet=hnetc+hnetr
FLUX(1)=hnet

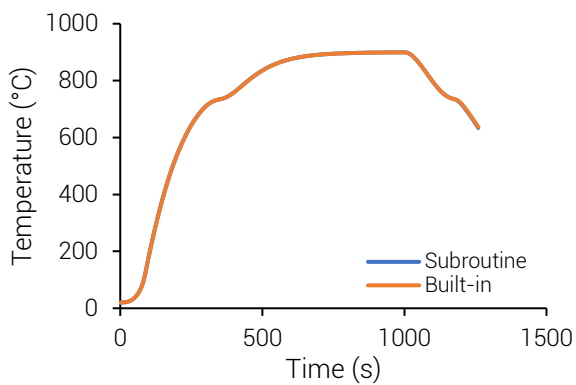
```

C

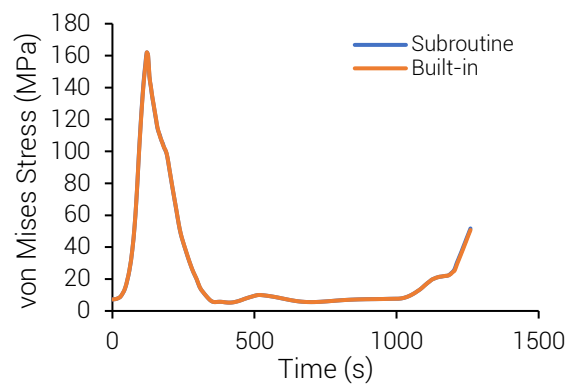
```

RETURN
END

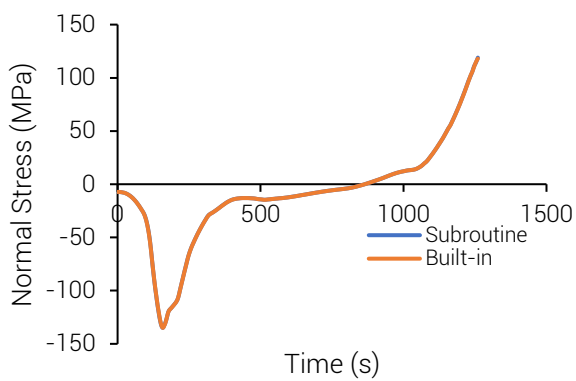
```



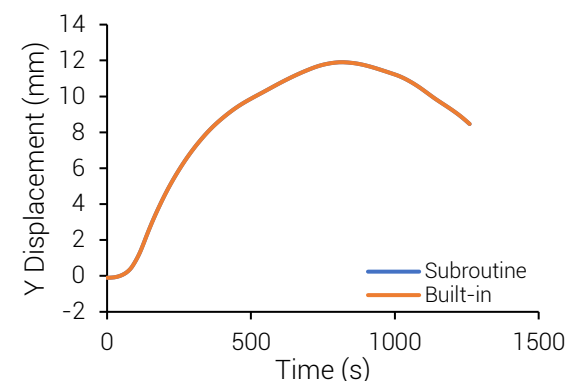
(a)



(b)



(c)



(d)

Figure F-2. Comparison of results for Case 2—Scenario 1: (a) temperature, (b) von Mises stress, (c) normal stress, and (d) displacement along y-direction.

Case 2—Scenario 2: Column at a Distance from the Localized Fire

The user subroutine for Case 2—Scenario is shown below followed by the comparison of results from several chosen nodes in Fig. F-3. The slight differences between the two is because there is no option to input the view factor from the fire. As a result, the radiation

contribution from the ambient surroundings could not be properly modelled. Nonetheless, the differences are small which means that the expected values are within that range. Therefore, the user subroutine passed the verification.

```

SUBROUTINE DFLUX(FLUX,SOL,KSTEP,KINC,TIME,NOEL,NPT,COORDS,
1 JLTYP,TEMP,PRESS,SNAME)
C
C   INCLUDE 'ABA_PARAM.INC'
C
C   DIMENSION FLUX(2), TIME(2), COORDS(3)
C   CHARACTER*80 SNAME
C
C   JLTYP=0
C
C   LOCALIZED FIRE CURVE (EN 1999-1-2 Annex C)
C   !Important parameters are already pre-calculated to simplify this code.
C
C   D = fuel diameter in m
C   Qmax = maximum HRR in W
C   Q = instantaneous total HRR in W
C   t = time in s
C   ta = time to reach HRR of 1 MW in s
C   tQmax = time to reach maximum HRR in s
C   tdecay = time to reach decay in s
C   tbo = time to reach burnout in s
C   fl = length of fire in m
C   Z = height along the flame axis in m
C   aL = horizontal distance from the center of the fire to the face of the column in m
C   Hii = height of the cylinder in m
C
C   !Manually input the value of these parameters.
C   D=1.0
C   Qmax=196349.5408
C   ta=300.0
C   tQmax=132.9340
C   tdecay=1350.8627
C   tbo=2432.7827
C   aL=1.0
C
C   t=TIME(1)
C
C   IF (t .LT. tQmax) THEN
C     Q=10.0**6.0*((t/ta)**2.0)
C   ELSE IF (t .GE. tQmax .AND. t .LT. tdecay) THEN
C     Q=Qmax
C   ELSE IF (t .GE. tdecay .AND. t .LT. tbo) THEN
C     Q=Qmax*((t-tbo)/(tdecay-tbo))
C   ELSE
C     Q=0.0

```

```

                                END IF
C
    Qc=0.8*Q
    fl=-1.02*D+0.0148*(Q**(2.0/5.0))
C
    IF (fl .LT. 0.0) THEN
        fl=0.0
    END IF
C
C   VIEW FACTOR CALCULATION (Shokri & Beyler, 2016)
C
    IF (SNAME .EQ. 'ASSEMBLY_EXPOSED_Y150') THEN
        Z=0.15
    ELSE IF (SNAME .EQ. 'ASSEMBLY_EXPOSED_Y450') THEN
        Z=0.45
    ELSE IF (SNAME .EQ. 'ASSEMBLY_EXPOSED_Y750') THEN
        Z=0.75
    ELSE IF (SNAME .EQ. 'ASSEMBLY_EXPOSED_Y1050') THEN
        Z=1.05
    ELSE IF (SNAME .EQ. 'ASSEMBLY_EXPOSED_Y1350') THEN
        Z=1.35
    ELSE IF (SNAME .EQ. 'ASSEMBLY_EXPOSED_Y1650') THEN
        Z=1.65
    ELSE IF (SNAME .EQ. 'ASSEMBLY_EXPOSED_Y1950') THEN
        Z=1.95
    ELSE IF (SNAME .EQ. 'ASSEMBLY_EXPOSED_Y2250') THEN
        Z=2.25
    ELSE IF (SNAME .EQ. 'ASSEMBLY_EXPOSED_Y2550') THEN
        Z=2.55
    ELSE IF (SNAME .EQ. 'ASSEMBLY_EXPOSED_Y2850') THEN
        Z=2.85
    END IF
C
    IF (Z .GE. fl) THEN
        H12=Z-fl
    ELSE
        H12=fl-Z
    END IF
C
    H11=Z
    S=2.0*aL/D
    ah11=2.0*H11/D
    ah12=2.0*H12/D
    B=(1.0+S**2.0)/(2.0*S)
    A11=(ah11**2.0+S**2.0+1.0)/(2.0*S)
    A12=(ah12**2.0+S**2.0+1.0)/(2.0*S)
C
    PI=3.1416
C
    F11a=(1.0/(PI*S))*ATAN(ah11/SQRT(S**2.0-1.0))-(ah11/(PI*S))*ATAN(SQRT((S-
1.0)/(S+1.0)))

```

```

      F11b=((A11*ah11)/(PI*S*SQRT(A11**2.0-1.0))*ATAN(SQRT(((A11+1.0)*(S-
1.0))/((A11-1.0)*(S+1.0))))
      F11=F11a+F11b
C
      F12a=(1.0/(PI*S))*ATAN(ah12/SQRT(S**2.0-1.0))-(ah12/(PI*S))*ATAN(SQRT((S-
1.0)/(S+1.0)))
      F12b=((A12*ah12)/(PI*S*SQRT(A12**2.0-1.0))*ATAN(SQRT(((A12+1.0)*(S-
1.0))/((A12-1.0)*(S+1.0))))
      F12=F12a+F12b
C
      IF (Z .GE. fl) THEN
      F=F11-F12
      ELSE
      F=F11+F12
      END IF
C
C TEMPERATURE-DEPENDENT EMISSIVITY MODEL (EN 1993-1-2)
C
C TS = surface temperature in degrees C
C Em = surface emissivity
C
      TS=SOL
      Em=0.7
C
C NET SURFACE HEAT FLUX (Improved EN 1991-1-2 Section 3.1 Formulation by
Hostikka (2003))
C
C hnet = net surface heat flux in W/m^2
C hnetc = net convective heat flux in W/m^2
C hnetr = net radiative heat flux in W/m^2
C Ac = convective heat transfer coefficient = 35 W/m^2/K (EN 1991-1-2 Section 3.3.1.1)
C F = configuration factor
C Em = surface emissivity as defined above
C Ef = emissivity of the fire = 1 (EN 1991-1-2 Section 3.1(6))
C Ea = emissivity of the ambient surroundings
C Ta = temperature of the ambient surroundings
C SBC = Stefan-Boltzmann constant = 5.67*10^-8 W/m^2/K^4
C
      Ea=1.0
      TA=20.0
      SBC=5.67*(10.0**-8.0)
C
      IF (SNAME .EQ. 'ASSEMBLY_UNEXPOSED_SURFACES') THEN
      Ac=4.0 !for unexposed side of members
      hnetc=Ac*(TA-TS)
      hnetr=Em*Ea*SBC*((TA+273.15)**4.0)-Em*SBC*((TS+273.15)**4.0)
      hnet=hnetc+hnetr
      FLUX(1)=hnet
      ELSE IF (SNAME .EQ. 'ASSEMBLY_TOP') THEN
      Ac=4.0 !for unexposed side of members
      hnetc=Ac*(TA-TS)
      hnetr=Em*Ea*SBC*((TA+273.15)**4.0)-Em*SBC*((TS+273.15)**4.0)

```

```

hnet=hnetc+hnetr
FLUX(1)=hnet
ELSE
Ac=35.0
hnetc=Ac*(TA-TS)
hnetr=Em*(58.0*(10.0**(-0.00823*D)))*(10.0**3.0)*F+(1.0-
F)*Em*Ea*SBC*((TA+273.15)**4.0)-Em*SBC*((TS+273.15)**4.0)
hnet=hnetc+hnetr
FLUX(1)=hnet
END IF

```

```

C
RETURN
END

```

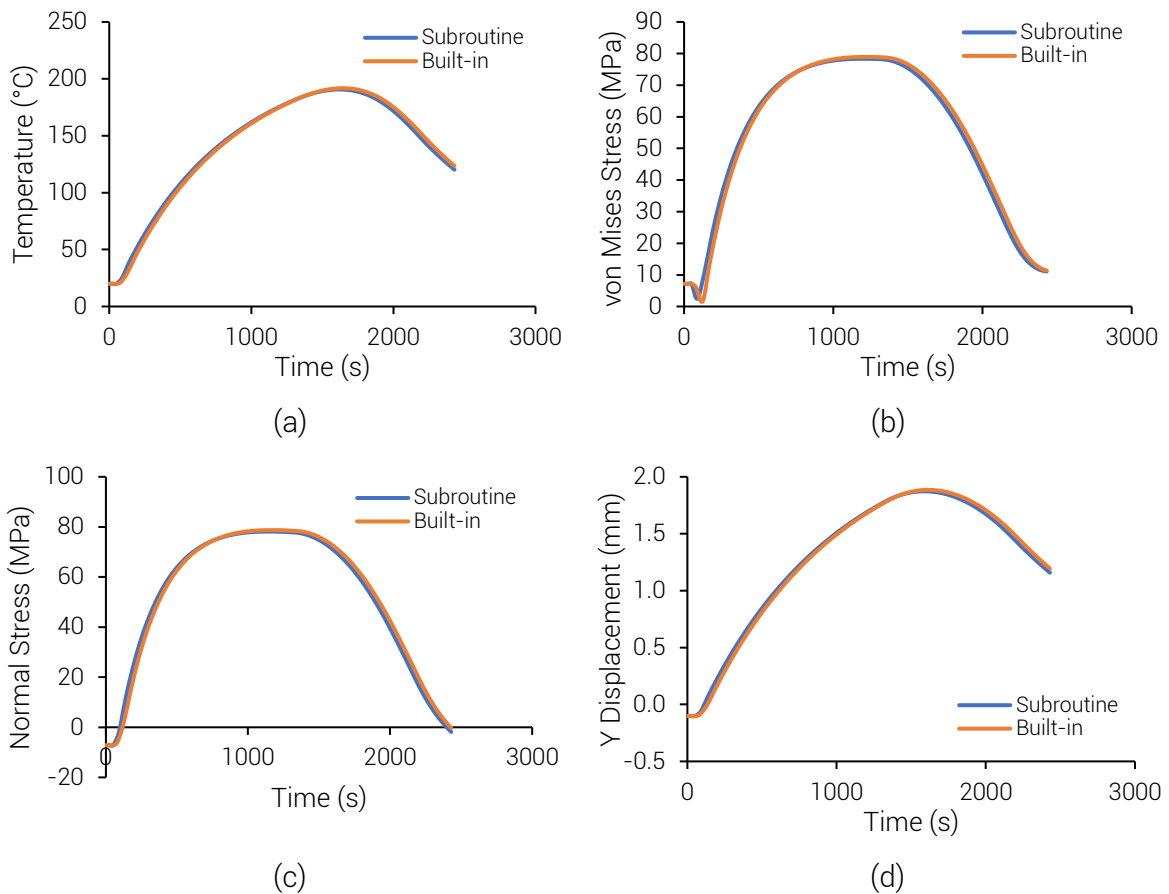


Figure F-3. Comparison of results for Case 2—Scenario 2: (a) temperature, (b) von Mises stress, (c) normal stress, and (d) displacement along y-direction.

Case 2—Scenario 3: Beam Directly Above the Localized Fire

The user subroutine for Case 2—Scenario 3 is shown below followed by the comparison of results as shown in Fig. F-4. It can be seen that there are considerable differences between

the results from the user subroutine and the built-in function. This is mostly due to the limitation of the software and partly due to the limitation of the fire model used in the user subroutine. Firstly, there is no option in the software to input the value of the emissivity of the gas surrounding the member. This had a huge impact on the results because in this scenario, the beam is engulfed by the smoke and therefore receiving radiation from that as well. Secondly, apart from there is no option to input the view factor from the fire, the fire model used does not calculate the view factor from the fire to the surface. Because of that, the effect of radiation from the surroundings was not considered both in the user subroutine and in the input to the software. Nonetheless, the results from the built-in function gave an idea on the order of the expected values. The user subroutine can be considered to pass the verification.

```

SUBROUTINE DFLUX(FLUX,SOL,KSTEP,KINC,TIME,NOEL,NPT,COORDS,
1 JLTYP,TEMP,PRESS,SNAME)
C
C   INCLUDE 'ABA_PARAM.INC'
C
C   DIMENSION FLUX(2), TIME(2), COORDS(3)
C   CHARACTER*80 SNAME
C
C   JLTYP=0
C
C   LOCALIZED FIRE CURVE (EN 1999-1-2 Annex C)
C   !Important parameters are already pre-calculated to simplify this code.
C
C   D = fuel diameter in m
C   Qmax = maximum HRR in W
C   Q = instantaneous total HRR in W
C   Qr = radiative portion of the HRR in W
C   t = time in s
C   ta = time to reach HRR of 1 MW in s
C   tQmax = time to reach maximum HRR in s
C   tdecay = time to reach decay in s
C   tbo = time to reach burnout in s
C   fl = length of fire in m
C   flm = mid-height of the fire in m
C   TGC_j = instantaneous ceiling jet temperature in degrees C
C   X = horizontal distance from the center of the fire in m
C   y = height of the beam in m
C   H = height of the ceiling in m
C   r_j = horizontal distance from the center of the ceiling jet in m
C   R = distance from the mid-height of the flame to the target surface in m
C   Theta = angle between the normal of the target surface and the line of sight from the
source to the target in rad
C
C   !Manually input the value of these parameters.
      D=1.0

```



```

Qmax=196349.5408
ta=300.0
tQmax=132.9340
tdecay=1350.8627
tbo=2432.7827
y=0.3
H=3.0
C
t=TIME(1)
C
IF (t .LT. tQmax) THEN
Q=10.0**6.0*((t/ta)**2.0)
  ELSE IF (t .GE. tQmax .AND. t .LT. tdecay) THEN
Q=Qmax
  ELSE IF (t .GE. tdecay .AND. t .LT. tbo) THEN
Q=Qmax*((t-tbo)/(tdecay-tbo))
  ELSE
Q=0.0
  END IF
C
fl=-1.02*D+0.0148*(Q**(2.0/5.0))
C
IF (fl .LE. 0.0) THEN
flm=0.0
  ELSE
flm=fl/2.0
  END IF
C
POINT SOURCE METHOD (Beyler, 2016)
C
IF (SNAME .EQ. 'ASSEMBLY_BOTTOM_150') THEN
X=0.15
  ELSE IF (SNAME .EQ. 'ASSEMBLY_BOTTOM_450') THEN
X=0.45
  ELSE IF (SNAME .EQ. 'ASSEMBLY_BOTTOM_750') THEN
X=0.75
  ELSE IF (SNAME .EQ. 'ASSEMBLY_BOTTOM_1050') THEN
X=1.05
  ELSE IF (SNAME .EQ. 'ASSEMBLY_BOTTOM_1350') THEN
X=1.35
  END IF
C
R=SQRT((H-y-flm)**2.0+X**2.0)
COS_Theta=(H-y-flm)/R
Qr=(0.21-0.0034*D)*Q
C
ALPERT'S CEILING JET CORRELATION (Quintiere, 2000)
C
For surfaces named 'Other'
C
IF (SNAME .EQ. 'ASSEMBLY_OTHER_150') THEN
ro=0.15
  ELSE IF (SNAME .EQ. 'ASSEMBLY_OTHER_450') THEN

```

```

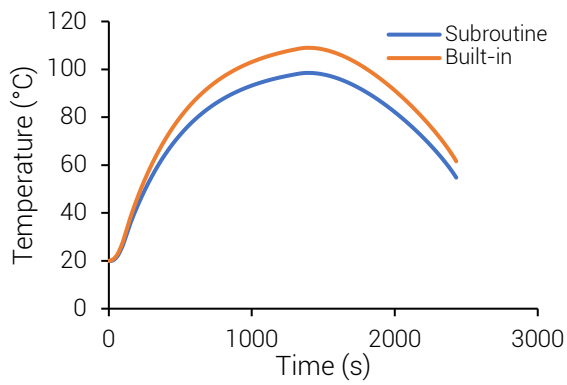
ro=0.45
ELSE IF (SNAME .EQ. 'ASSEMBLY_OTHER_750') THEN
ro=0.75
ELSE IF (SNAME .EQ. 'ASSEMBLY_OTHER_1050') THEN
ro=1.05
ELSE IF (SNAME .EQ. 'ASSEMBLY_OTHER_1350') THEN
ro=1.35
END IF
C
IF (ro/H .LT. 0.18) THEN
TGCo=20.0+16.9*((Q/1000.0)**(2.0/3.0))/(H**(5.0/3.0))
ELSE
TGCo=20.0+5.38*(((Q/1000.0)/ro)**(2.0/3.0))/H
END IF
C
C
For surfaces named 'Bottom'
IF (SNAME .EQ. 'ASSEMBLY_BOTTOM_150') THEN
rb=0.15
ELSE IF (SNAME .EQ. 'ASSEMBLY_BOTTOM_450') THEN
rb=0.45
ELSE IF (SNAME .EQ. 'ASSEMBLY_BOTTOM_750') THEN
rb=0.75
ELSE IF (SNAME .EQ. 'ASSEMBLY_BOTTOM_1050') THEN
rb=1.05
ELSE IF (SNAME .EQ. 'ASSEMBLY_BOTTOM_1350') THEN
rb=1.35
END IF
C
IF (rb/H .LT. 0.18) THEN
TGCb=20.0+16.9*((Q/1000.0)**(2.0/3.0))/(H**(5.0/3.0))
ELSE
TGCb=20.0+5.38*(((Q/1000.0)/rb)**(2.0/3.0))/H
END IF
C
C
TEMPERATURE-DEPENDENT EMISSIVITY MODEL (EN 1993-1-2)
C
C
TS = surface temperature in degrees C
C
Em = surface emissivity
C
C
TS=SOL
Em=0.7
C
C
NET SURFACE HEAT FLUX (Improved EN 1991-1-2 Section 3.1 Formulation by
Hostikka (2003))
C
C
hnet = net surface heat flux in W/m^2
C
hnetc = net convective heat flux in W/m^2
C
hnetf = net radiative heat flux from the fire in W/m^2
C
hnetg = net radiative heat flux from the ceiling jet in W/m^2
C
hnetr = net radiative heat flux in W/m^2
C
Ac = convective heat transfer coefficient = 35 W/m^2/K (EN 1991-1-2 Section 3.3.1.1)
C
Em = surface emissivity as defined above

```

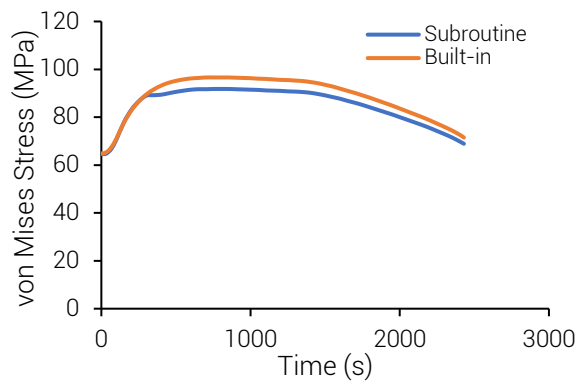
```

C      Eg = emissivity of the gas in the ceiling jet
C      SBC = Stefan-Boltzmann constant = 5.67*10^-8 W/m^2/K^4
C
C      Ac=35.0
C      SBC=5.67*(10.0**-8.0)
C      PI=3.1416
C
C      TEMPERATURE-DEPENDENT EMISSIVITY OF THE SMOKE LAYER (Gou-wei et al.,
2014)
C
C      Egb=0.458-1.29*(10.0**-4.0)*TGCb
C      Ego=0.458-1.29*(10.0**-4.0)*TGCo
C
C      hnetf=Em*(1.0-Egb)*(Qr*cos_Theta)/(4*PI*R**2.0)
C
C      hnetcb=Ac*(TGCb-TS)
C      hnetco=Ac*(TGCo-TS)
C
C      hnetgb=Em*Egb*SBC*((TGCb+273.15)**4.0)
C      hnetgo=Em*Ego*SBC*((TGCo+273.15)**4.0)
C
C      hnetb=hnetcb+hnetf+hnetgb-Em*SBC*((TS+273.15)**4.0)
C      hneto=hnetco+hnetgo-Em*SBC*((TS+273.15)**4.0)
C
C      IF (SNAME .EQ. 'ASSEMBLY_BOTTOM_150') THEN
C      FLUX(1)=hnetb
C      ELSE IF (SNAME .EQ. 'ASSEMBLY_BOTTOM_450') THEN
C      FLUX(1)=hnetb
C      ELSE IF (SNAME .EQ. 'ASSEMBLY_BOTTOM_750') THEN
C      FLUX(1)=hnetb
C      ELSE IF (SNAME .EQ. 'ASSEMBLY_BOTTOM_1050') THEN
C      FLUX(1)=hnetb
C      ELSE IF (SNAME .EQ. 'ASSEMBLY_BOTTOM_1350') THEN
C      FLUX(1)=hnetb
C      END IF
C
C      IF (SNAME .EQ. 'ASSEMBLY_OTHER_150') THEN
C      FLUX(1)=hneto
C      ELSE IF (SNAME .EQ. 'ASSEMBLY_OTHER_450') THEN
C      FLUX(1)=hneto
C      ELSE IF (SNAME .EQ. 'ASSEMBLY_OTHER_750') THEN
C      FLUX(1)=hneto
C      ELSE IF (SNAME .EQ. 'ASSEMBLY_OTHER_1050') THEN
C      FLUX(1)=hneto
C      ELSE IF (SNAME .EQ. 'ASSEMBLY_OTHER_1350') THEN
C      FLUX(1)=hneto
C      END IF
C
C      RETURN
C      END

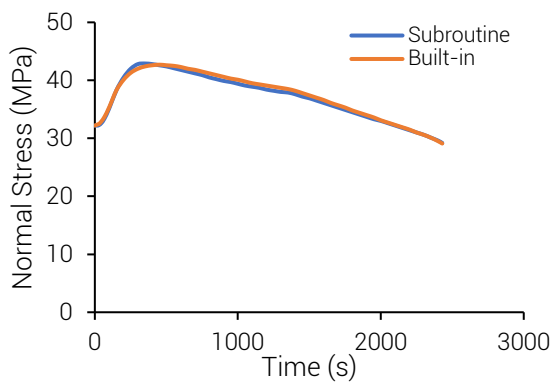
```



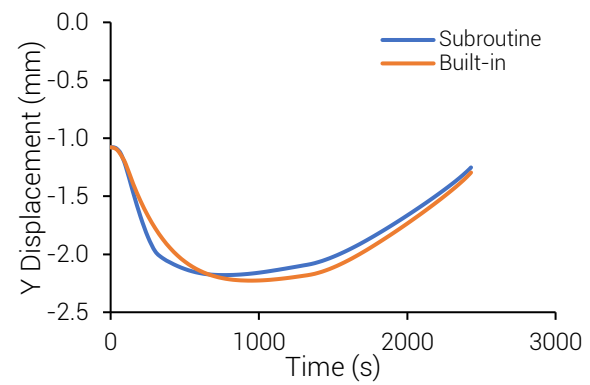
(a)



(b)



(c)



(d)

Figure F-4. Comparison of results for Case 2–Scenario 3: (a) temperature, (b) von Mises stress, (c) normal stress, and (d) displacement along y-direction.